

**Comparison of several active suspension strategies
using computer simulation**

by

Paul Kenneth Warner

**A Thesis Submitted to the
Graduate Faculty in Partial Fulfillment of the
Requirements for the Degree of
MASTER OF SCIENCE**

Major: Mechanical Engineering

Signatures have been redacted for privacy

**Iowa State University
Ames, Iowa
1988**

TABLE OF CONTENTS

ACKNOWLEDGEMENTS		xii
LIST OF NOMENCLATURE		xiii
1 INTRODUCTION		1
2 LITERATURE REVIEW		3
2.1 Theoretical Studies		3
2.2 Active Suspension Applications		4
2.3 Actuators		6
3 LINEAR FULL STATE FEEDBACK WITH IDEAL ACTUATORS		9
3.1 Seven Degree of Freedom Dynamic Model		9
3.2 System Optimization		12
3.3 Frequency Response		17
3.4 Vehicle Simulation		20
4 LIMITED STATE FEEDBACK		30
4.1 Road Height Removed From State Vector		30
4.2 Optimal Reconstruction of State Variables		37
5 HYDRAULIC ACTUATORS		51
5.1 Hydraulic Equations of Motion		52
5.2 Effects of Actuator Dynamics on Suspension Performance		55
6 VARIABLE DAMPING SEMI-ACTIVE ACTUATORS		64
6.1 On/Off Damper		64
6.2 Active Damper		74
7 CONCLUSIONS		80

8	BIBLIOGRAPHY	82
9	APPENDIX A - PARAMETERS USED IN THIS THESIS . . .	84
10	APPENDIX B - FEEDBACK GAIN MATRICES	85
11	APPENDIX C - SYSTEM EQUATIONS AND MATRICES . .	89

LIST OF FIGURES

Figure 3.1	Seven degree of freedom model of vehicle	10
Figure 3.2	Block diagram of regulator system	14
Figure 3.3	Bounce frequency response for varying phase angles between front and rear tires of the passive suspension (vehicle 1) . .	21
Figure 3.4	Bounce frequency response for varying phase angles between front and rear tires of the active suspension (vehicle 2) . . .	21
Figure 3.5	Pitch frequency response for varying phase angles between front and rear tires of the passive suspension (vehicle 1) . .	22
Figure 3.6	Pitch frequency response for varying phase angles between front and rear tires of the active suspension (vehicle 2) . . .	22
Figure 3.7	Roll frequency response for varying phase angles between left and right tires of the passive suspension (vehicle 1) . .	23
Figure 3.8	Roll frequency response for varying phase angles between left and right tires of the active suspension (vehicle 2) . . .	23
Figure 3.9	Slanted half sine wave road profile	24
Figure 3.10	Step road profile	24
Figure 3.11	Bounce response of the vehicle with an active suspension (vehicle 2) to a slanted bump input compared to that of the passive suspension (vehicle 1)	25

Figure 3.12	Pitch response of the vehicle with an active suspension (vehicle 2) to a slanted bump input compared to that of the passive suspension (vehicle 1)	26
Figure 3.13	Roll response of the vehicle with an active suspension (vehicle 2) to a slanted bump input compared to that of the passive suspension (vehicle 1)	26
Figure 3.14	Bounce response of the vehicle with an active suspension (vehicle 2) to a step input compared to that of the passive suspension (vehicle 1)	27
Figure 3.15	Pitch response of the vehicle with an active suspension (vehicle 2) to a step input compared to that of the passive suspension (vehicle 1)	28
Figure 4.1	Bounce frequency response for varying phase angles between front and rear tires of the active suspension (vehicle 3) . . .	31
Figure 4.2	Pitch frequency response for varying phase angles between front and rear tires of the active suspension (vehicle 3) . . .	32
Figure 4.3	Roll frequency response for varying phase angles between front and rear tires of the active suspension (vehicle 3) . . .	32
Figure 4.4	Bounce response of the vehicle with road height removed from the state variables (vehicle 3) to a slanted bump input compared to that of the active (vehicle 2) and passive (vehicle 1) suspensions	33
Figure 4.5	Pitch response of the vehicle with road height removed from the state variables (vehicle 3) to a slanted bump input compared to that of the active (vehicle 2) and passive (vehicle 1) suspensions	34
Figure 4.6	Roll response of the vehicle with road height removed from the state variables (vehicle 3) to a slanted bump input compared to that of the active (vehicle 2) and passive (vehicle 1) suspensions	34

Figure 4.7	Bounce response of the vehicle with road height removed from the state variables (vehicle 3) to a step bump compared to that of the active (vehicle 2) and passive (vehicle 1) suspensions	35
Figure 4.8	Pitch response of the vehicle with road height removed from the state variables (vehicle 3) to a step bump input compared to that of the active (vehicle 2) and passive (vehicle 1) suspensions	35
Figure 4.9	Block diagram of optimal observer system	40
Figure 4.10	Bounce frequency response for varying phase angles between front and rear tires of the optimal observer suspension (vehicle 4)	45
Figure 4.11	Pitch frequency response for varying phase angles between front and rear tires of the optimal observer suspension (vehicle 4)	45
Figure 4.12	Roll frequency response for varying phase angles between front and rear tires of the optimal observer suspension (vehicle 4)	46
Figure 4.13	Bounce response of the vehicle with an optimal observer (vehicle 4) to a slanted bump input compared to that of the active (vehicle 2) and passive (vehicle 1) suspensions	46
Figure 4.14	Pitch response of the vehicle with an optimal observer (vehicle 4) to a slanted bump input compared to that of the active (vehicle 2) and passive (vehicle 1) suspensions	47
Figure 4.15	Roll response of the vehicle with an optimal observer (vehicle 4) to a slanted bump input compared to that of the active (vehicle 2) and passive (vehicle 1) suspensions	47
Figure 4.16	Bounce response of the vehicle with an optimal observer (vehicle 4) to a step input compared to that of the active (vehicle 2) and passive (vehicle 1) suspensions	48

Figure 4.17	Pitch response of the vehicle with an optimal observer (vehicle 4) to a step input compared to that of the active (vehicle 2) and passive (vehicle 1) suspensions	48
Figure 5.1	Servo-valve and Piston system	52
Figure 5.2	Bounce frequency response for varying phase angles between front and rear tires of the active suspension with a first order actuator ($\tau_h = 1$)	57
Figure 5.3	Bounce frequency response for varying phase angles between front and rear tires of the active suspension with a first order actuator ($\tau_h = 0.1$)	57
Figure 5.4	Bounce frequency response for varying phase angles between front and rear tires of the active suspension with a first order actuator ($\tau_h = 0.01$)	58
Figure 5.5	Percent improvement in roll, pitch and bounce peak values verses first order actuator frequency for a slanted bump	59
Figure 5.6	Percent improvement in cost integral values verses first order actuator frequency for a slanted bump	59
Figure 5.7	Bounce frequency response for varying phase angles between front and rear tires of the active suspension with a second order actuator ($\omega_n = 0.5$)	60
Figure 5.8	Bounce frequency response for varying phase angles between front and rear tires of the active suspension with a second order actuator ($\omega_n = 2$)	61
Figure 5.9	Bounce frequency response for varying phase angles between front and rear tires of the active suspension with a second order actuator ($\omega_n = 10$)	61
Figure 5.10	Percent improvement in roll, pitch and bounce peak values verses second order actuator frequency for a slanted bump	62

Figure 5.11	Percent improvement in cost integral values verses second order actuator frequency for a slanted bump	62
Figure 6.1	Block diagram of on/off suspension system applied to a two degree of freedom model of a vehicle	65
Figure 6.2	Bounce response of the vehicle with an on/off suspension system (vehicle 5) to a slanted bump input compared to that of the passive (vehicle 1) and active (vehicle 2) suspensions	66
Figure 6.3	Pitch response of the vehicle with an on/off suspension system (vehicle 5) to a slanted bump input compared to that of the passive (vehicle 1) and active (vehicle 2) suspensions	67
Figure 6.4	Roll response of the vehicle with an on/off suspension system (vehicle 5) to a slanted bump input compared to that of the passive (vehicle 1) and active (vehicle 2) suspensions . . .	67
Figure 6.5	Bounce response of the vehicle with an on/off suspension system (vehicle 5) to a step input compared to that of the passive suspension (vehicle 1)	68
Figure 6.6	Pitch response of the vehicle with an on/off suspension system (vehicle 5) to a step input compared to that of the passive suspension (vehicle 1)	69
Figure 6.7	Bounce response of the vehicle with an on/off suspension system having twice the damping (vehicle 7) to a slanted bump input compared to that of the passive suspensions (vehicle 1 and vehicle 6, twice damping)	70
Figure 6.8	Pitch response of the vehicle with an on/off suspension system having twice the damping (vehicle 7) to a slanted bump input compared to that of the passive suspensions (vehicle 1 and vehicle 6, twice damping)	71

Figure 6.9	Roll response of the vehicle with an on/off suspension system having twice the damping (vehicle 7) to a slanted bump input compared to that of the passive suspensions (vehicle 1 and vehicle 6, twice damping)	71
Figure 6.10	Bounce response of the vehicle with an on/off suspension system having twice the damping (vehicle 7) to a step input compared to that of the passive suspensions (vehicle 1 and vehicle 6, twice damping)	72
Figure 6.11	Pitch response of the vehicle with an on/off suspension system having twice the damping (vehicle 7) to a step input compared to that of the passive suspensions (vehicle 1 and vehicle 6, twice damping)	73
Figure 6.12	Bounce response of the vehicle with an active damper (vehicle 8) suspension system to a slanted bump input compared to that of the passive (vehicle 1) and active (vehicle 2) suspensions	75
Figure 6.13	Pitch response of the vehicle with an active damper (vehicle 8) suspension system to a slanted bump input compared to that of the passive (vehicle 1) and active (vehicle 2) suspensions	76
Figure 6.14	Roll response of the vehicle with an active damper (vehicle 8) suspension system to a slanted bump input compared to that of the passive (vehicle 1) and active (vehicle 2) suspensions	76
Figure 6.15	Bounce response of the vehicle with an active damper (vehicle 8) suspension system to a step input compared to that of the passive (vehicle 1) and active (vehicle 2) suspensions	77
Figure 6.16	Pitch response of the vehicle with an active damper (vehicle 8) suspension system to a step input compared to that of the passive (vehicle 1) and active (vehicle 2) suspensions	78

LIST OF TABLES

Table 3.1	Response characteristics of the vehicle with an active suspension. (vehicle 2) to a slanted bump input compared to that of the passive suspension (vehicle 1)	27
Table 3.2	Response characteristics of the vehicle with an active suspension (vehicle 2) to a step bump input compared to that of the passive suspension (vehicle 1)	28
Table 4.1	Response characteristics of the vehicle with road height removed from the state vector (vehicle 3) to a slanted bump input compared to that of the active (vehicle 2) and passive (vehicle 1) suspensions	36
Table 4.2	Response characteristics of the vehicle with road height removed from the state vector (vehicle 3) to a step input compared to that of the active (vehicle 2) and passive (vehicle 1) suspensions	36
Table 4.3	Response characteristics of the vehicle with an optimal observer (vehicle 4) to a slanted bump input compared to that of the active (vehicle 2) and passive (vehicle 1) suspensions	49
Table 4.4	Response characteristics of the vehicle with an optimal observer (vehicle 4) to a step input compared to that of the active (vehicle 2) and passive (vehicle 1) suspensions	49
Table 6.1	Response characteristics of the vehicle with an on/off suspension system (vehicle 5) to a slanted bump compared to that of the active (vehicle 2) and passive (vehicle 1) suspensions	68

Table 6.2	Response characteristics of the vehicle with an on/off suspension system (vehicle 5) to a step input compared to that of the active (vehicle 2) and passive (vehicle 1) suspensions	69
Table 6.3	Response characteristics of the vehicle with an on/off suspension system having twice the damping (vehicle 7) to a slanted bump input compared to that of the passive suspensions (vehicle 1 and vehicle 6, twice damping)	72
Table 6.4	Response characteristics of the vehicle with an on/off suspension system having twice the damping (vehicle 7) to a step input compared to that of the passive suspensions (vehicle 1 and vehicle 6, twice damping)	73
Table 6.5	Response characteristics of the vehicle with an active damper (vehicle 8) suspension system to a slanted bump input compared to that of the active (vehicle 2) and passive (vehicle 1) suspensions	77
Table 6.6	Response characteristics of the vehicle with an active damper (vehicle 8) suspension system to a step compared to that of the active (vehicle 2) and passive (vehicle 1) suspensions .	78

ACKNOWLEDGEMENTS

I would like to express my gratitude and appreciation to my advisor and good friend, Martin Vanderploeg, for his encouragement and assistance throughout my graduate program. I would also like to thank Professors Bernard and Huston for their input while serving on my thesis committee.

I wish to give special thanks to my wife, Julia, for her love and support in my work.

In addition, I thank my colleagues, Alan Hufnagel, Alan Lynch, Jay Shannan, Jeff Trom, and Don Dusenberry for their valuable suggestions and support.

LIST OF NOMENCLATURE

a	Longitudinal distance from sprung mass center of gravity to the front axle centerline
A	System matrix relating \mathbf{x} to $\dot{\mathbf{x}}$
\tilde{A}	System matrix relating $\tilde{\mathbf{x}}$ to $\dot{\tilde{\mathbf{x}}}$
A_p	Piston area
b	Longitudinal distance from sprung mass center of gravity to the rear axle centerline
B	System matrix relating control force to $\dot{\mathbf{x}}$
\tilde{B}_1	System matrix relating control force to $\dot{\tilde{\mathbf{x}}}$
\tilde{B}_2	System matrix relating road height velocity vector to $\dot{\tilde{\mathbf{x}}}$
c	Hydraulic valve coefficient
c_f	Front suspension damping coefficient
c_r	Rear suspension damping coefficient
C	System matrix relating the state vector to the observed variable vector
e	Error vector between the state vector and the approximated state vector
F	Estimator system matrix relating the reconstructed state variables to their derivatives

- F_a Total suspension force applied to the left front corner of the sprung mass and the left front unsprung mass
- F_{act} Sum of the control forces
- F_b Total suspension force applied to the left rear corner of the sprung mass and the left rear unsprung mass
- F_c Total suspension force applied to the right front corner of the sprung mass and the right front unsprung mass
- F_d Total suspension force applied to the right rear corner of the sprung mass and the right rear unsprung mass
- F_{damp} Sum of the damping forces measured from equilibrium
- F_{des} Force desired from actuator
- F_{out} Output force from hydraulic piston
- F_s Sum of the spring forces measured from equilibrium
- F_{t1} Left front force due to the compression of the tire
- F_{t2} Left rear force due to the compression of the tire
- F_{t3} Right front force due to the compression of the tire
- F_{t4} Right rear force due to the compression of the tire
- G Optimal observer system matrix relating the observed variables to the derivative of the approximated state vector
- H Optimal observer system matrix relating the control force vector to the derivative of the approximated state vector
- $H(j\omega)$ Frequency response matrix of a linear system
- $H'(j\omega)$ Modified frequency response matrix of a linear system

I_x	Mass moment of inertia of the sprung mass about its longitudinal axis through its center of gravity
I_y	Mass moment of inertia of the sprung mass about its lateral axis through its center of gravity
J	Integral of the cost function, Π
j	Imaginary number, $\sqrt{-1}$
k_f	Front suspension spring constant
k_r	Rear suspension spring constant
K	Optimum linear constant gain matrix for the tracking system
K_r	Optimum linear constant gain matrix for the regulator system
K_e	Optimum linear constant gain matrix for the optimal observer system
k_1	Linearized hydraulic equation parameter
k_2	Linearized hydraulic equation parameter
k_3	Linearized hydraulic equation parameter
l	Dimension of the state vector
M_s	Sprung mass
M_1	Left front unsprung mass
M_2	Left rear unsprung mass
M_3	Right front unsprung mass
M_4	Right rear unsprung mass
n	Dimension of the observed variable vector

p_L	Load pressure
p_{L0}	Initial load pressure to be linearized about
p_s	Supply pressure
p_0	Sump pressure
p_1	Pressure in lower chamber of actuator piston
p_2	Pressure in upper chamber of actuator piston
P	Solution matrix of the algebraic Riccati equation
q_1	Weighting coefficient on relative chassis motion
q_2	Weighting coefficient on chassis velocity
q_3	Weighting coefficient on tire compression
q_4	Weighting coefficient on spring force
q_5	Weighting coefficient on damping force
q_6	Weighting coefficient on control force
Q	Symmetric weighting matrix developed by q_1, \dots, q_5
Q_L	Load flow in hydraulic piston
Q_1	Hydraulic flow rate through servo-valve port number 1
Q_2	Hydraulic flow rate through servo-valve port number 2
Q_3	Hydraulic flow rate through servo-valve port number 3
Q_4	Hydraulic flow rate through servo-valve port number 4
R	Symmetric weighting matrix developed by q_6

t	Independent variable, time
t_f	distance between centerlines of front tires
t_r	distance between centerlines of rear tires
u	Control force vector
V	Noise intensity matrix
V_0	Total volume in actuator piston
V_1	Volume in lower chamber of actuator piston
V_2	Volume in upper chamber of actuator piston
V_{11}	Intensity matrix of the state excitation noise
V_{12}	Intensity matrix of the correlation of the state excitation noise and the measurement noise
V_{21}	Intensity matrix of the correlation of the state excitation noise and the measurement noise
V_{22}	Intensity matrix of the measurement noise
w	Road height velocity vector
w_m	Vector of steady state input magnitudes
\bar{w}^2	Mean squared value of the measurement noise
w_1	State excitation noise vector
w_2	Measurement noise vector
x	Linearized valve opening
x_0	Initial valve opening to be linearized about

x_1	Valve opening at servo-valve port number 1
x_2	Valve opening at servo-valve port number 2
x_3	Valve opening at servo-valve port number 3
x_4	Valve opening at servo-valve port number 4
x	Regulator system state vector
x_m	Vector of steady state response magnitudes
\hat{x}	Approximated regulator system state vector
\tilde{x}	Tracking system state vector
y	Observed variable vector
\hat{y}	Approximation of the observed variable vector made from the approximated state vector
z	Vertical distance of the sprung mass from its static equilibrium position
\bar{z}_r^2	Mean square of the road profile
z'	Vertical distance of the sprung mass from its static equilibrium position measured relative to the road
z'_a	Vertical distance from the road to the left front corner of the chassis measured from static equilibrium
z'_b	Vertical distance from the road to the left rear corner of the chassis measured from static equilibrium
z'_c	Vertical distance from the road to the right front corner of the chassis measured from static equilibrium
z'_d	Vertical distance from the road to the right rear corner of the chassis measured from static equilibrium

z_1	Vertical distance of the left front unsprung mass from its static equilibrium position
z'_1	Vertical distance of the left front unsprung mass from its static equilibrium position measured relative to the road
z_2	Vertical distance of the left rear unsprung mass from its static equilibrium position
z'_2	Vertical distance of the left rear unsprung mass from its static equilibrium position measured relative to the road
z_3	Vertical distance of the right front unsprung mass from its static equilibrium position
z'_3	Vertical distance of the right front unsprung mass from its static equilibrium position measured relative to the road
z_4	Vertical distance of the right rear unsprung mass from its static equilibrium position
z'_4	Vertical distance of the right rear unsprung mass from its static equilibrium position measured relative to the road
β	Bulk modulus of hydraulic fluid
ζ	Damping ratio of second order actuator
η	Steady state time response to a sinusoidal input
θ	Absolute measure of angle about the sprung mass lateral axis through its center of gravity
θ'	Measure of the angle between the road and the chassis about the sprung mass lateral axis through its center of gravity
μ	Steady state input
$\hat{\mu}$	Magnitude of steady state input

Π	Weighted sum of the square of the deviation of the state variables of a regulator system from zero
σ	Phase angle of input
ϕ	Absolute measure of angle about the sprung mass longitudinal axis through its center of gravity
ϕ'	Measure of the angle between the road and the chassis about the sprung mass longitudinal axis through its center of gravity
ψ	Phase angle of response
ω	Frequency in radians per second
ω_n	Natural frequency of second order actuator
T	Indicates transpose of a matrix
\cdot	Indicates first derivative with respect to time
$\ddot{}$	Indicates second derivative with respect to time
E	Expectation operator
δ	Delta function
diag	Forms a diagonal matrix from the components given
sign	Gives the sign of its argument

1 INTRODUCTION

Many studies have shown that active suspensions can greatly improve suspension performance over passive suspensions. Much of the active suspension research has been devoted to control theory applied to ideal systems. These ideal system models may not give accurate predictions of an actual system because they include state variables in the feedback loop that are difficult if not impossible to measure, and because they ignore actuator dynamics. The purpose of this study is to quantify the effects of several more realistic active and semi-active suspension strategies on ride performance. A linearized dynamic model of a vehicle is used which has as its seven degrees of freedom bounce, pitch, and roll of the sprung mass and the four vertical unsprung mass positions. Frequency response and selected time responses are used for evaluation of suspension performance.

Chapter 2 reviews articles on active suspension theory and applied active suspensions. Chapter 3 presents the seven degree of freedom linear model and the optimal linear control methods that are used throughout this thesis. An ideal active system is presented which has full state feedback and ideal actuators. As expected, this system yields excellent improvements in ride, and is used throughout the thesis to compare less ideal systems. Chapter 4 investigates the effects of removing difficult to measure state variables from the feedback loop and shows how recon-

struction of the state vector from easily measured variables yields improvements in ride which compare well with the ideal system. Chapter 5 looks at the effects of hydraulic actuators, which are approximated as first and second order systems. Chapter 6 investigates semi-active actuators including an active damping actuator and an on/off damping actuator.

All of the non-ideal systems studied result in improvements over the passive suspension system, but to a varying degree. As expected, none of the non-ideal systems result in improvements equaling those of the ideal active suspension system.

2 LITERATURE REVIEW

In recent years, active and semi-active suspension systems have attracted considerable attention from the research community and from automotive manufacturers. Research in the academic community has appeared regularly in the literature, but deals primarily with simple ideal analytical models. Research conducted by automotive firms for the most part has been kept out of the literature due to proprietary concerns. This literature review will present some relevant theoretical studies, and then concentrate on the more applied literature.

2.1 Theoretical Studies

Thompson [1] presented an analysis of a quarter car model with an active suspension. A performance index was defined that was a weighted sum of the system state variables. The algebraic Riccati equation was then solved to find the optimum feedback gains. Through digital simulation, this control scheme was shown to result in significant improvements in vibration isolation. Thompson and Pearce [2] extended this study to the analysis of a half car model with two active suspensions. This model included pitch and bounce as the state variables. Using the same performance index as in his earlier paper, optimal feedback gains were found. Again, the active suspension system resulted in significant improvement over the

passive suspension.

Shannan [3] conducted a study of a seven degree of freedom car model with a fully active suspension. This model's feedback state variables included bounce, pitch, roll, vertical wheel corner positions, and road height. The performance index was similar to the one used by Thompson [1]. Performance of the active suspension was judged against the passive suspension by simulation over bumps to compare ride and by simulation through steering and braking maneuvers to compare handling. It was shown that the active suspension improved ride significantly. In addition, it was shown that active suspension systems can affect the handling, and that sprung mass motions are significantly reduced during handling maneuvers.

2.2 Active Suspension Applications

Although many automotive manufacturers have active research programs dealing with active suspensions, very little has appeared in the literature.

The Lotus Turbo Esprit [4] was the pioneering effort in active suspensions. The suspension was designed to maintain near constant ride height to take advantage of ground effects for racing, and still give an acceptable ride. The system consisted of 18 transducers to measure various loads, displacements and accelerations. The signals generated were fed into a microprocessor which output signals to the hydraulic servo-valve which controls the actuator. This system resulted in a more comfortable ride than standard racing cars without sacrificing good handling.

Toyota developed a semi-active system for the 1983 Soarer [5]. This system sensed speed, steering, throttle position and braking to determine which of two damping modes, hard or soft, would be used. The system achieved a 15% - 30%

decrease of squat, a 20% - 30% decrease of roll angle, a 10% - 30% decrease of nose dive and a 30% - 40% decrease of shift squat.

Mitsubishi used a similar system in its 1984 Gallant, but also used variable springs and more sensors [6]. This system sensed speed, steering, body acceleration, and throttle position and switched between a hard and soft mode by changing the spring rate and damping rate when certain conditions were met. Variable spring rate was achieved by changing the volume in an air spring. Variable damping was achieved by switching between two different oil paths. A constant ride height was maintained by varying the pressure in the air springs.

The 1987 Ford Thunderbird Turbo Coupe [7] with the Programmed Ride Control option was another production automobile with a semi-active suspension. It utilized fast acting rotary solenoids to change damping between a ride optimized and a handling optimized rate. Its three manually selected modes were ride, handling, and automatic. In automatic mode, signals from sensors determined the mode of the adjustable shocks. Steer angle and velocity was measured from which lateral acceleration was estimated. Hard braking was determined from braking pressure. Acceleration was sensed whenever a high power condition existed in the engine.

The conditions in which the device switched damping from soft to hard ride were these: hard braking (brake pressure greater than 400 psi), high speed (velocity greater than 83 mph), hard cornering (lateral acceleration greater than .35 g), and acceleration (engine vacuum greater than an 8 psi. boost or greater than 90% throttle). The performance was judged by examining the quickness of the change from ride to handling optimized mode. These conditions were selected so that changes from soft to stiff mode were fast enough during a maneuver that it appeared

to the driver to have been in stiff mode all along.

2.3 Actuators

Because actuators are an essential component of an active suspension system, and often are the limiting factor in the performance of the system, this section will give a short review of the literature covering actuator dynamics as they relate to active suspensions. Several different types of actuators have been suggested or used for active suspension systems. Two most common are variable rate springs and dampers, and hydraulic systems.

Variable rate springs and dampers have been studied by several researchers and already exist in a limited sense on many production vehicles [5,6,7]. A semi-active system using an active damper to generate the control forces was proposed by Crosby and Karnopp [8]. The active (or variable) damper system uses the same feedback gains as the fully active suspension to determine the damping rate. The force was generated by the relative velocities of the attachment points. This system required very little external energy to implement. When the command force and the available force were opposite (i.e., velocity in the same direction as command force) the damping rate was set to the minimum value. When command force and the available force were in the same direction the damping was set proportional to the command force. This system was simulated using a one degree of freedom model and showed significant improvement over passive suspensions and rivaled the isolation possible with a fully active suspension. The limitations of such a system included the following:

1. It can produce force only when a relative velocity exists across the attachment

points.

2. When the force available is not in the same direction as the control force required, no control force is available.
3. When the force required exceeds that available through a finite damping ratio, the damper is locked up.

Sharp and Hassan [9] studied the use of the active damper in vehicles by using a two degree of freedom quarter car model. By examining a passenger discomfort parameter and wheel load during digital simulation, the suspension was found to give substantially better ride comfort and better wheel load control for rough roads but only improved ride comfort for smoother roads.

Hydraulic actuation systems have received limited attention in the literature dealing with active suspensions for automobiles. Sutton [10] analyzed an active hydraulic system for a two degree of freedom quarter car model and also experimentally tested its performance.

Hydraulic systems have been studied extensively as actuators in a variety of active vibration isolation applications. Merritt [11] gives a summary of the advantages and disadvantages of hydraulic power. Those applicable to active suspensions are the following:

- Advantages

1. Large power to weight ratios are available.
2. Long component life is possible.
3. Hydraulic machines are not limited as electric machines are by magnetic saturation and electrical losses.
4. Hydraulic actuators have a higher speed of response than electric actuators.
5. Closed loop control of hydraulic actuators is relatively simple using valves and pumps.

6. Transmission of power is moderately easy with hydraulic lines and energy storage is accomplished with accumulators.

- Disadvantages

1. Hydraulic control analysis is difficult because of the nonlinear differential equations involved.
2. Small allowable tolerances result in high costs of hydraulic components.

Sherman and Lance [12] examined the use of hydraulic actuators in a positioning system for a weapon. A linearized model was used to obtain an optimal feedback control loop. The dynamics of the servo-valve were neglected. The controller, designed using the linearized equations, was found to give good control when the nonlinear equations of motion were simulated. Lopez and Lance [13] examined the use of hydraulic actuators in an agricultural tractor to control implement depth. A linearized model was used to obtain a control law, but servo-valve dynamics were also included. Again, good control was obtained for the non-linear system simulated using a control law defined from the linearized approximations.

3 LINEAR FULL STATE FEEDBACK WITH IDEAL ACTUATORS

This chapter examines suspension performance using a seven degree of freedom dynamic model as used by Shannan [3]. The control system presented in this section is an ideal system and is used as a measure for comparing other more feasible approaches. The results in this section are similar to those of Shannan, however, the control problem has been reformulated as a tracking problem. In addition, the system is examined not only in the time domain but also using two input frequency response plots.

3.1 Seven Degree of Freedom Dynamic Model

The seven degrees of freedom for the math model are the bounce, pitch and roll of the sprung mass, and the vertical displacements of the four unsprung masses as shown in Figure 3.1. The vertical tire forces acting between the unsprung mass and the road profile are modeled as linear springs with no damping. The suspension forces consist of spring forces, damper forces, and actuator forces. The passive suspension is retained to decrease the control effort and to provide a backup suspension should the active suspension fail. The model is linear, and therefore valid only for small deflections from equilibrium.

The linearized equations of motion for the three sprung mass degrees of freedom

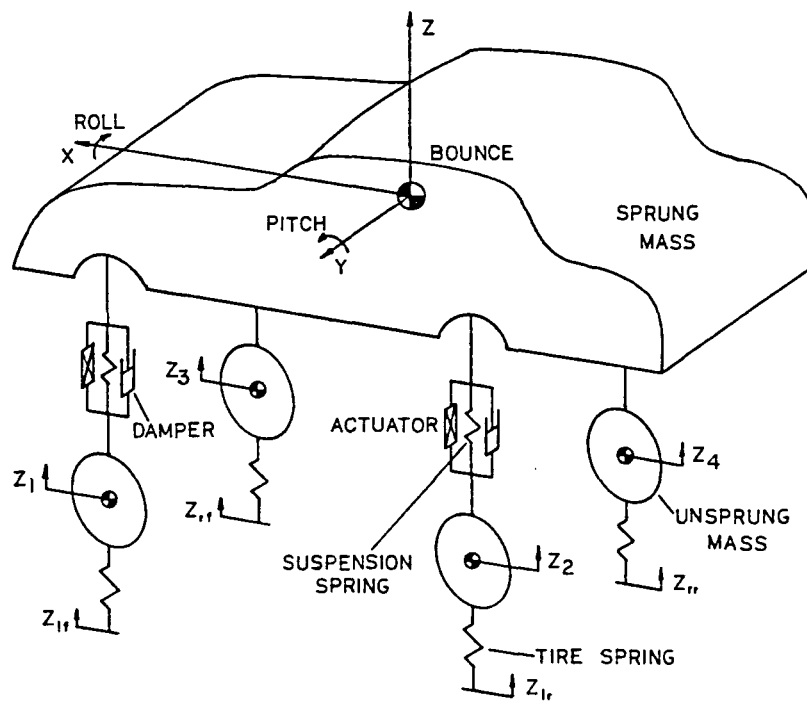


Figure 3.1: Seven degree of freedom model of vehicle

are

$$I_x \ddot{\phi} = \frac{t_f F_a}{2} + \frac{t_r F_b}{2} - \frac{t_f F_c}{2} - \frac{t_r F_d}{2} \quad (3.1)$$

$$I_y \ddot{\theta} = -a F_a + b F_b - a F_c + b F_d \quad (3.2)$$

$$M_s \ddot{z} = F_a + F_b + F_c + F_d \quad (3.3)$$

where F_a, \dots, F_d are suspension forces including spring, damping, and actuator forces, as defined in Appendix C. The linearized equations of motion for the four unsprung masses are

$$M_1 \ddot{z}_1 = F_{t1} - F_a \quad (3.4)$$

$$M_1 \ddot{z}_2 = F_{t2} - F_b \quad (3.5)$$

$$M_1 \ddot{z}_3 = F_{t3} - F_c \quad (3.6)$$

$$M_1 \ddot{z}_4 = F_{t4} - F_d \quad (3.7)$$

where F_{t1}, \dots, F_{t4} are vertical tire forces also defined in Appendix C.

To facilitate computer simulation, the seven second order equations of motion are converted to fourteen first order differential equations. To obtain an optimum control, it is desired to include the road heights at the four corners as state variables which requires using the road height velocities as input. The fourteen system equations and four road height equations can be represented by the matrix equation

$$\dot{\tilde{\mathbf{x}}} = \tilde{\mathbf{A}}\tilde{\mathbf{x}} + \tilde{\mathbf{B}}_1 \mathbf{u} + \tilde{\mathbf{B}}_2 \mathbf{w} \quad (3.8)$$

where $\tilde{\mathbf{A}}$, $\tilde{\mathbf{B}}_1$, and $\tilde{\mathbf{B}}_2$ are system matrices, $\tilde{\mathbf{x}}$ is the state vector, \mathbf{u} is the control force vector representing the forces that are applied between the four unsprung masses and the sprung mass, and \mathbf{w} is the road height velocity vector at each of the four

tires.

$$\tilde{\mathbf{x}}^T = \left[\dot{\phi} \quad \dot{\theta} \quad \phi \quad \theta \quad z \quad \dot{z} \quad z_1 \quad \dot{z}_1 \quad z_2 \quad \dot{z}_2 \quad z_3 \quad \dot{z}_3 \quad z_4 \quad \dot{z}_4 \quad z_{lf} \quad z_{lr} \quad z_{rf} \quad z_{rr} \right] \quad (3.9)$$

$$\mathbf{u}^T = \left[F_1 \quad F_2 \quad F_3 \quad F_4 \right] \quad (3.10)$$

$$\mathbf{w}^T = \left[\dot{z}_{lf} \quad \dot{z}_{lr} \quad \dot{z}_{rf} \quad \dot{z}_{rr} \right] \quad (3.11)$$

3.2 System Optimization

The problem of optimizing the control of a linear mechanism can be accomplished by finding an optimum linear constant gain matrix, K , such that

$$\mathbf{u}(t) = -K\tilde{\mathbf{x}}(t) \quad (3.12)$$

For the case of automotive ride, Kwakernaak and Sivan [14] defined this type of problem to be a tracking problem because it is desired to have the car follow the contours of the road. If it is taken as a regulator problem then a change in road height, or in slope would result in a steady state error. Thus, the desired control should allow the car to follow the hills, slopes and banked turns without any steady state error.

The method to determine an optimal control criteria is to convert this tracking problem to a regulator problem which can then be solved using the algebraic Riccati equation. New state variables are chosen which describe the vehicle position with respect to the road. This facilitates regulating them to zero. For this problem ϕ' is the angle between the car and the road about the X axis, θ' is the angle between the car and the road about the Y axis, and z' is the vertical distance from the ground

to the vehicle's center of gravity, z . The references for these new state variables are weighted averages of the road height at the four tires.

$$\phi' = \phi - \frac{1}{2} \left(\frac{z_{lf} - z_{rf}}{t_f} + \frac{z_{lr} - z_{rr}}{t_r} \right) \quad (3.13)$$

$$\theta' = \theta - \frac{1}{2} \left(\frac{z_{lf} - z_{lr}}{a+b} + \frac{z_{rf} - z_{rr}}{a+b} \right) \quad (3.14)$$

$$z' = z - \frac{b}{a+b} \left(\frac{z_{lf} + z_{rf}}{2} \right) - \frac{a}{a+b} \left(\frac{z_{lr} + z_{rr}}{2} \right) \quad (3.15)$$

If the velocity terms are assumed to be zero in a steady state condition the previous state velocity variables can be used.

Unsprung mass positions are also converted from absolute to relative variables by using the distance from the road to the wheel as the new variable.

$$z'_1 = z_1 - z_{lf} \quad (3.16)$$

$$z'_2 = z_2 - z_{lr} \quad (3.17)$$

$$z'_3 = z_3 - z_{rf} \quad (3.18)$$

$$z'_4 = z_4 - z_{rr} \quad (3.19)$$

Again the previous state velocity variables are used.

Now, the regulator state variables, \mathbf{x} , are related to the tracking state variables, $\tilde{\mathbf{x}}$, by

$$\mathbf{x} = D\tilde{\mathbf{x}} \quad (3.20)$$

where

$$\mathbf{x}^T = \left[\dot{\phi} \quad \dot{\theta} \quad \phi' \quad \theta' \quad z' \quad \dot{z} \quad \dot{z}'_1 \quad \dot{z}'_2 \quad \dot{z}'_3 \quad \dot{z}'_4 \quad z_{lf} \quad z_{lr} \quad z_{rf} \quad z_{rr} \right] \quad (3.21)$$

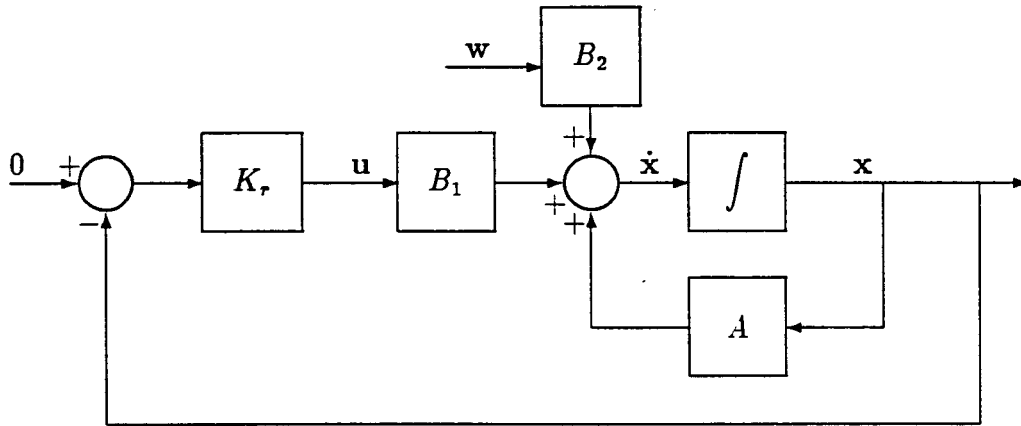


Figure 3.2: Block diagram of regulator system

and D is the linear constant transformation matrix. A new equation of motion using the regulator state variables can be found by substituting equation 3.20 into equation 3.8 yielding

$$\dot{\mathbf{x}} = D\tilde{A}D^{-1}\mathbf{x} + D\tilde{B}_1\mathbf{u} + D\tilde{B}_2\mathbf{w} \quad (3.22)$$

or

$$\dot{\mathbf{x}} = A\mathbf{x} + B_1\mathbf{u} + B_2\mathbf{w} \quad (3.23)$$

This equation is represented by the block diagram in Figure 3.2.

The problem of finding the tracker optimal control is the same as in equation 3.12 but in terms of the new state variables. In this case

$$\mathbf{u}(t) = -K_r\mathbf{x}(t). \quad (3.24)$$

The feedback gain matrix, K_r , can be found using linear optimal control theory as described in Kwakernaak and Sivan [14]. The cost function, Π , is a weighted sum of the square of the deviation of the state variables of a regulator system from zero.

Different weights are assigned to each state to achieve a desired objective. For this problem, the cost function is defined as

$$\begin{aligned}
\Pi = & q_1 (\phi'^2 + \theta'^2 + z'^2) \\
& + q_2 (\dot{\phi}^2 + \dot{\theta}^2 + \dot{z}^2) \\
& + q_3 (z_1'^2 + z_2'^2 + z_3'^2 + z_4'^2) \\
& + q_4 \left\{ (k_f(z'_1 - z'_a))^2 + (k_r(z'_2 - z'_b))^2 + (k_f(z'_3 - z'_c))^2 + (k_r(z'_4 - z'_d))^2 \right\} \\
& + q_5 \left\{ (c_f(\dot{z}'_1 - \dot{z}'_a))^2 + (c_r(\dot{z}'_2 - \dot{z}'_b))^2 + (c_f(\dot{z}'_3 - \dot{z}'_c))^2 + (c_r(\dot{z}'_4 - \dot{z}'_d))^2 \right\} \\
& + q_6 (F_1^2 + F_2^2 + F_3^2 + F_4^2) \tag{3.25}
\end{aligned}$$

where

$$z'_a \approx z' + \frac{t_f}{2} \phi' - a\theta' \tag{3.26}$$

$$z'_b \approx z' + \frac{t_r}{2} \phi' + b\theta' \tag{3.27}$$

$$z'_c \approx z' - \frac{t_f}{2} \phi' - a\theta' \tag{3.28}$$

$$z'_d \approx z' - \frac{t_r}{2} \phi' + b\theta' \tag{3.29}$$

The constants, q_1, \dots, q_6 , can be chosen to change the influence of a certain state on the control. If improved tracking is desired, then q_1 , the weighting of the chassis position with respect to the road, should be increased. If less body velocity is desired, then q_2 , the weighting of the chassis absolute velocity should be increased. If wheel hop is of lesser importance, then q_3 , the weighting on the wheel deflections can be decreased. If less body acceleration is desired then q_4, q_5 and q_6 , the weightings of the forces transmitted to the chassis, should be increased.

Optimization of a suspension depends upon a number of performance measures of vehicle ride and handling. These performance measures are rather subjective and

not well defined. Therefore, what is considered optimal for one application may not be for another, and selecting weighting factors is usually accomplished by trial and error.

Having chosen a cost function, $\Pi(\mathbf{x}(t))$, the optimal control is that which minimizes the integral of the cost function over a given time interval.

$$J = \int_0^t \Pi(\mathbf{x}(t)) dt \quad (3.30)$$

This integral can also be written in the form

$$J = \int_0^t \{\mathbf{x}^T(t)Q\mathbf{x}(t) + \mathbf{u}^T(t)R\mathbf{u}(t)\} dt \quad (3.31)$$

The classic solution to this problem is found by solving the algebraic Riccati equation,

$$0 = Q - PBR^{-1}B^T P + A^T P + PA \quad (3.32)$$

with

$$K_r = R^{-1}B^T P \quad (3.33)$$

As previously stated, good suspension performance depends upon proper selection of the cost weighting coefficients in equation 3.25. These constants change the contribution of each grouping of state variables to the performance function which is to be minimized. As a constant is increased, it tends to decrease the deviation of its variables from a zero state. Therefore, the choice of weighting coefficients is a compromise. After selecting a set of weighting coefficients, the gain matrix is found by numerically solving the algebraic Riccati equation and the control system is evaluated via frequency response, root locus and simulation. In a design scenario, the weighting constants are then adjusted to improve the response. Several iterations through this procedure are often necessary to achieve a desirable feedback gain

matrix. The weighting constants used throughout this thesis are $q_1 = 10$, $q_2 = 7.5$, $q_3 = 50$, $q_4 = 5(10)^{-7}$, $q_5 = 5(10)^{-7}$, and $q_6 = 5(10)^{-7}$. These were selected such that the contribution of each cost term is of the same order of magnitude. This choice gives good results in a general sense, and since there is no specific design objective for this thesis, these weighting coefficients are not iterated and are used throughout this thesis.

3.3 Frequency Response

The frequency response of the linear system gives a general view of the improvements possible with active suspensions. The input to the linear system is assumed to be

$$\mathbf{w}(t) = \mathbf{w}_m e^{j\omega t} \quad (3.34)$$

The steady state response is

$$\mathbf{x}(t) = \mathbf{x}_m e^{j\omega t} \quad (3.35)$$

Combining equations 3.23 and 3.24 gives

$$\dot{\mathbf{x}}(t) = (A - B_1 K_r) \mathbf{x}(t) + B_2 \mathbf{w}(t) \quad (3.36)$$

The steady state response of this system is

$$\mathbf{x}(t) = H(j\omega) \mathbf{w}_m e^{j\omega t} \quad (3.37)$$

where

$$H(j\omega) = [j\omega I - (A - B_1 K_r)] B_2 \quad (3.38)$$

and is the frequency response matrix of the system. This response to complex periodic inputs can also be applied to sinusoidal inputs. The k -th component of the

input is represented by

$$\mu_k(t) = \hat{\mu}_k \sin(\omega t + \sigma_k) \quad (3.39)$$

where σ_k is the phase lag of the k -th input. Assuming all other components are zero then the i -th component of the response is given by

$$\eta_i(t) = \|H_{ik}(j\omega)\| \hat{\mu}_k \sin(\omega t + \sigma_k + \psi_{ik}) \quad (3.40)$$

where ψ_{ik} is the phase angle of $H_{ik}(j\omega)$. A general road surface can be approximated by sinusoidal inputs of different phases at each of the four wheels.

$$z_{lf} = \sin(\omega t + \sigma_1) \quad (3.41)$$

$$z_{lr} = \sin(\omega t + \sigma_2) \quad (3.42)$$

$$z_{rf} = \sin(\omega t + \sigma_3) \quad (3.43)$$

$$z_{rr} = \sin(\omega t + \sigma_4) \quad (3.44)$$

Using the principle of superposition, the total response of the vehicle to these four inputs is the vector sum of their individual responses.

$$\eta_{i,\text{total}}(t) = \sum_{k=1}^4 \|H_{ik}(j\omega)\| \hat{\mu}_k \sin(\omega t + \sigma_k + \psi_{ik}) \quad (3.45)$$

To study bounce and pitch responses, the phase angles of the front wheel inputs are assumed to be zero while the phase angles of the rear wheel inputs are varied together. The phase angles of the rear wheel inputs are related to the wavelength of the road, T , and the wheelbase, $a + b$, by

$$\sigma_2 = \sigma_4 = 2\pi \frac{a + b}{T} \quad (3.46)$$

To study roll frequency response, the phase angle of the left side wheel inputs is set to zero while the phase angle of the right side wheels is varied together.

Because road height velocity is the input to this linear system, the frequency response will not relate road height to magnitude. If the road input for the left front wheel is

$$z_{lf} = \sin(\omega t + \sigma_1) \quad (3.47)$$

then the corresponding road height velocity is

$$\dot{z}_{lf} = \omega \sin(\omega t + \pi/2 + \sigma_1) \quad (3.48)$$

Since the magnitude of $\sin(\omega t + \sigma_1)$ and $\sin(\omega t + \pi/2 + \sigma_1)$ is the same,

$$\|\dot{z}_{lf}\| = \|\omega z_{lf}\| \quad (3.49)$$

In this case the i -th component of the response to the road height input is given by

$$\eta_i(t) = \|H_{ik}(j\omega)\| \omega \sin(\omega t + \sigma_k + \psi_{ik} + \pi/2) \quad (3.50)$$

Therefore, the frequency response function relating a state variable to the road height input, $H'_{ik}(j\omega)$, can be defined in terms of the frequency response to road height velocity as

$$H'_{ik}(j\omega) = \omega H_{ik}(j\omega) \quad (3.51)$$

Since all components of the response have the same additional phase lag, the magnitude of the vector sum will not be affected and its phase will be shifted by $\pi/2$.

To examine the frequency response of the bounce, pitch and roll of the vehicle the tracking state variables are used since they give the absolute measure of bounce, pitch and roll. The system equation used to find $H(j\omega)$ is

$$\dot{\bar{\mathbf{x}}}(t) = (\tilde{A} - \tilde{B}_1 K_r D) \bar{\mathbf{x}} + \tilde{B}_2 \mathbf{w} \quad (3.52)$$

Figures 3.3 and 3.5 present the bounce and pitch angle frequency response for the passive system (vehicle 1). Figures 3.4 and 3.6 give the frequency response for the ideal active system (vehicle 2). Figures 3.7 and 3.8 present the roll frequency response for the passive and active systems.

These results show that the active suspension system significantly decreases the magnitudes of response around the bounce, pitch and roll natural frequencies of the sprung mass, 1.38 Hz, 0.91 Hz, and 1.31 Hz respectively. However, there is limited improvement for the active suspension near the natural frequencies of the unsprung masses, 6.46 Hz for the front and 8.71 Hz for the rear.

3.4 Vehicle Simulation

This section presents the results of two simulations. The equations of motion of the vehicle model described in Section 3.1 are integrated with two different input road profiles, a slanted half sine wave bump and a step as shown in Figures 3.9 and 3.10. The slanted bump road profile is the same as used by Shannan [3]. For the vehicle traveling at 24.59 m/sec (55 mph) this profile excites the roll mode of the sprung mass at the roll natural frequency, while also exciting pitch and bounce modes. The step is similar to the one used by Thompson [1] who showed that if the system is optimal for a unit step input at a given velocity, it will also be optimal for random signal inputs of a road which has as its power spectral density

$$\Phi(\omega) = \frac{cV}{\omega^2} \quad (3.53)$$

where c is a road roughness constant and V is the vehicle velocity. This profile tends to excite wheel hop.

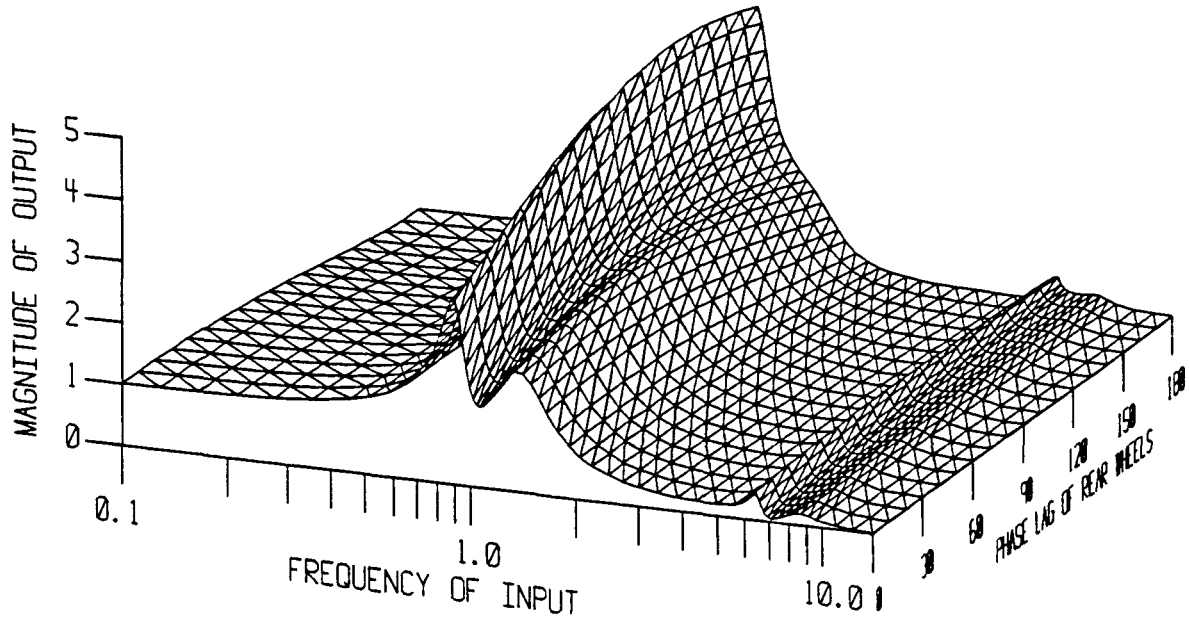


Figure 3.3: Bounce frequency response for varying phase angles between front and rear tires of the passive suspension (vehicle 1)

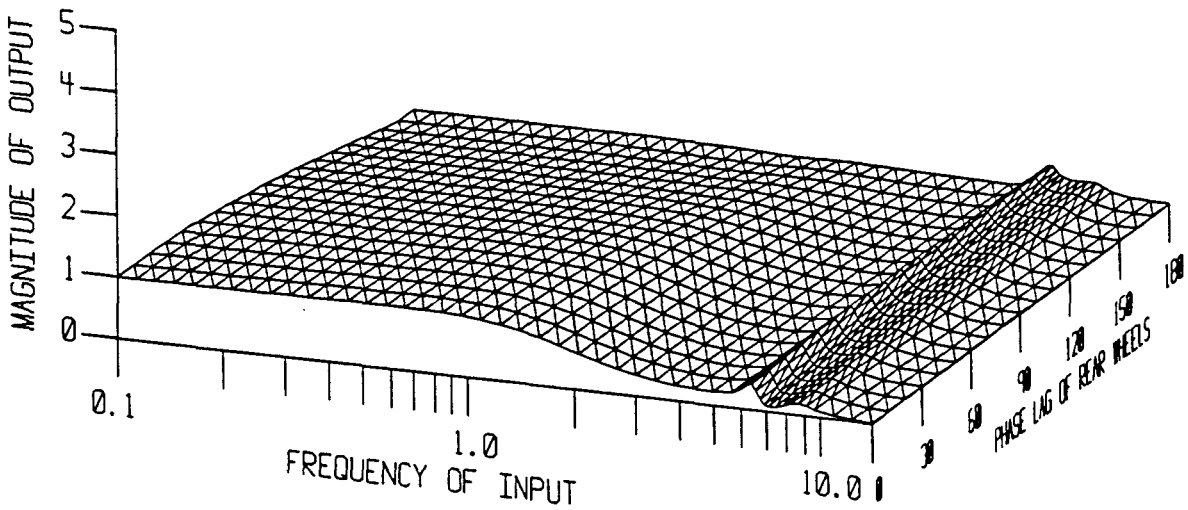


Figure 3.4: Bounce frequency response for varying phase angles between front and rear tires of the active suspension (vehicle 2)

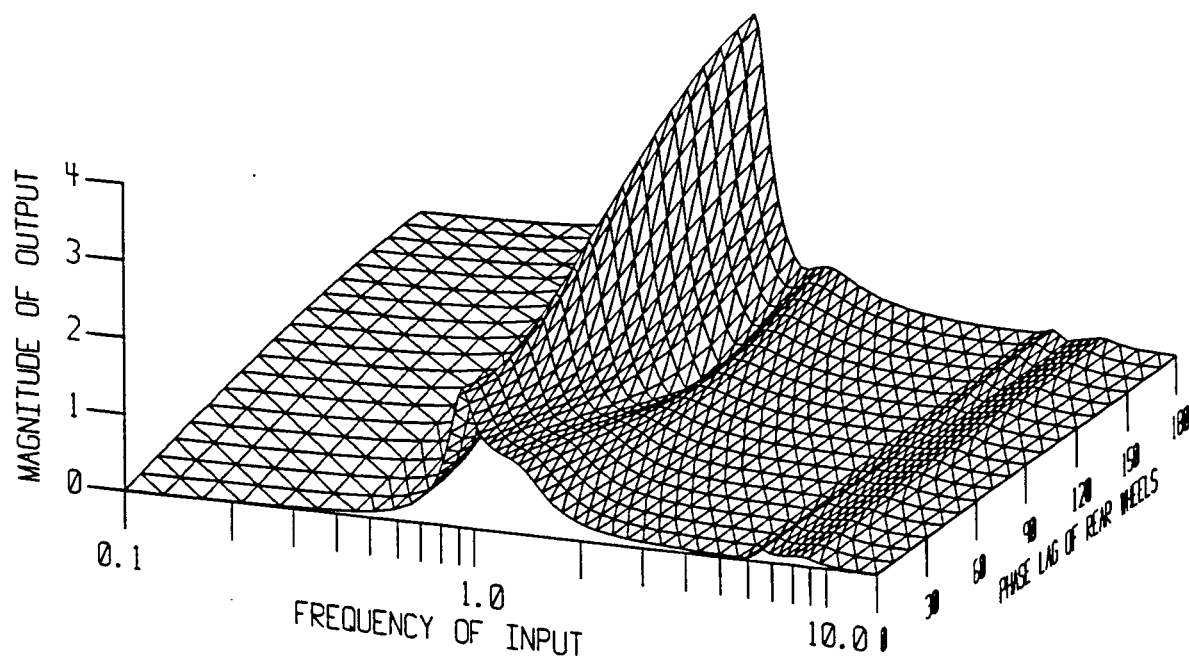


Figure 3.5: Pitch frequency response for varying phase angles between front and rear tires of the passive suspension (vehicle 1)

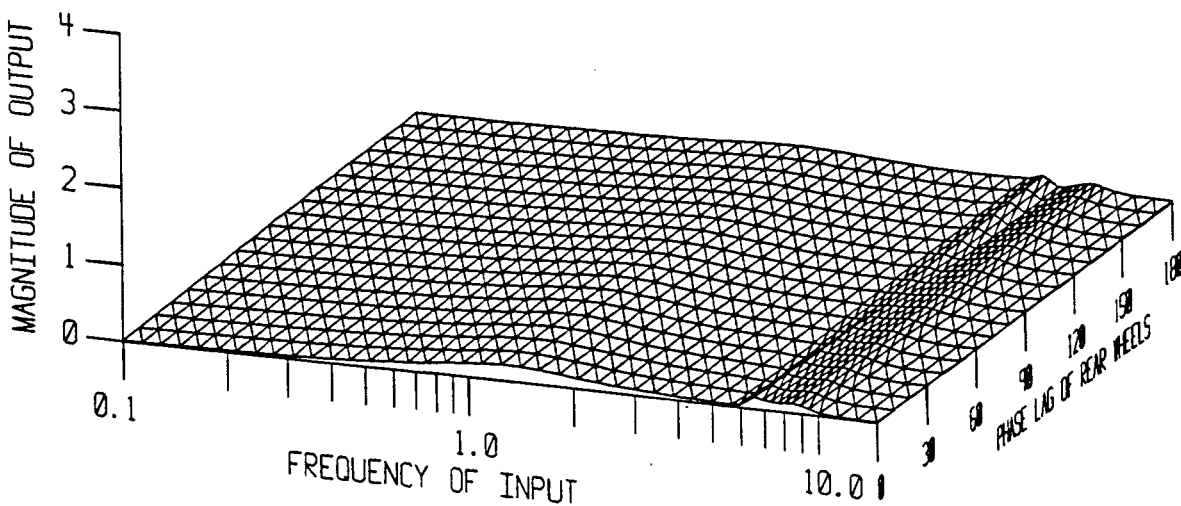


Figure 3.6: Pitch frequency response for varying phase angles between front and rear tires of the active suspension (vehicle 2)

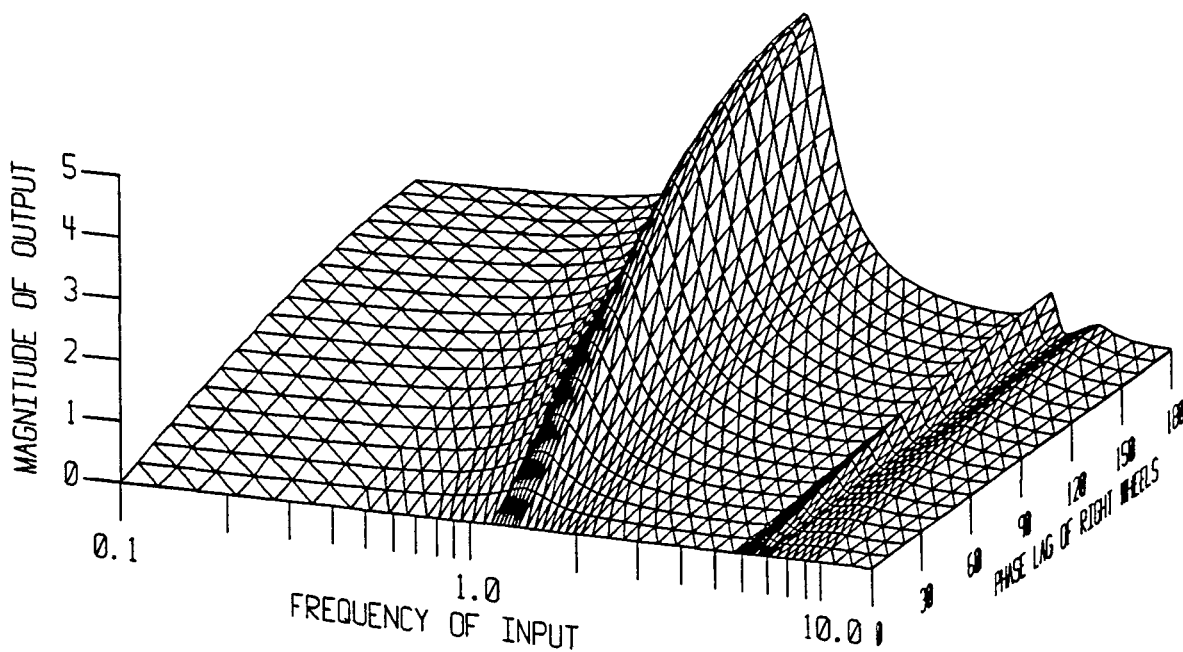


Figure 3.7: Roll frequency response for varying phase angles between left and right tires of the passive suspension (vehicle 1)

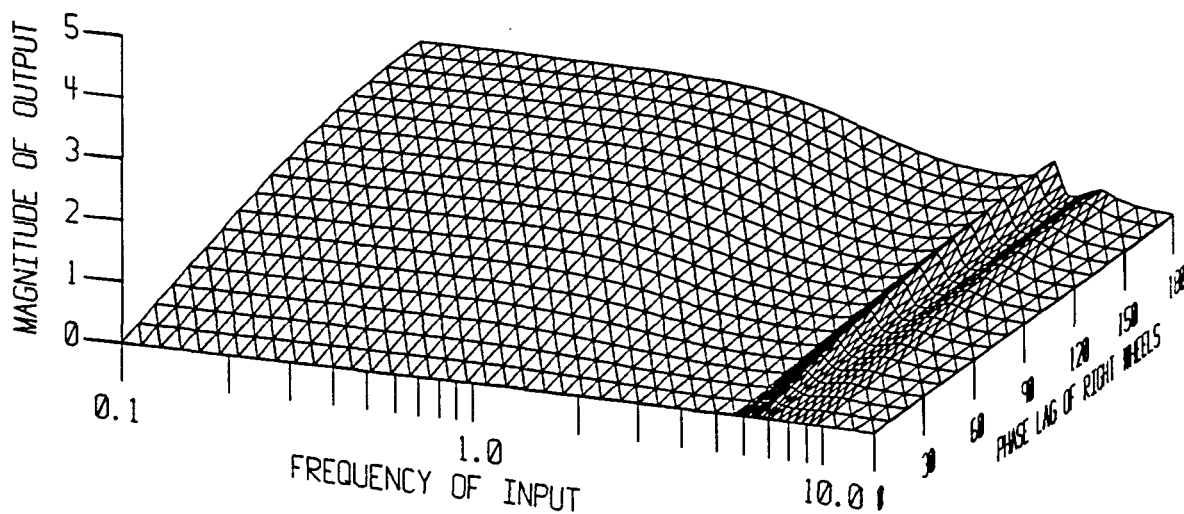


Figure 3.8: Roll frequency response for varying phase angles between left and right tires of the active suspension (vehicle 2)

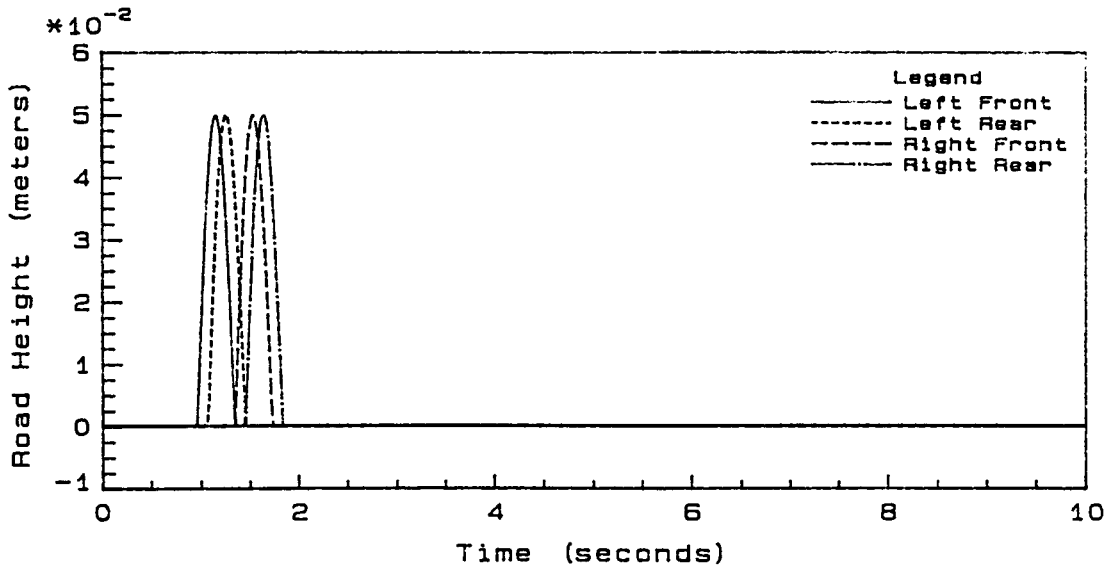


Figure 3.9: Slanted half sine wave road profile

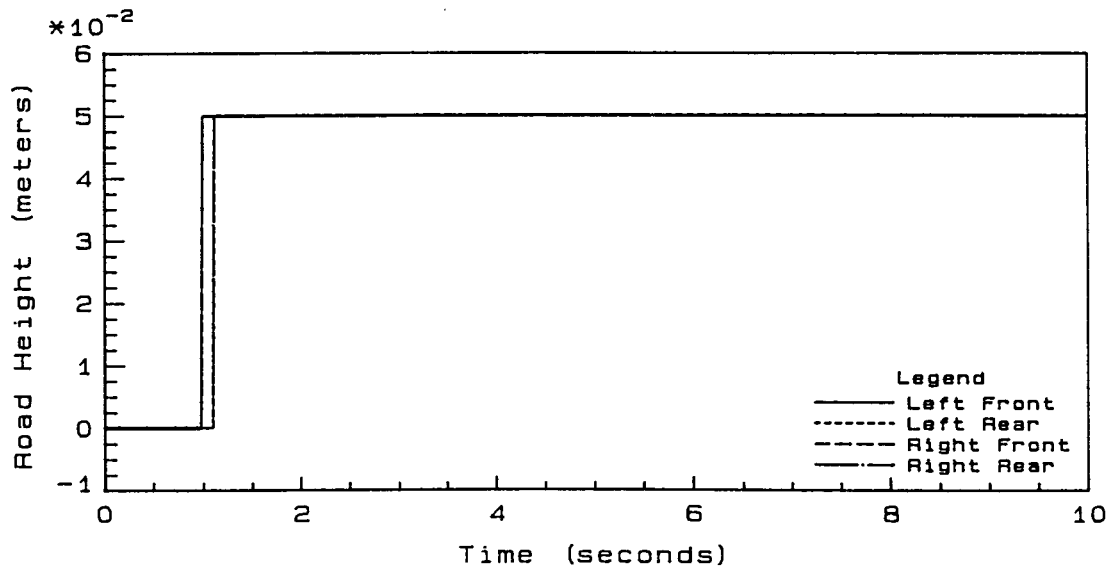


Figure 3.10: Step road profile

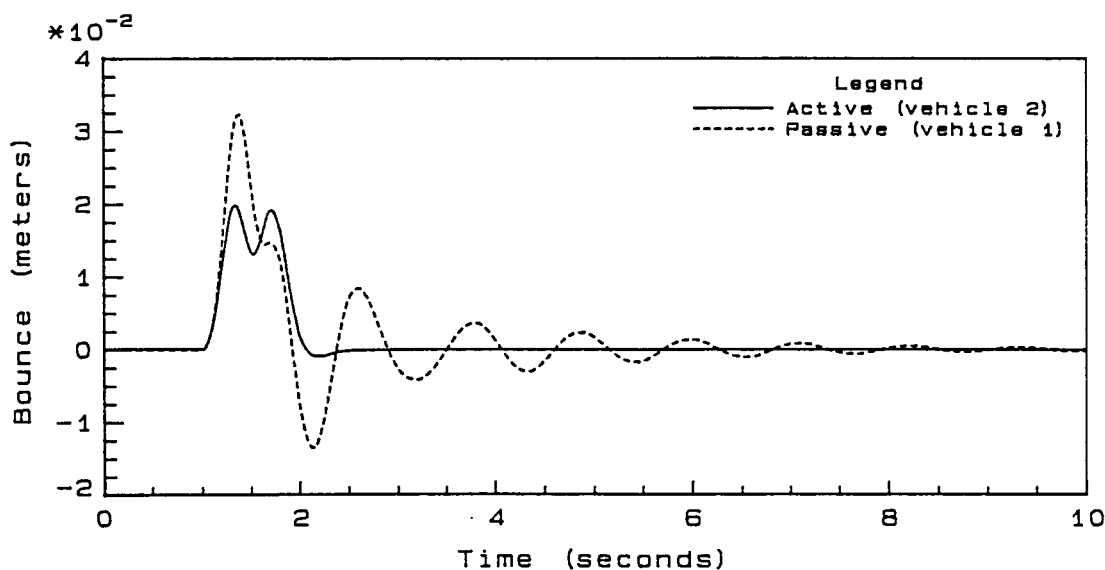


Figure 3.11: Bounce response of the vehicle with an active suspension (vehicle 2) to a slanted bump input compared to that of the passive suspension (vehicle 1)

Bounce, pitch, and roll response to the slanted bump are shown in Figures 3.11, 3.12, and 3.13 respectively for both the active and passive suspensions. Table 3.1 lists the peak force transmitted, and the integrals of the components of the performance function, J , for the slanted bump. Figures 3.14 and 3.15 show the pitch and bounce responses of the vehicle to the step input. Table 3.2 lists the peak force transmitted, and the integrals of the components of the performance function for the step input.

The simulation results show that this particular active suspension gives very good low frequency ride response as compared to the passive suspension. In each graph the peak amplitudes and residual vibrations are greatly reduced. Specifically, for the slanted bump, peak bounce is reduced by 38.7%, peak roll by 63.8%, and peak pitch by 48.1%. Roll response settles out 66.6% faster, pitch 77.8% faster, and

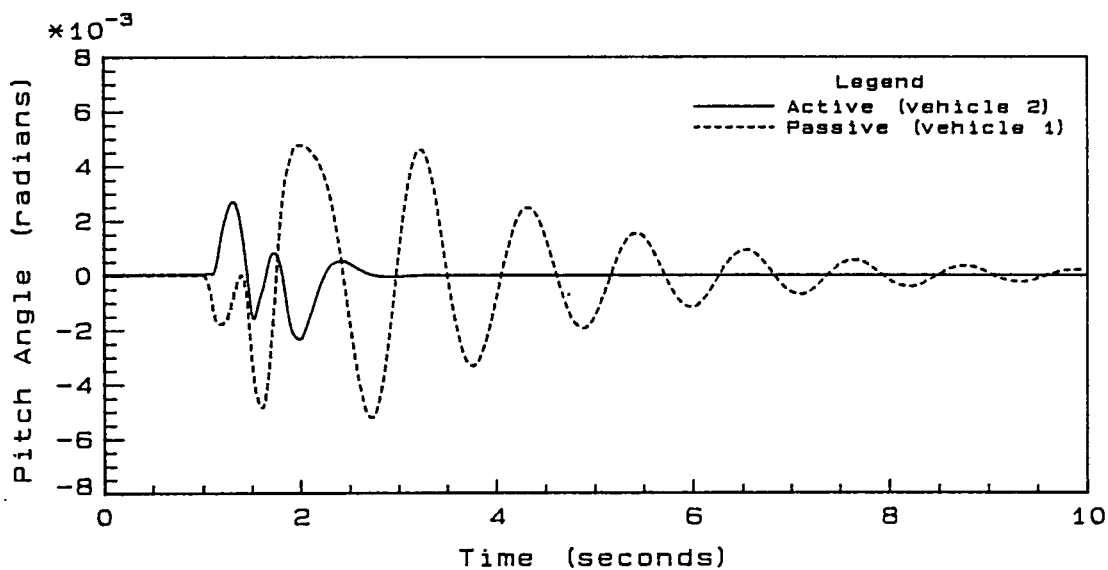


Figure 3.12: Pitch response of the vehicle with an active suspension (vehicle 2) to a slanted bump input compared to that of the passive suspension (vehicle 1)

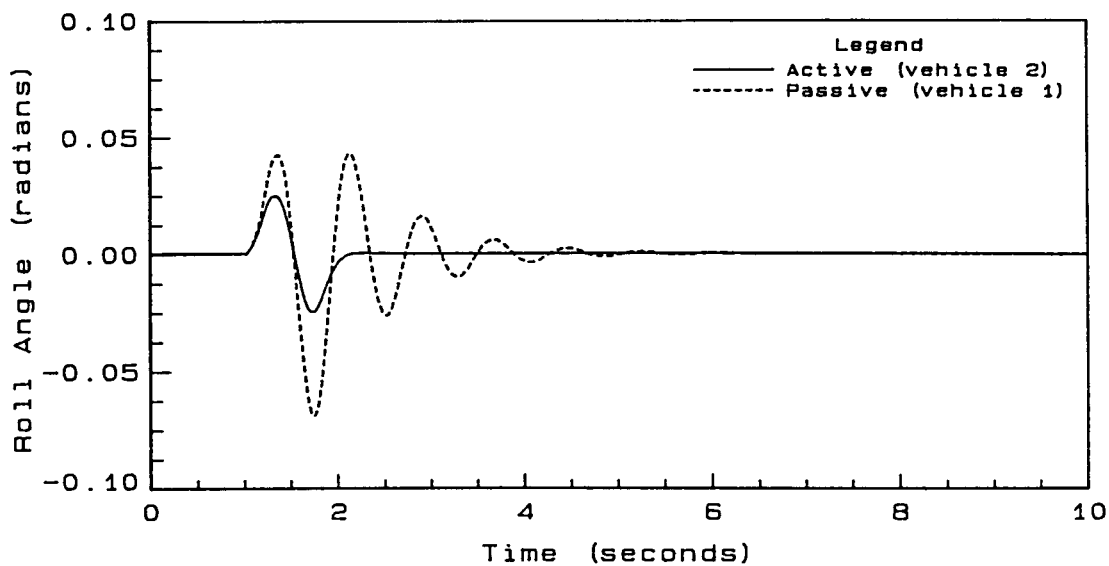


Figure 3.13: Roll response of the vehicle with an active suspension (vehicle 2) to a slanted bump input compared to that of the passive suspension (vehicle 1)

Table 3.1: Response characteristics of the vehicle with an active suspension (vehicle 2) to a slanted bump input compared to that of the passive suspension (vehicle 1)

	vehicle 1	vehicle 2	% Improvement
Peak Force Transmitted (Newtons)	928.98	608.03	34.55
$\int_0^t q_1(\dot{\phi}^2 + \dot{\theta}^2 + \dot{z}^2)dt$.0181	.0037	79.56
$\int_0^t q_2(\dot{\phi}^2 + \dot{\theta}^2 + \dot{z}^2)dt$.9338	.1187	87.3
$\int_0^t q_3(z_1'^2 + z_2'^2 + z_3'^2 + z_4'^2)dt$.0028	.0024	14.29
$\int_0^t (q_4 F_s^2 + q_5 F_{\text{damp}}^2 + q_6 F_{\text{act}}^2)dt$.4752	.2255	52.55

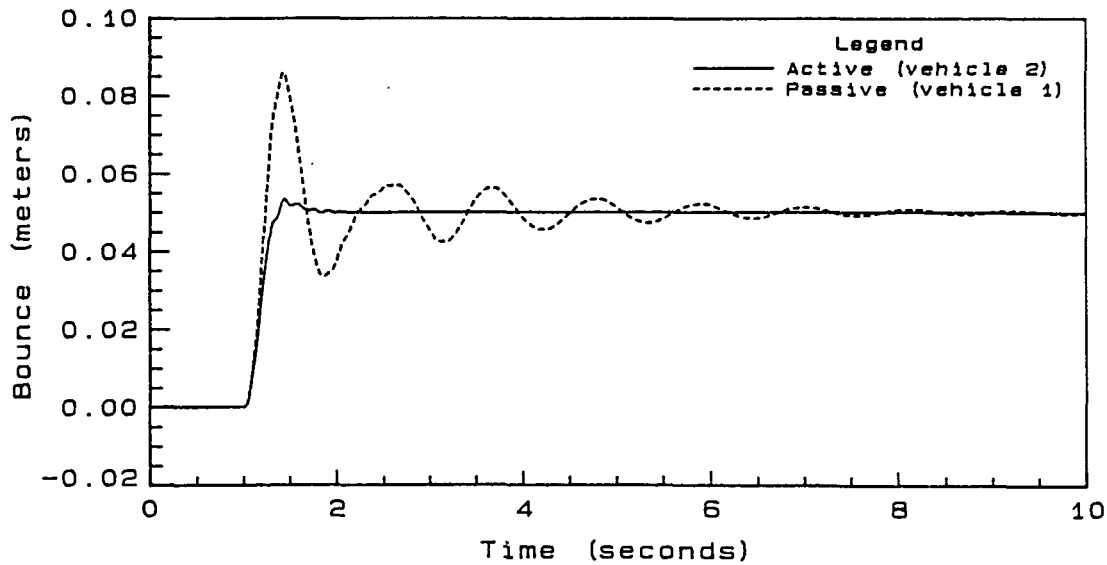


Figure 3.14: Bounce response of the vehicle with an active suspension (vehicle 2) to a step input compared to that of the passive suspension (vehicle 1)

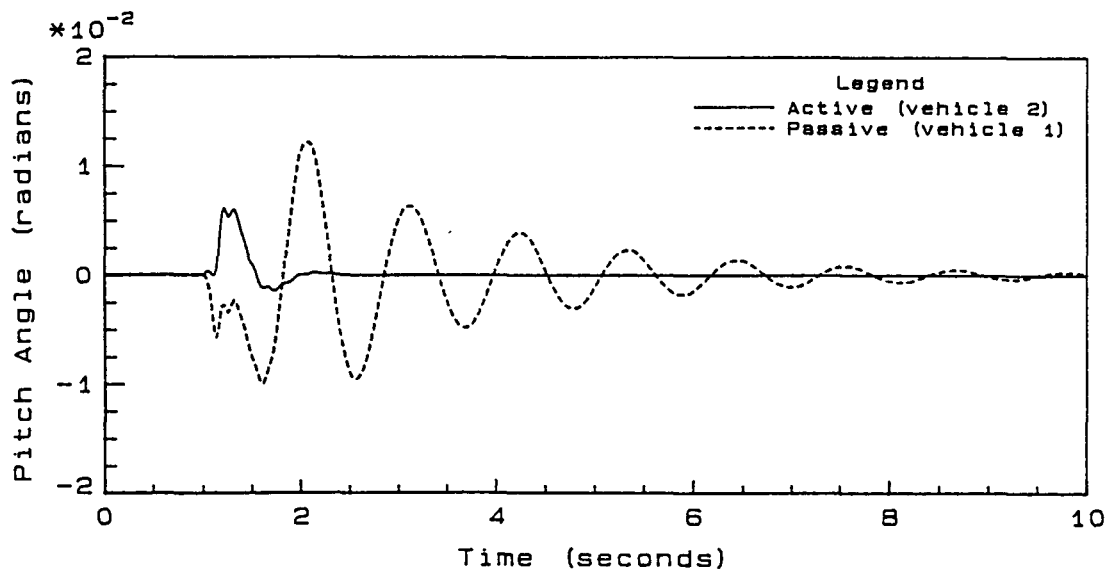


Figure 3.15: Pitch response of the vehicle with an active suspension (vehicle 2) to a step input compared to that of the passive suspension (vehicle 1)

Table 3.2: Response characteristics of the vehicle with an active suspension (vehicle 2) to a step bump input compared to that of the passive suspension (vehicle 1)

	vehicle 1	vehicle 2	% Improvement
Peak Force Transmitted (Newtons)	2222.9	1830.0	17.68
$\int_0^t q_1(\phi'^2 + \theta'^2 + z'^2)dt$.0072	.0021	70.83
$\int_0^t q_2(\dot{\phi}^2 + \dot{\theta}^2 + \dot{z}^2)dt$.2800	.0725	74.11
$\int_0^t q_3(z_1'^2 + z_2'^2 + z_3'^2 + z_4'^2)dt$..0607	.0526	13.34
$\int_0^t (q_4 F_s^2 + q_5 F_{\text{damp}}^2 + q_6 F_{\text{act}}^2)dt$.6724	.5606	16.63

bounce 79.2% faster. For the step response, peak bounce overshoot is reduced by 90.3% while peak pitch is reduced by 49.2%. The settling time for the step response is 90.2% faster for bounce and 85.6% faster for pitch.

The integrals of the components of the performance function show the mean squared of the difference from zero of the different state variable combinations. The first integral in Tables 3.1 and 3.2 shows the improvement in the chassis road tracking. The second integral shows the improvement in chassis velocity remaining close to zero. The third integral gives the improvement in wheel hop. The fourth integral shows the improvement in total force transmitted to the chassis. All indicate that the active suspension gives improved performance compared to the passive suspension.

Large improvements in the response of the vehicle with the active suspension is not surprising in light of the ideal nature of the active system. The model presented in this chapter assumes that all state variables can be measured and that the actuators are ideal. In reality, these types of improvements can not be obtained. The remainder of this thesis will develop more realistic models of active systems. This will include assuming that some variables can not be measured, and therefore are not available for feedback, and introducing some limitations on the actuators. These more realistic systems will then be compared to the passive and ideal active systems to identify how much of the improvements shown in this chapter can actually be realized.

4 LIMITED STATE FEEDBACK

The results of Chapter 3 show that an ideal active suspension is capable of giving both improved vibration isolation and improved road tracking. However, it is assumed that all of the state variables can be measured. Current technology limits the ability to measure such quantities as road height, distance from the road to the sprung mass, tire compression, angles of the chassis with respect to the ground, and the velocities of the above quantities. This chapter will study active suspension systems that do not depend on measurement of all of these variables.

4.1 Road Height Removed From State Vector

One approach to the problem of incomplete measurement is to remove unmeasurable quantities from the state vector. However, since the algebraic Riccati solution requires the entire state vector for feedback, removal of variables from the state vector necessitates a change in the equations of motion. The only variables that could be eliminated in this manner are the road heights at the four tires. With this change in \mathbf{x} , the new state vector is

$$\mathbf{x}^T = \left[\phi' \quad \dot{\phi} \quad \theta' \quad \dot{\theta} \quad z' \quad \dot{z} \quad z'_1 \quad \dot{z}_1 \quad z'_2 \quad \dot{z}_2 \quad z'_3 \quad \dot{z}_3 \quad z'_4 \quad \dot{z}_4 \right] \quad (4.1)$$

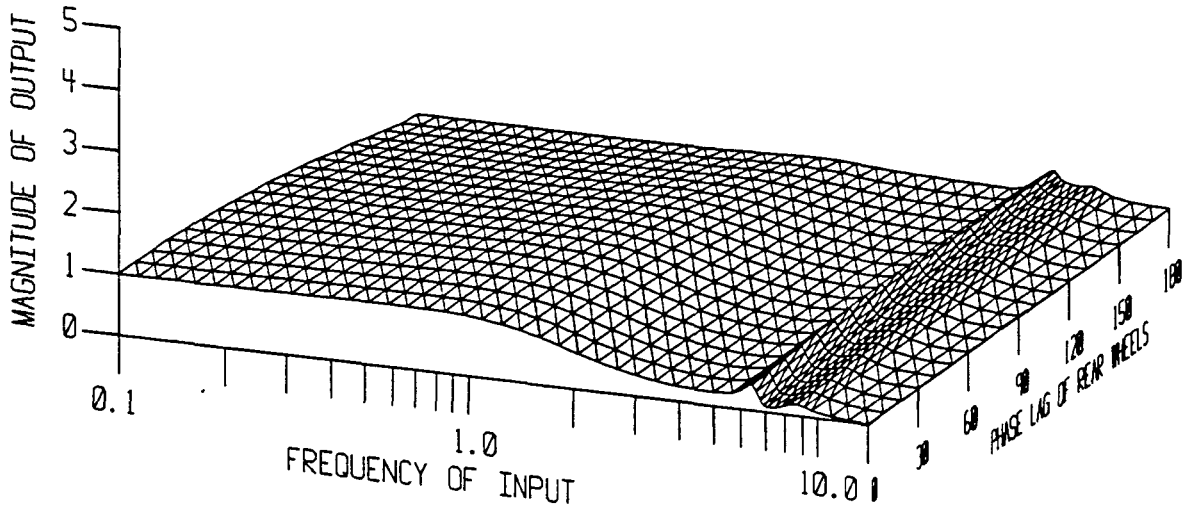


Figure 4.1: Bounce frequency response for varying phase angles between front and rear tires of the active suspension (vehicle 3)

The new equations of motion for the system are

$$\dot{\mathbf{x}}(t) = \mathbf{A}\mathbf{x}(t) + \mathbf{B}\mathbf{u}(t) \quad (4.2)$$

$$\mathbf{u}(t) = -\mathbf{K}_r\mathbf{x}(t) \quad (4.3)$$

The same performance function used in Chapter 3 is used with the new equations of motion to find the feedback gain matrix, \mathbf{K}_r .

The steady state frequency response of this linear system (vehicle 3) is found in a similar manner to that presented in the previous chapter. However, since the input is the actual road height, no transformation is necessary for the frequency response function, $H(j\omega)$. Figures 4.1, 4.2, and 4.3 give the frequency response for this active system.

The frequency responses for this vehicle are virtually the same as for the vehicle with the ideal active suspension (vehicle 2), which indicates that removing

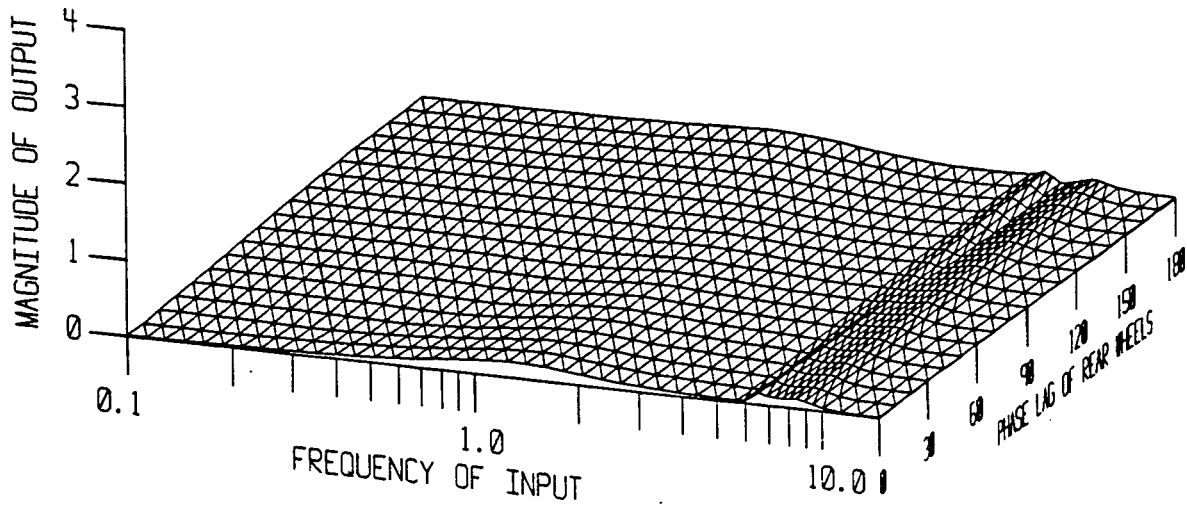


Figure 4.2: Pitch frequency response for varying phase angles between front and rear tires of the active suspension (vehicle 3)

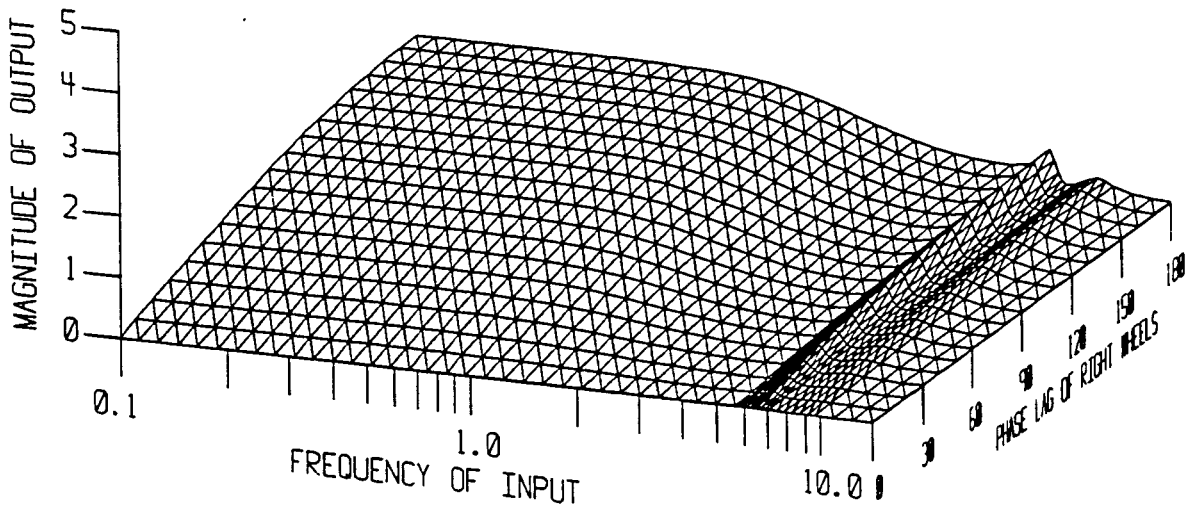


Figure 4.3: Roll frequency response for varying phase angles between front and rear tires of the active suspension (vehicle 3)

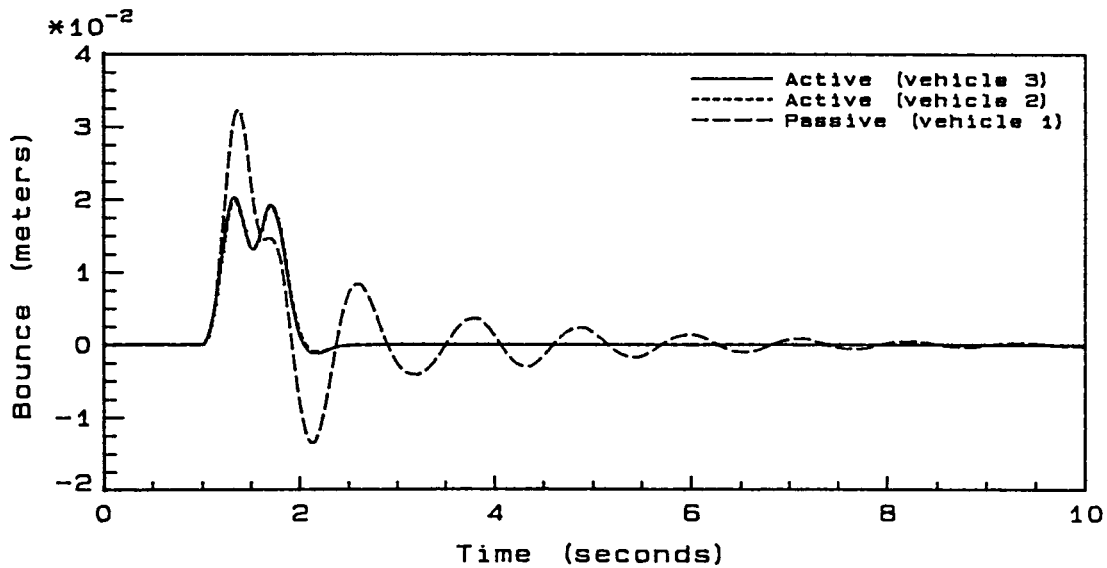


Figure 4.4: Bounce response of the vehicle with road height removed from the state variables (vehicle 3) to a slanted bump input compared to that of the active (vehicle 2) and passive (vehicle 1) suspensions

road height feedback does not significantly affect the performance of the active suspension.

These new equations of motion are integrated with the road profile inputs shown in Figures 3.9 and 3.10. The bounce, pitch and roll responses of this suspension are compared graphically to those of the fully active and passive suspensions in Figures 4.4, 4.5 and 4.6 for the slanted bump. The bounce and pitch responses were compared for the step in Figures 4.7 and 4.8. Table 4.1 lists peak force transmitted, and the integral of the performance function, J , for the slanted bump input. Table 4.2 lists the values for the step input.

The simulation results show that this particular active suspension gives about the same improvement in overall ride response as the fully active suspension. In each graph the peak amplitudes and residual vibrations are greatly reduced. Specifically,

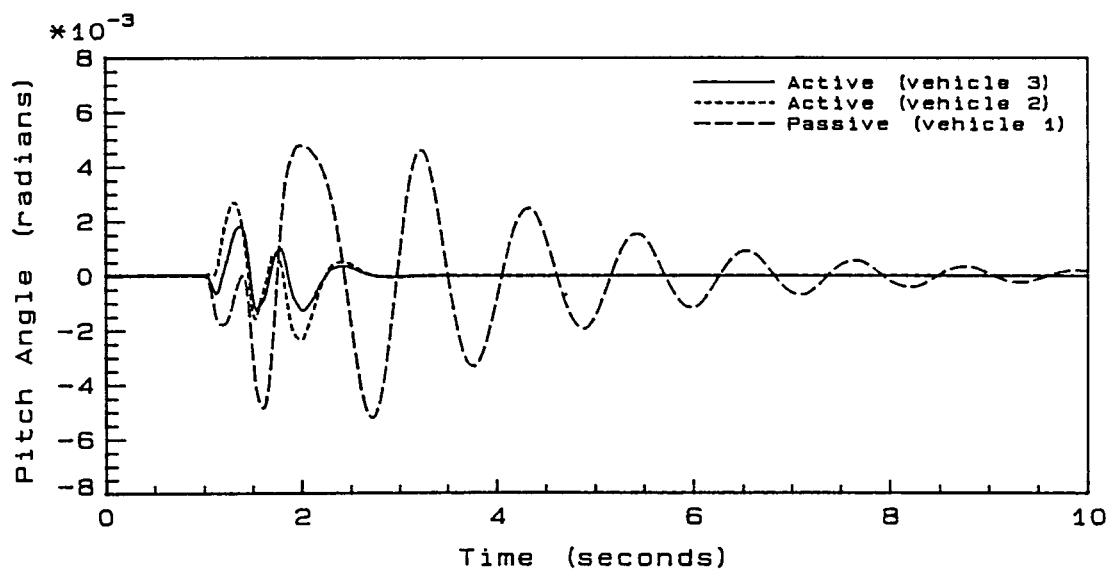


Figure 4.5: Pitch response of the vehicle with road height removed from the state variables (vehicle 3) to a slanted bump input compared to that of the active (vehicle 2) and passive (vehicle 1) suspensions

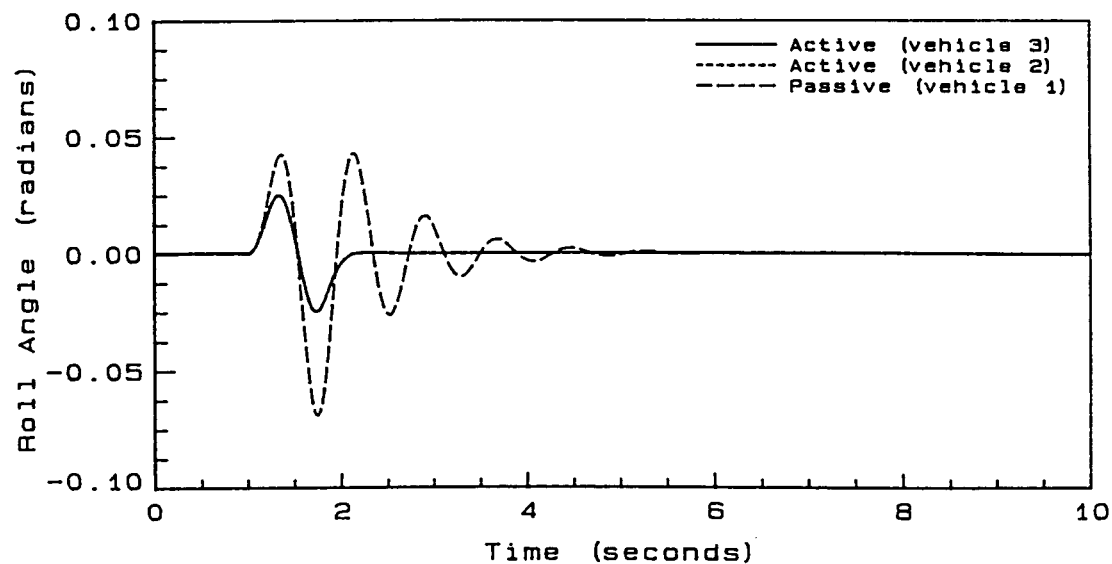


Figure 4.6: Roll response of the vehicle with road height removed from the state variables (vehicle 3) to a slanted bump input compared to that of the active (vehicle 2) and passive (vehicle 1) suspensions

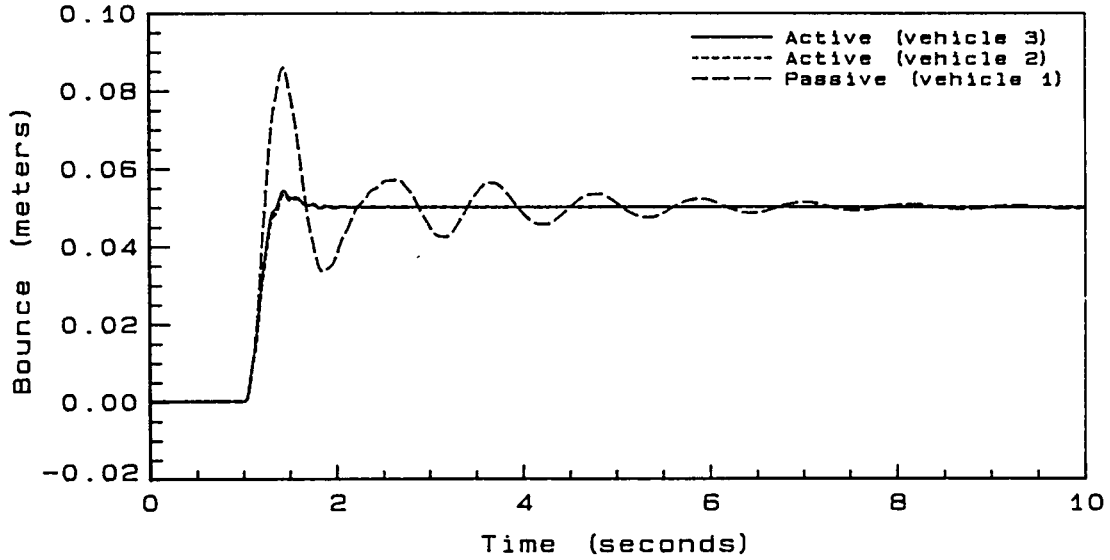


Figure 4.7: Bounce response of the vehicle with road height removed from the state variables (vehicle 3) to a step bump compared to that of the active (vehicle 2) and passive (vehicle 1) suspensions

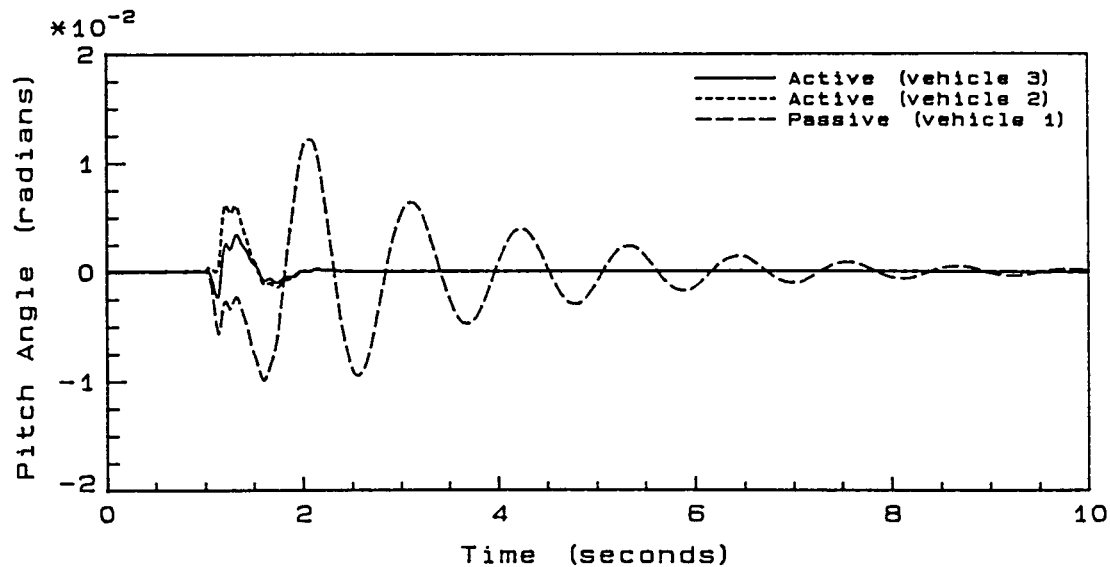


Figure 4.8: Pitch response of the vehicle with road height removed from the state variables (vehicle 3) to a step bump input compared to that of the active (vehicle 2) and passive (vehicle 1) suspensions

Table 4.1: Response characteristics of the vehicle with road height removed from the state vector (vehicle 3) to a slanted bump input compared to that of the active (vehicle 2) and passive (vehicle 1) suspensions

	vehicle 1	vehicle 3	% Improvement	
			vehicle 2	vehicle 3
Peak Force Transmitted (N)	928.98	645.17	34.55	31.00
$\int_0^t q_1(\dot{\phi}^2 + \dot{\theta}^2 + \dot{z}^2)dt$.0181	.0039	79.56	78.45
$\int_0^t q_2(\dot{\phi}^2 + \dot{\theta}^2 + \dot{z}^2)dt$.9338	.1192	87.30	87.23
$\int_0^t q_3(z_1'^2 + z_2'^2 + z_3'^2 + z_4'^2)dt$.0028	.0023	14.29	17.86
$\int_0^t (q_4 F_s^2 + q_5 F_{\text{damp}}^2 + q_6 F_{\text{act}}^2)dt$.4752	.2172	52.55	52.55

Table 4.2: Response characteristics of the vehicle with road height removed from the state vector (vehicle 3) to a step input compared to that of the active (vehicle 2) and passive (vehicle 1) suspensions

	vehicle 1	vehicle 3	% Improvement	
			vehicle 2	vehicle 3
Peak Force Transmitted (N)	2222.9	1952.2	17.68	12.18
$\int_0^t q_1(\dot{\phi}^2 + \dot{\theta}^2 + \dot{z}^2)dt$.0072	.0024	70.83	66.67
$\int_0^t q_2(\dot{\phi}^2 + \dot{\theta}^2 + \dot{z}^2)dt$.2800	.0740	74.11	73.57
$\int_0^t q_3(z_1'^2 + z_2'^2 + z_3'^2 + z_4'^2)dt$.0607	.0501	13.34	17.46
$\int_0^t (q_4 F_s^2 + q_5 F_{\text{damp}}^2 + q_6 F_{\text{act}}^2)dt$.6724	.5273	16.63	21.53

for the slanted bump, peak bounce is reduced by 37.2%, peak roll by 63.8%, and peak pitch by 65.4%. Roll response settles out 66.7% faster, pitch more than 77.8% faster, and bounce 80.0% faster. For the step response, peak bounce is reduced by 36.7% while peak pitch is reduced by 72.1%. The settling time for the step response is 90.2% faster for bounce and more than 84.4% faster for pitch.

Tables 4.1 and 4.2 show that the suspension modeled without using road height feedback gives very similar results as compared to the fully active suspension with the exception of peak force transmitted. Even this higher value of peak force has a significant improvement over the passive suspension. Therefore, it can be concluded that the performance of the suspension with road height removed from the state vector is improved over that of a passive system and is near that of the fully active system.

4.2 Optimal Reconstruction of State Variables

Another method of implementing the optimal control system described in Chapter 3 in a system with an incomplete state vector measurement is to reconstruct the state variables from the observed variables. An optimal observer is defined to be a system that reconstructs the state variables from a reduced set of observed variables with the minimum error from the actual state variables. The optimal observer formulation used in this thesis is from Kwakernaak and Sivan [14] and is as follows.

The regulator system shown in Figure 3.2 with disturbance input, $w(t)$, removed has system equations,

$$\dot{x}(t) = Ax(t) + Bu(t) \quad (4.4)$$

and the optimal linear regulator control law,

$$\mathbf{u}(t) = -K_r \mathbf{x}(t) \quad (4.5)$$

Assuming the observed variables for this system are linear combinations of the actual state variables,

$$\mathbf{y}(t) = C\mathbf{x}(t), \quad (4.6)$$

where $\mathbf{x}(t)$ is the n dimension vector of state variables and $\mathbf{y}(t)$ is the l dimension vector of measured variables ($l < n$). Knowing $\mathbf{y}(t)$, it is thus desirable to reconstruct the state variables such that if $\hat{\mathbf{x}}(t_0) = \mathbf{x}(t_0)$, then

$$\hat{\mathbf{x}}(t) = \mathbf{x}(t), \quad (4.7)$$

for all $t > t_0$ where $\hat{\mathbf{x}}(t)$ is the n dimension vector of reconstructed state variables.

In order to find an optimal observer, its form is assumed to be a function of past observations. The derivatives of the reconstructed state variables are a linear combination of the reconstructed state variables, observed variables and control input variables.

$$\dot{\hat{\mathbf{x}}}(t) = F\hat{\mathbf{x}}(t) + G\mathbf{y}(t) + H\mathbf{u}(t) \quad (4.8)$$

By subtracting equation 4.8 from 4.4 and including 4.6 the following differential equation is obtained for the error in the reconstructed state.

$$\dot{\mathbf{x}}(t) - \dot{\hat{\mathbf{x}}}(t) = A\mathbf{x}(t) + B\mathbf{u}(t) - F\hat{\mathbf{x}}(t) - GC\mathbf{x}(t) - H\mathbf{u}(t) \quad (4.9)$$

Equation 4.9 can be reduced to

$$\dot{\mathbf{x}}(t) - \dot{\hat{\mathbf{x}}}(t) = (A - GC)\mathbf{x}(t) - F\hat{\mathbf{x}}(t) - B\mathbf{u}(t) - H\mathbf{u}(t) \quad (4.10)$$

Since it is desired that equation 4.7 be satisfied, then

$$\dot{\mathbf{x}}(t) = \dot{\hat{\mathbf{x}}}(t) \quad (4.11)$$

for all $t > t_0$ must also be satisfied. Substituting equation 4.11 and 4.7 in equation 4.10 yields the following equation:

$$0 = [(A - GC) - F]\mathbf{x}(t) + (B - H)\mathbf{u}(t) \quad (4.12)$$

Assuming that $\mathbf{x}(t)$ is independent of $\mathbf{u}(t)$, and solving equation 4.12 for F and H gives

$$F = A - GC \quad (4.13)$$

$$H = B \quad (4.14)$$

Substituting these into equation 4.8 yields

$$\dot{\hat{\mathbf{x}}}(t) = (A - GC)\hat{\mathbf{x}}(t) + G\mathbf{y}(t) + B\mathbf{u}(t) \quad (4.15)$$

To understand this expression better, it can be written as

$$\dot{\hat{\mathbf{x}}}(t) = A\hat{\mathbf{x}}(t) + G(\mathbf{y}(t) - \hat{\mathbf{y}}(t)) + B\mathbf{u}(t) \quad (4.16)$$

G can then be renamed K_e which is the feedback gain applied to the error between the observed variables, $\mathbf{y}(t)$, and the reconstructed observed variables, $\hat{\mathbf{y}}(t)$. Thus the system equations are

$$\dot{\mathbf{x}}(t) = A\mathbf{x}(t) + B\mathbf{u}(t) \quad (4.17)$$

$$\mathbf{u}(t) = -K_r\hat{\mathbf{x}}(t) \quad (4.18)$$

$$\dot{\hat{\mathbf{x}}}(t) = A\hat{\mathbf{x}}(t) + K_e(\mathbf{y}(t) - \hat{\mathbf{y}}(t)) + B\mathbf{u}(t) \quad (4.19)$$

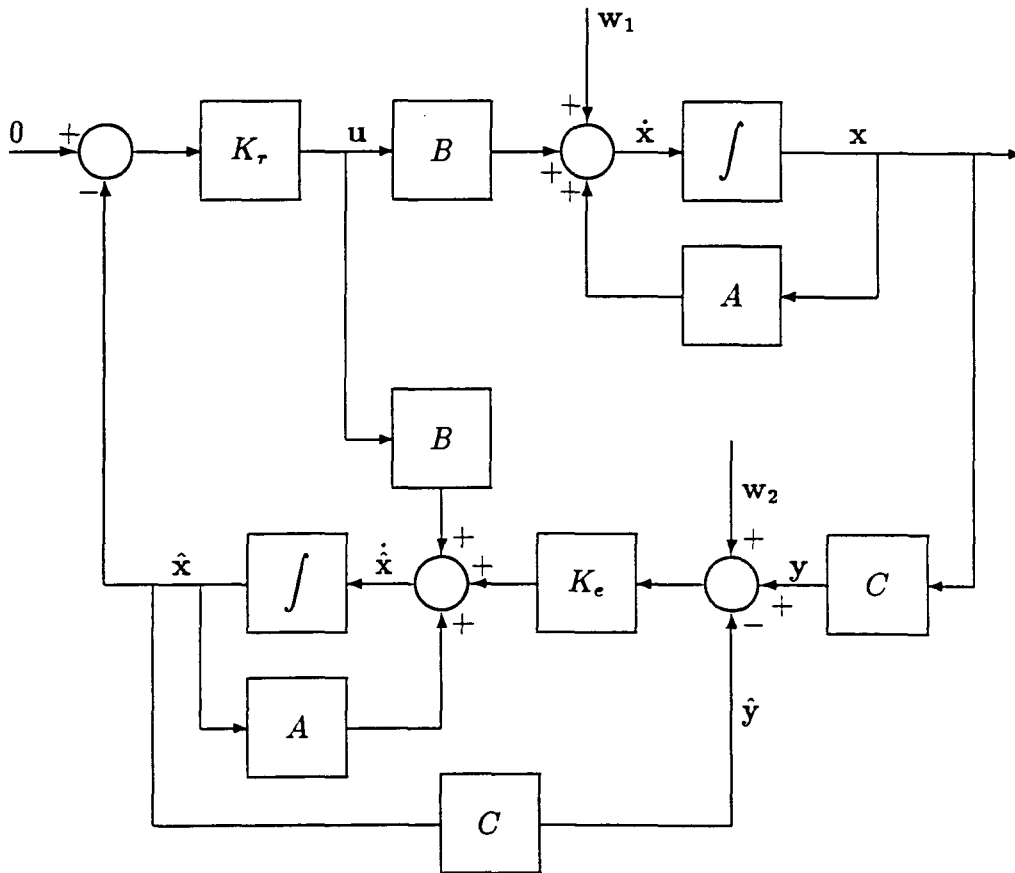


Figure 4.9: Block diagram of optimal observer system

and the system block diagram is shown in Figure 4.9. Equations 4.17, 4.18 and 4.19 can be simplified to the matrix form

$$\begin{pmatrix} \dot{\mathbf{x}}(t) \\ \dot{\hat{\mathbf{x}}}(t) \end{pmatrix} = \begin{pmatrix} A & -BK_r \\ K_e C & A - K_e C - BK_r \end{pmatrix} \begin{pmatrix} \mathbf{x}(t) \\ \hat{\mathbf{x}}(t) \end{pmatrix} \quad (4.20)$$

Finding K_e to optimize the observer requires a stochastic approach. Using the regulator equations and introducing the state excitation noise vector, $\mathbf{w}_1(t)$, and the measurement noise vector, $\mathbf{w}_2(t)$, results in the following equations:

$$\dot{\mathbf{x}}(t) = A\mathbf{x}(t) + B\mathbf{u}(t) + \mathbf{w}_1(t) \quad (4.21)$$

$$\mathbf{y}(t) = C\mathbf{x}(t) + \mathbf{w}_2(t) \quad (4.22)$$

The vector, $\left[\mathbf{w}_1^T(t) \quad \mathbf{w}_2^T(t) \right]^T$ is assumed to be a white noise process with intensities

$$V(t) = \begin{bmatrix} V_{11}(t) & V_{12}(t) \\ V_{21}(t) & V_{22}(t) \end{bmatrix} \quad (4.23)$$

such that

$$V(t_1)\delta(t_1 - t_2) = E \left\{ \begin{bmatrix} \mathbf{w}_1(t_1) \\ \mathbf{w}_2(t_1) \end{bmatrix} \begin{bmatrix} \mathbf{w}_1^T(t_2) & \mathbf{w}_2^T(t_2) \end{bmatrix}^T \right\} \quad (4.24)$$

where E is the expectation operator and $\delta(t_1 - t_2)$ is the delta function of $t_1 - t_2$. If $\mathbf{w}_1(t)$ and $\mathbf{w}_2(t)$ are uncorrelated then $V_{12}(t) = V_{21}(t) = 0$. Furthermore, if intensity is assumed constant for all $t > t_0$ then the intensity matrix becomes

$$V = \begin{bmatrix} V_{11} & 0 \\ 0 & V_{22} \end{bmatrix} \quad (4.25)$$

Now, the problem of finding the optimum K_e becomes minimizing the mean square reconstruction error,

$$E\{\mathbf{e}^T(t)\mathbf{e}(t)\}, \quad (4.26)$$

where

$$\mathbf{e}(t) = \mathbf{x}(t) - \hat{\mathbf{x}}(t) \quad (4.27)$$

The Kalman-Bucy filter [14] minimizes the mean squared reconstruction error and is used in this thesis. This solution to the optimal observer problem is obtained by choosing for the gain matrix

$$K_e = PCV_{22}^{-1} \quad (4.28)$$

where P is the solution to the algebraic Riccati equation

$$0 = AP + PA^T + V_{11} - PC^T V_{22}^{-1} CP. \quad (4.29)$$

The equations of motion for the system with the optimal observer circuit and input noise, $\mathbf{w}_1(t)$, and measurement noise, $\mathbf{w}_2(t)$, are

$$\dot{\mathbf{x}}(t) = A\mathbf{x}(t) + B\mathbf{u}(t) + \mathbf{w}_1(t) \quad (4.30)$$

$$\mathbf{u}(t) = -K_r \hat{\mathbf{x}}(t) \quad (4.31)$$

$$\mathbf{y}(t) = C\mathbf{x}(t) + \mathbf{w}_2(t) \quad (4.32)$$

$$\dot{\hat{\mathbf{x}}}(t) = (A - K_e C)\hat{\mathbf{x}}(t) + K_e \mathbf{y}(t) + B\mathbf{u}(t) \quad (4.33)$$

For the active suspension application, the observed variables are defined as the suspension deflections and their velocities. These were chosen because they can be

practically measured.

$$\mathbf{y} = \begin{bmatrix} z'_a - z'_1 \\ \dot{z}'_a - \dot{z}'_1 \\ z'_b - z'_2 \\ \dot{z}'_b - \dot{z}'_2 \\ z'_c - z'_3 \\ \dot{z}'_c - \dot{z}'_3 \\ z'_d - z'_4 \\ \dot{z}'_d - \dot{z}'_4 \end{bmatrix} \quad (4.34)$$

If the components of $\mathbf{w}_1(t)$ and $\mathbf{w}_2(t)$ are uncorrelated, the intensity matrix is diagonal with components being the mean squared values of each component in $\mathbf{w}_1(t)$ and $\mathbf{w}_2(t)$. Intensities are chosen as the mean squared acceleration imparted in the unsprung mass from a mean squared value of the road height, \bar{z}_r^2 . Thus,

$$V_{11} = k_t^2 \bar{z}_r^2 \times \text{diag} \left[0 \ 0 \ 0 \ 0 \ 0 \ 0 \ 0 \ 0 \ 1/M_1^2 \ 0 \ 1/M_2^2 \ 0 \ 1/M_3^2 \ 0 \ 1/M_4^2 \right] \quad (4.35)$$

The noise in each measurement is assumed to have the same mean squared value.

$$V_{22} = \bar{w}_2^2 I \quad (4.36)$$

Increasing the components of V_{11} has the effect of increasing the gains and the eigenvalues of the estimator system. Decreasing V_{22} has the same effect. This is desirable since the eigenvalues of the observer should be larger than those of the regulator so that the reconstructed state vector is corrected faster than the system is changing. However, the larger eigenvalues also create a need for a smaller integration step size which may not be possible in an actual on board microcomputer. The

values of $\bar{z}_r^2 = 6.375(10)^{-7}$ and $\bar{w}_2^2 = 1(10)^{-6}$ give a fairly good compromise between reconstructability and step size of the integration. The actual step size needed in the simulation is .002 seconds using a fourth order Kutta-Merson integration algorithm.

The system equation used to find the frequency response matrix for the optimal observer is

$$\begin{pmatrix} \dot{\mathbf{x}}(t) \\ \dot{\hat{\mathbf{x}}}(t) \end{pmatrix} = \begin{pmatrix} A & -\tilde{B}_1 K_r \\ K_e C & A - K_e C - B K_r \end{pmatrix} \begin{pmatrix} \mathbf{x}(t) \\ \hat{\mathbf{x}}(t) \end{pmatrix} + \begin{pmatrix} \tilde{B}_2 \\ K_e C D_2 \end{pmatrix} \mathbf{w}(t) \quad (4.37)$$

where D_2 is the first 14 rows and last 4 columns of D .

Figures 4.10, 4.11 and 4.12 give the frequency response for the active system. These plots show an increase in response magnitude at the natural frequencies for bounce, pitch, and roll when compared to the ideal active suspension for all three modes. However, the magnitudes at these frequencies are still much reduced when compared with the passive suspension's results.

Using the same feedback gain matrix, K_r , and the optimal observer, the equations of motion are integrated with the slanted bump and step road profile inputs shown in Figures 3.9 and 3.10. The bounce, pitch and roll responses of this suspension are compared to those of the active and passive suspensions in Figures 4.13, 4.14 and 4.15 for the slanted bump. The bounce and pitch responses are compared for the step in Figures 4.16 and 4.17. Table 4.3 lists peak force transmitted, and the integrals of the components of the performance function, J , for the slanted bump input and Table 4.4 lists the values for the step input.

The simulation results show that this particular active suspension with an optimal observer gives good low frequency ride response as compared to the passive suspension. However, the performance is less than that of the fully active suspension

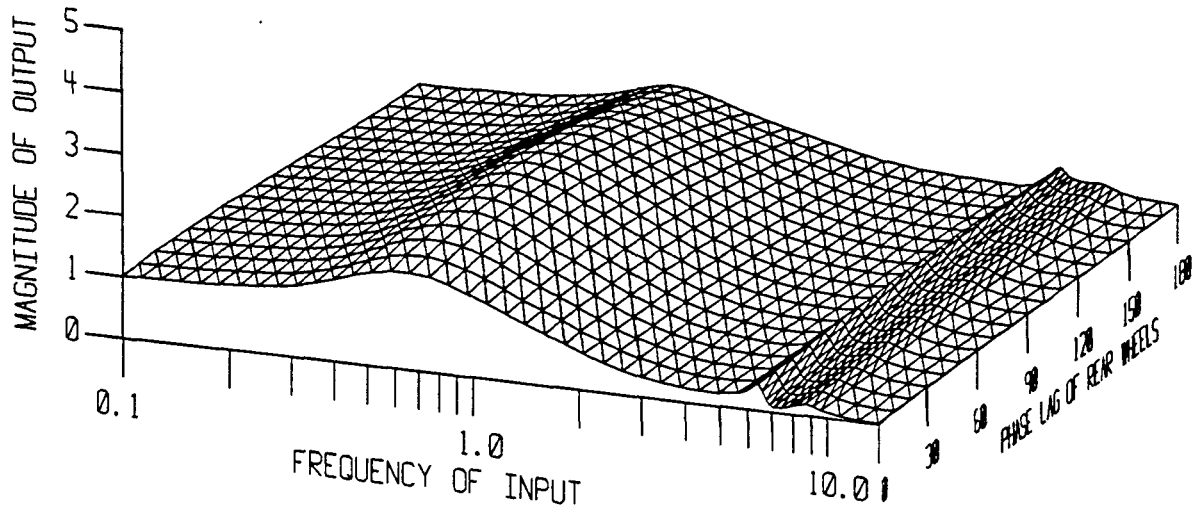


Figure 4.10: Bounce frequency response for varying phase angles between front and rear tires of the optimal observer suspension (vehicle 4)

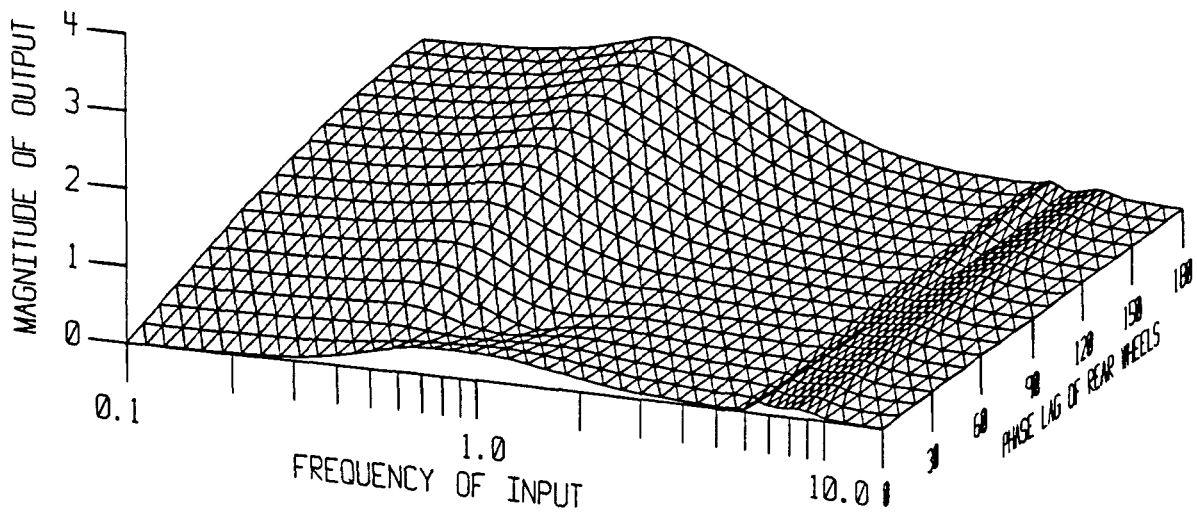


Figure 4.11: Pitch frequency response for varying phase angles between front and rear tires of the optimal observer suspension (vehicle 4)

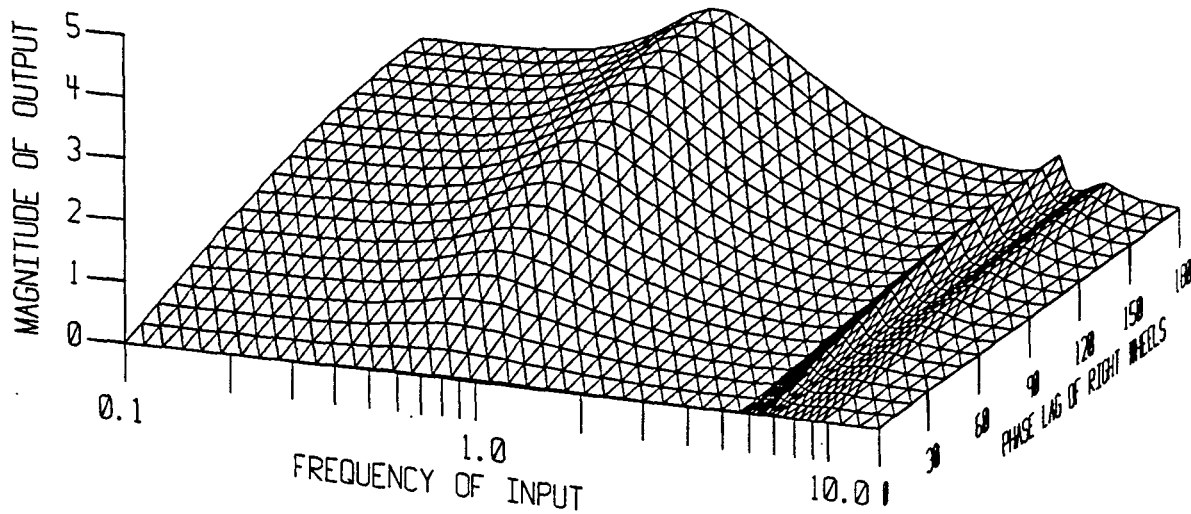


Figure 4.12: Roll frequency response for varying phase angles between front and rear tires of the optimal observer suspension (vehicle 4)

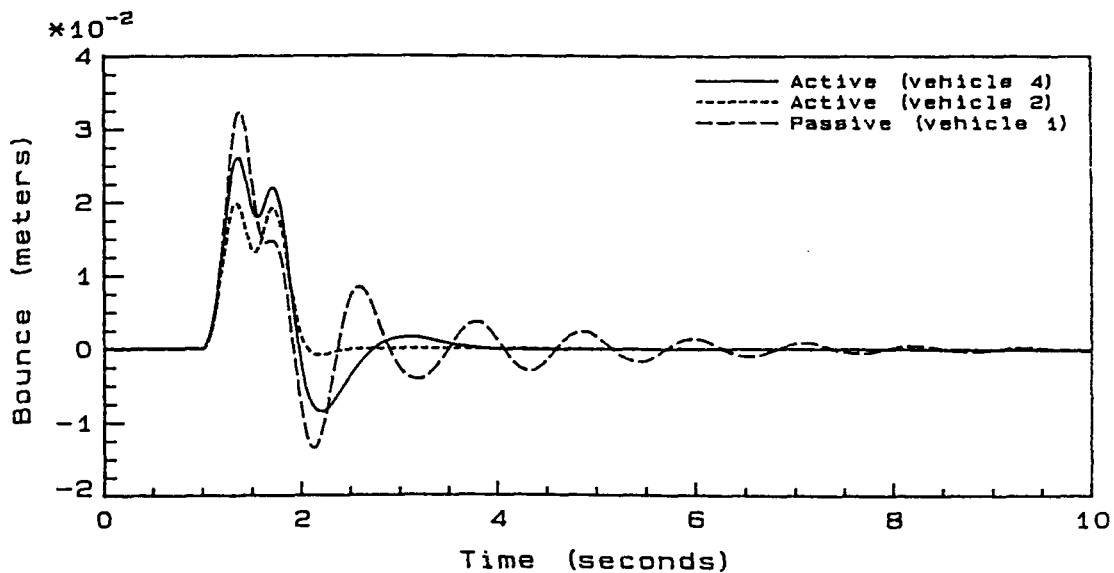


Figure 4.13: Bounce response of the vehicle with an optimal observer (vehicle 4) to a slanted bump input compared to that of the active (vehicle 2) and passive (vehicle 1) suspensions

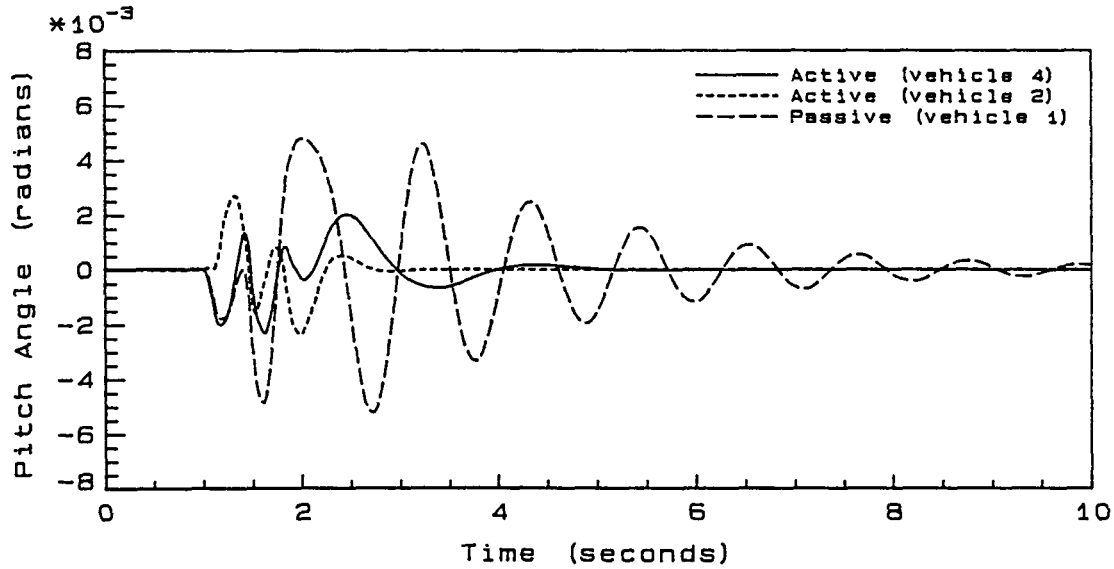


Figure 4.14: Pitch response of the vehicle with an optimal observer (vehicle 4) to a slanted bump input compared to that of the active (vehicle 2) and passive (vehicle 1) suspensions

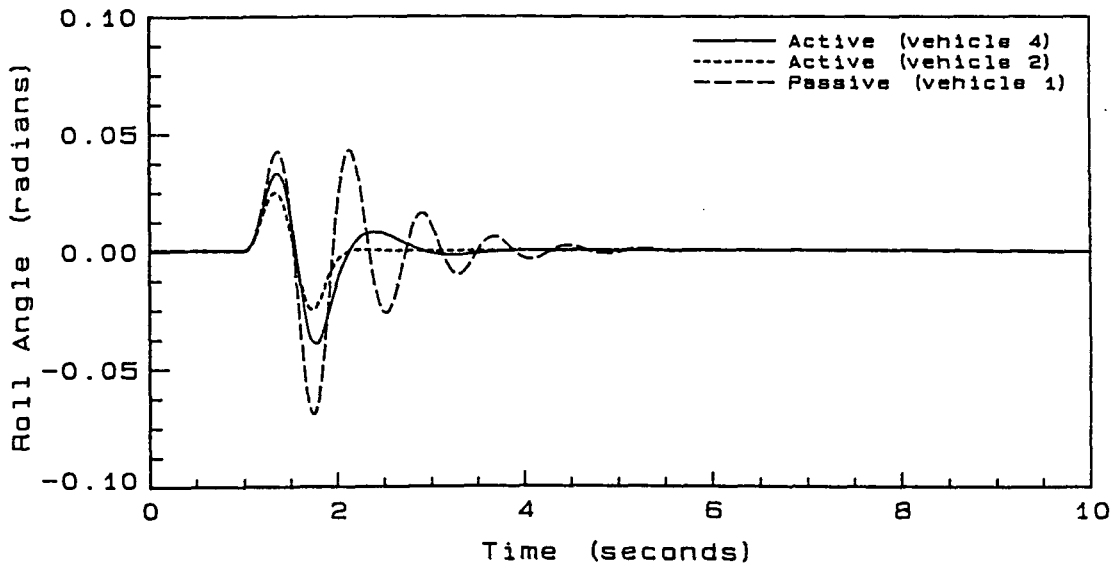


Figure 4.15: Roll response of the vehicle with an optimal observer (vehicle 4) to a slanted bump input compared to that of the active (vehicle 2) and passive (vehicle 1) suspensions

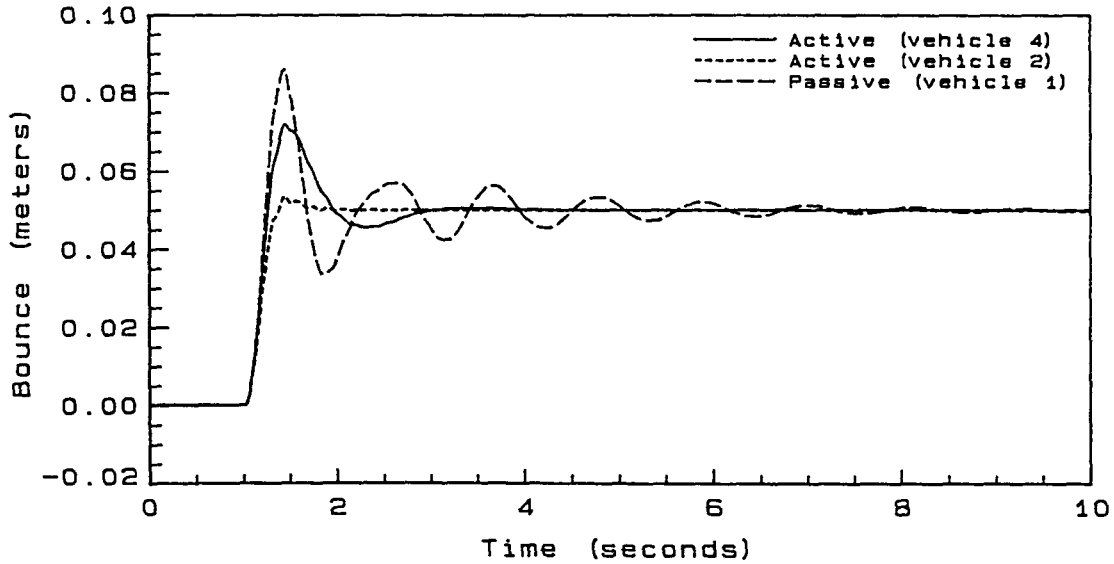


Figure 4.16: Bounce response of the vehicle with an optimal observer (vehicle 4) to a step input compared to that of the active (vehicle 2) and passive (vehicle 1) suspensions

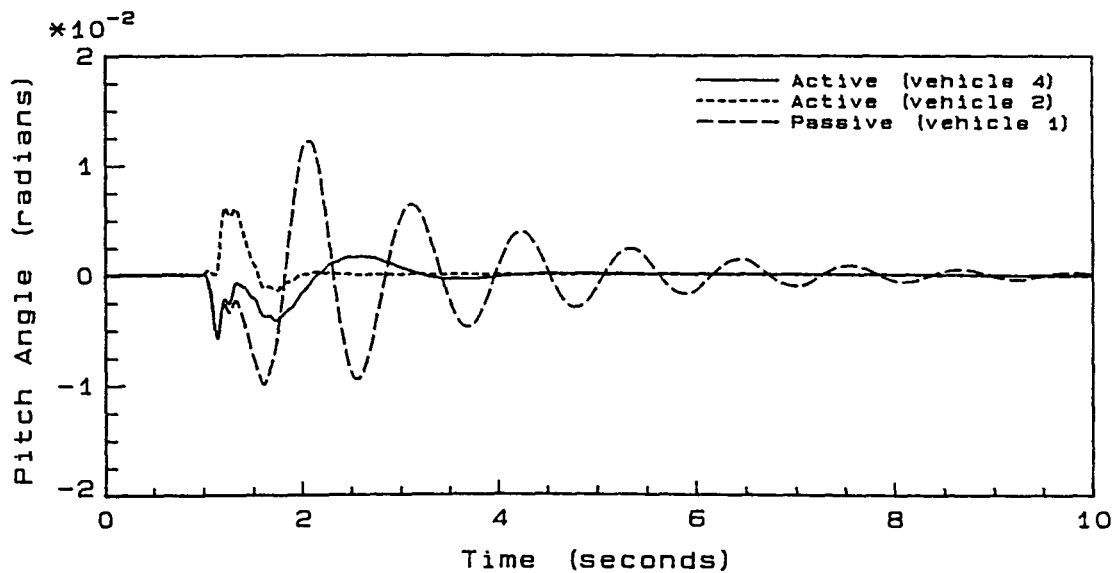


Figure 4.17: Pitch response of the vehicle with an optimal observer (vehicle 4) to a step input compared to that of the active (vehicle 2) and passive (vehicle 1) suspensions

Table 4.3: Response characteristics of the vehicle with an optimal observer (vehicle 4) to a slanted bump input compared to that of the active (vehicle 2) and passive (vehicle 1) suspensions

	vehicle 1	vehicle 4	% Improvement	
			vehicle 2	vehicle 4
Peak Force Transmitted (N)	928.98	753.14	34.55	18.93
$\int_0^t q_1(\dot{\phi}^2 + \dot{\theta}^2 + \dot{z}^2)dt$.0181	.0074	79.56	59.12
$\int_0^t q_2(\dot{\phi}^2 + \dot{\theta}^2 + \dot{z}^2)dt$.9338	.2364	87.30	74.68
$\int_0^t q_3(z_1'^2 + z_2'^2 + z_3'^2 + z_4'^2)dt$.0028	.0022	14.29	21.43
$\int_0^t (q_4 F_s^2 + q_5 F_{\text{damp}}^2 + q_6 F_{\text{act}}^2)dt$.4752	.2891	52.55	39.16

Table 4.4: Response characteristics of the vehicle with an optimal observer (vehicle 4) to a step input compared to that of the active (vehicle 2) and passive (vehicle 1) suspensions

	vehicle 1	vehicle 4	% Improvement	
			vehicle 2	vehicle 4
Peak Force Transmitted (N)	2222.9	2179.4	17.68	1.96
$\int_0^t q_1(\dot{\phi}^2 + \dot{\theta}^2 + \dot{z}^2)dt$.0072	.0038	70.83	47.22
$\int_0^t q_2(\dot{\phi}^2 + \dot{\theta}^2 + \dot{z}^2)dt$.2800	.1273	74.11	54.54
$\int_0^t q_3(z_1'^2 + z_2'^2 + z_3'^2 + z_4'^2)dt$.0607	.0475	13.34	21.75
$\int_0^t (q_4 F_s^2 + q_5 F_{\text{damp}}^2 + q_6 F_{\text{act}}^2)dt$.6724	.5392	16.63	19.81

and the active suspension without road height in its state vector. In each graph the peak amplitudes and residual vibrations are reduced. Specifically, for the slanted bump, peak bounce is reduced by 36.2%, peak roll by 43.0%, and peak pitch by 55.8%. Roll response settles out 38.1% faster, pitch more than 57.8% faster, and bounce 60.0% faster. For the step response, peak bounce is reduced by 16.3% while peak pitch is reduced by 52.5%. The settling time for the step response is 70.5% faster for bounce and more than 66.7% faster for pitch.

Tables 4.3 and 4.4 show that the suspension using the optimal observer results in significant improvement over the passive suspension yet not as good as the fully active suspension. It can be concluded based on these simulations that an active suspension using an optimal observer is capable of giving good performance compared to a passive suspension even when all state variables are not available to be measured.

5 HYDRAULIC ACTUATORS

The results of Chapter 4 show that an active suspension is capable of producing good performance even when all the state variables cannot be measured. However, the previous system models assumed that the actuator could produce any force of any magnitude in any direction and at any frequency. This chapter will include the dynamics of hydraulic actuators into the system models used in previous chapters and examine the effects of the actuators on the performance of the systems.

Hydraulic actuators have been used in many prototype research vehicles, but their practicality for production vehicles is questionable due to weight, cost, maintenance, and power usage. Figure 5.1 presents a schematic of a hydraulic actuator which consists of a spool valve and piston combination. These systems are typically non-linear, but some success has come from deriving control strategies from linearizations [12,13]. The system can be modeled as a first order system if the electro-mechanical spool valve dynamics are left out, or as a third order system if they are retained.

The response characteristics of the actuator systems vary dramatically based on system parameters such as supply pressure, valve coefficients, piston areas, and volumes. Because of this, generic models are chosen in which the system is described using a time constant for the first order hydraulic system, and a natural frequency

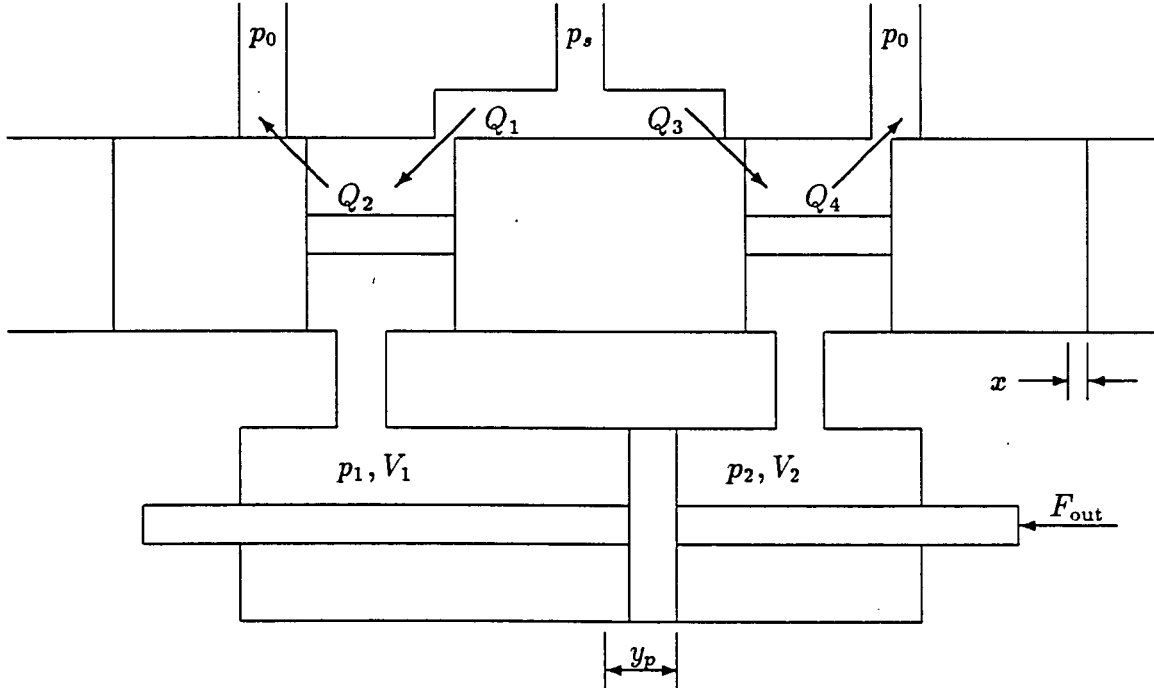


Figure 5.1: Servo-valve and Piston system

and damping ratio for the second order spool-valve system. The next section will relate these system constants to the parameters of the hydraulic system.

5.1 Hydraulic Equations of Motion

Figure 5.1 presents the four way spool valve and piston combination used in this section. Electro-mechanical spool valve dynamics and leakage across the piston are neglected. The flow rates in the valve are given by

$$Q_1 = cx_1 \sqrt{|p_s - p_1|} \text{sign}(p_s - p_1) \quad (5.1)$$

$$Q_2 = cx_2 \sqrt{|p_1 - p_0|} \text{sign}(p_1 - p_0) \quad (5.2)$$

$$Q_3 = cx_3\sqrt{|p_s - p_2|} \text{sign}(p_s - p_2) \quad (5.3)$$

$$Q_4 = cx_4\sqrt{|p_2 - p_0|} \text{sign}(p_2 - p_0) \quad (5.4)$$

where for $x \geq 0$, $x_1 = x_4 = x$ and $x_2 = x_3 = 0$; and for $x < 0$, $x_1 = x_4 = 0$ and $x_2 = x_3 = -x$. Applying continuity to the control volumes, V_1 and V_2 , gives

$$Q_1 - Q_2 = \frac{V_1}{\beta} \dot{p}_1 + A_p \dot{y}_p \quad (5.5)$$

$$Q_3 - Q_4 = \frac{V_2}{\beta} \dot{p}_2 - A_p \dot{y}_p \quad (5.6)$$

rearranging these gives the differential equations for pressure,

$$\dot{p}_1 = \frac{\beta}{V_1} (Q_1 - Q_2 - A_p \dot{y}_p) \quad (5.7)$$

$$\dot{p}_2 = \frac{\beta}{V_2} (Q_3 - Q_4 + A_p \dot{y}_p) \quad (5.8)$$

The force output from the piston is

$$F_{\text{out}} = A_p(p_1 - p_2) \quad (5.9)$$

A linear form of these equations is made by using load pressure, $p_L = p_1 - p_2$, and assuming $x \geq 0$. Thus, $Q_2 = Q_3 = 0$. Assuming $p_0 = 0$ and $p_s - p_1 = p_2$ gives equal flow rates.

$$Q_L = Q_1 = Q_2 = Cx\sqrt{\frac{p_s - p_L}{2}} \quad (5.10)$$

Assuming equal volumes and small changes in volume about $V_0 = V_1 + V_2$ gives

$$\dot{p}_L = \frac{2\beta}{V_0} (Q_L - A_p \dot{y}_p) \quad (5.11)$$

The linearized forms of equations 5.10 and 5.11 are

$$Q_L = c\sqrt{\frac{p_s - p_{L0}}{2}}x - \frac{cx_0}{2\sqrt{2(p_s - p_{L0})}}p_L \quad (5.12)$$

$$\dot{p}_L = \frac{2\beta}{V_0} (Q_L - A_p \dot{y}_p) \quad (5.13)$$

The final linear equation for pressure is

$$\dot{p}_L = k_3(k_1x - k_2p_L - A_p\dot{y}_p) \quad (5.14)$$

where

$$k_1 = C\sqrt{\frac{p_s - p_{L0}}{2}} \quad (5.15)$$

$$k_2 = \frac{Cx_0}{2\sqrt{2(p_s - p_{L0})}} \quad (5.16)$$

$$k_3 = \frac{2\beta}{V_0} \quad (5.17)$$

The transfer function between output force and spool-valve position is

$$\frac{F_{\text{out}}}{x} = \frac{k_1k_3A_p}{s + k_2k_3} \quad (5.18)$$

Assuming a linear relationship between desired force and valve position and a steady state error of zero,

$$\frac{F_{\text{out}}}{F_{\text{des}}} = \frac{k_vk_1k_3A_p}{s + k_2k_3} \quad (5.19)$$

where

$$k_v = \frac{k_2}{k_1A_p} \quad (5.20)$$

The overall transfer function for force reduces to the first order system,

$$\frac{F_{\text{out}}}{F_{\text{des}}} = \frac{1}{\tau_h s + 1} \quad (5.21)$$

where the time constant is

$$\tau_h = \frac{1}{k_2k_3} = \frac{V_0\sqrt{2(p_s - p_{L0})}}{\beta Cx_0} \quad (5.22)$$

To include servo-valve dynamics it is assumed that the transfer function for valve opening to force desired is second order [11,13] and

$$\frac{x}{F_{\text{des}}} = \frac{k_v}{s^2 + 2\zeta\omega_n s + \omega_n^2} \quad (5.23)$$

Substituting this into equation 5.18 and assuming zero steady state error gives

$$k_v = \frac{\omega_n^2 k_2}{k_1 A_p} \quad (5.24)$$

The transfer function for force output compared to force desired is

$$\frac{F_{\text{out}}}{F_{\text{des}}} = \frac{1}{(\tau_h s + 1) \left(\frac{s^2}{\omega_n^2} + \frac{2\zeta}{\omega_n} s + 1 \right)} \quad (5.25)$$

5.2 Effects of Actuator Dynamics on Suspension Performance

If both hydraulic and electro-mechanical dynamics are included in a linear hydraulic actuator model, a third order system is obtained. As previously shown, the hydraulic portion is a first order system and the electro-mechanical spool valve is a second order system. In order to understand the effects of these components on the performance of the active suspensions, first and second order systems will be examined separately in the active model with the optimal observer. In this way, the sensitivity of system performance to the time constant in the first order case, and the natural frequency in the second order case can be studied. Because this model is linear, this type of analysis will give a good feel for the combined effects of these actuator parameters on the total system performance. This is because the system performance is limited primarily by the weakest link, that being either the hydraulics or the electro-mechanical components if in fact the actuator degrades the system. If the actuator has better response characteristics, i.e., higher response frequencies, than called upon by the control system, then the control system is the limiting system not the actuator.

This section examines a generalized first order actuator and will show the effects of the time constant of the actuator on the active suspension performance.

The transfer function for a first order system is

$$\frac{F_{out}}{F_{des}} = \frac{1}{\tau_h s + 1} \quad (5.26)$$

It is assumed that the actuator system parameters are fixed and its state variables can not be measured, and therefore can not be used as a feedback variable. The first order actuator model is included in the active suspension vehicle model with the optimal observer as used in Chapter 4.

Figures 5.2, 5.3, and 5.4 show frequency response plots for τ_h of 1, 0.1, and 0.01 seconds. These plots show that at a time constant of 1 second, the frequency response is very similar to that of the passive suspension shown in Figure 3.9, and that at 0.01 seconds, the frequency response is nearly as good as that of the active suspension with the optimal observer shown in Figure 4.10.

To demonstrate the effects of first order dynamics on suspension performance, the time constant of the actuators is varied from .01 to 1 seconds and the vehicle is simulated over the slanted bump road profile. Figure 5.5 shows the percentages of the improvements possible using ideal actuators in peak roll, pitch and bounce and Figure 5.6 shows the cost functions.

The results of this section show that for an actuator with time constant less than about 0.1 seconds, the performance curves flatten out. Thus, further decreasing the actuator time constant will not greatly improve performance. However, increasing the time constant above 0.1 seconds does dramatically decrease suspension performance.

This section examines the influence of a general second order actuator system and will show the effects of the natural frequency of the actuator on the active

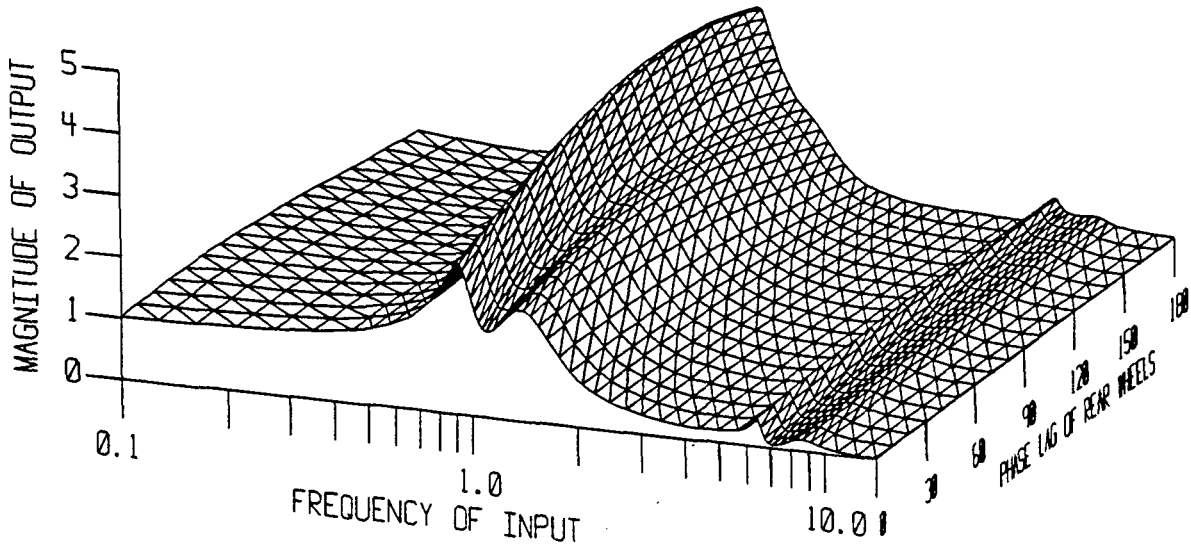


Figure 5.2: Bounce frequency response for varying phase angles between front and rear tires of the active suspension with a first order actuator ($\tau_h = 1$)

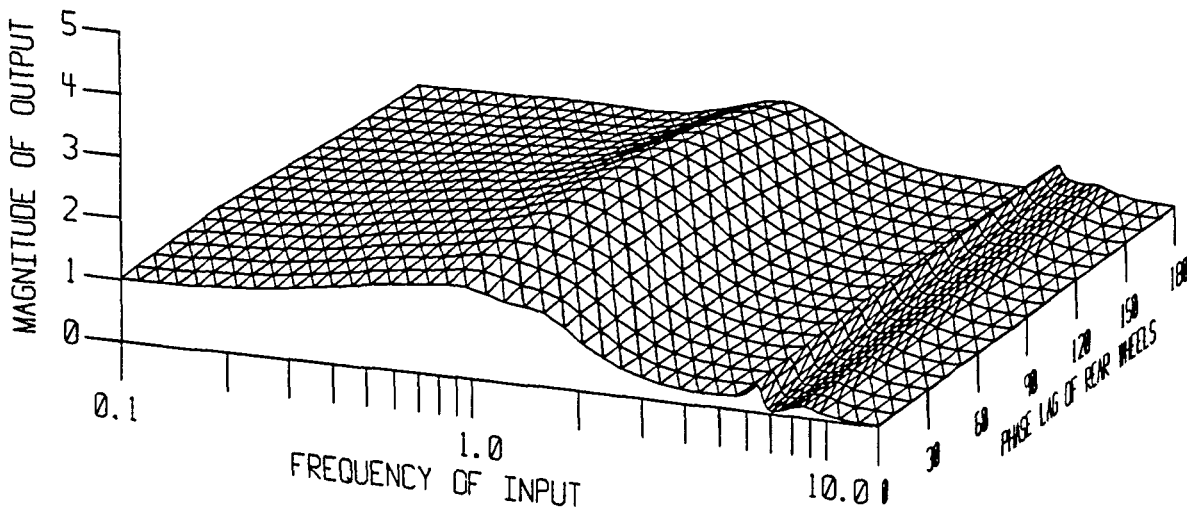


Figure 5.3: Bounce frequency response for varying phase angles between front and rear tires of the active suspension with a first order actuator ($\tau_h = 0.1$)

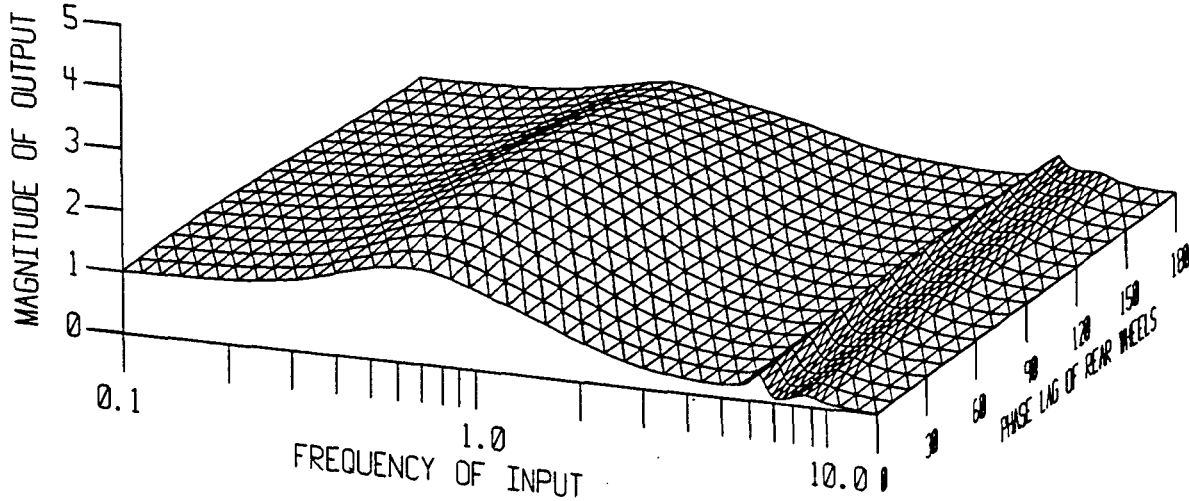


Figure 5.4: Bounce frequency response for varying phase angles between front and rear tires of the active suspension with a first order actuator ($\tau_h = 0.01$)

suspension performance. The transfer function for a second order force actuator is

$$\frac{F_{out}}{F_{des}} = \frac{1}{\omega_n^2 s^2 + \frac{2\zeta}{\omega_n} s + 1} \quad (5.27)$$

Again, it is assumed that the actuator state variables can not be used as feedback state variables. This actuator model is included in the active suspension vehicle model with the optimal observer as used in Chapter 4.

Frequency response plots for ω_n of 0.5, 2, and 10 Hertz are shown in Figures 5.7, 5.8, and 5.9. These plots show that at a natural frequency of 0.5 Hertz the frequency response is very similar to that of the passive suspension shown in Figure 3.9, and that at 10 Hertz the frequency response is nearly as good as that of the active suspension shown in Figure 3.10.

The results of several simulations are examined to investigate the effects of

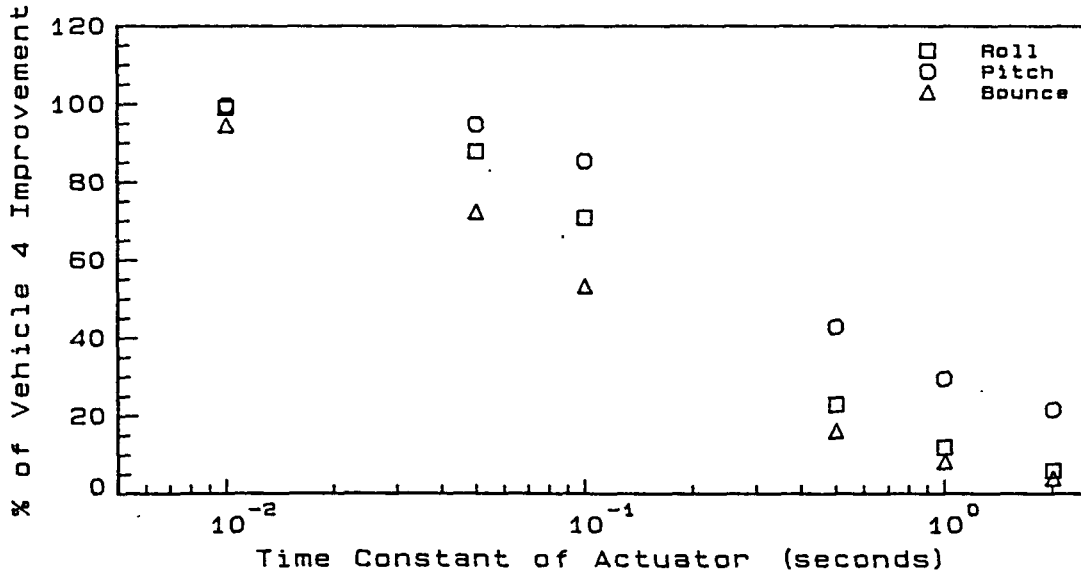


Figure 5.5: Percent improvement in roll, pitch and bounce peak values verses first order actuator frequency for a slanted bump

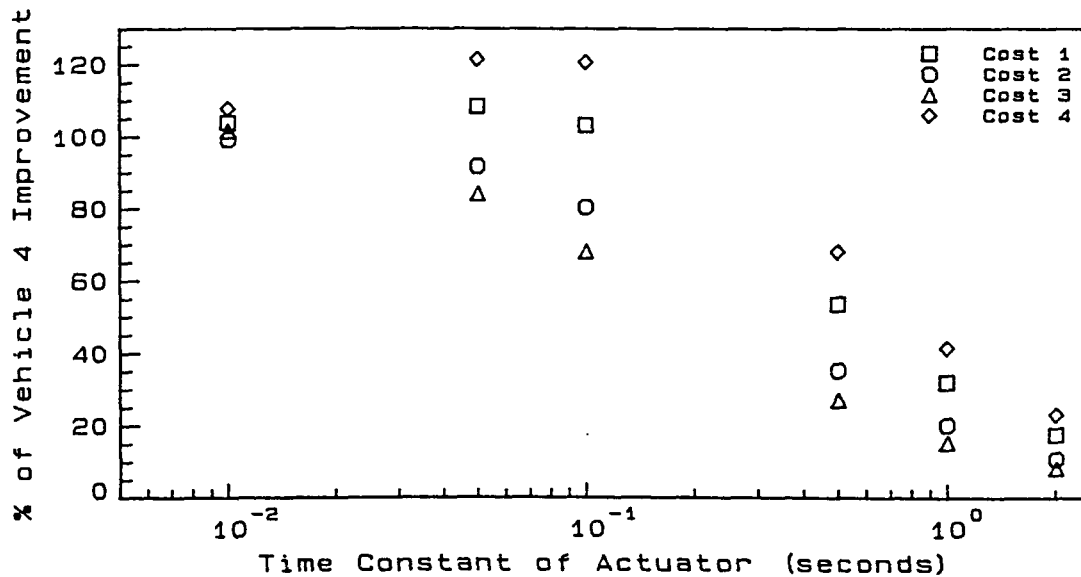


Figure 5.6: Percent improvement in cost integral values verses first order actuator frequency for a slanted bump

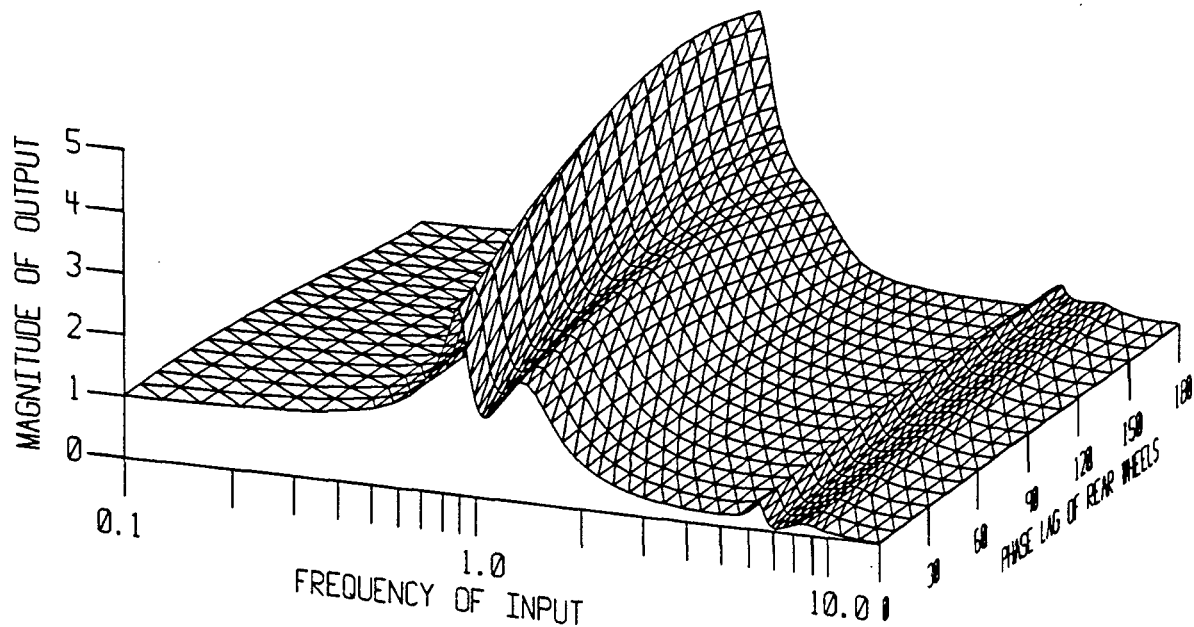


Figure 5.7: Bounce frequency response for varying phase angles between front and rear tires of the active suspension with a second order actuator ($\omega_n = 0.5$)

second order dynamics on suspension performance. The natural frequency of the actuators is varied from .5 to 20 Hertz with critical damping and the vehicle is simulated over the slanted bump road profile. The percentages of the improvements possible using ideal actuators in peak roll, pitch, and bounce are shown in Figure 5.10 and the cost functions are shown in Figure 5.11.

The results of this section demonstrate the effects of actuator natural frequency on suspension performance. At frequencies below about 1 Hertz, the performance is not significantly improved over the passive suspension. Above 10 Hertz, further improvement is not possible. This is not surprising since the bounce, pitch and roll natural frequencies are at values of 1.38 Hz, 0.91 Hz, and 1.31 Hz respectively, which corresponds to the rapid improvement found as the actuator frequency passes these lower natural frequencies. Also, the front and rear wheel hop natural frequencies

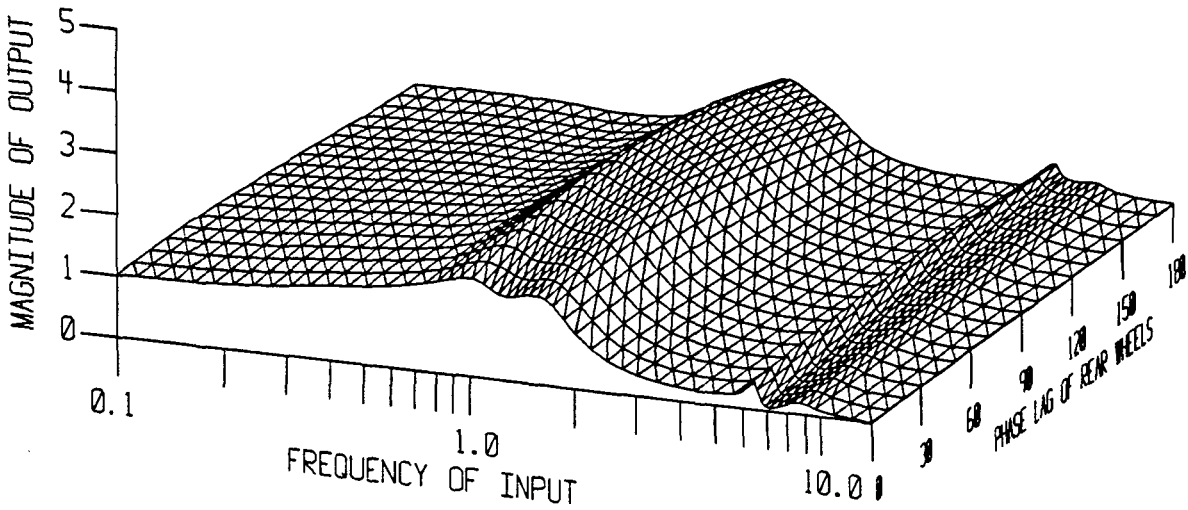


Figure 5.8: Bounce frequency response for varying phase angles between front and rear tires of the active suspension with a second order actuator ($\omega_n = 2$)

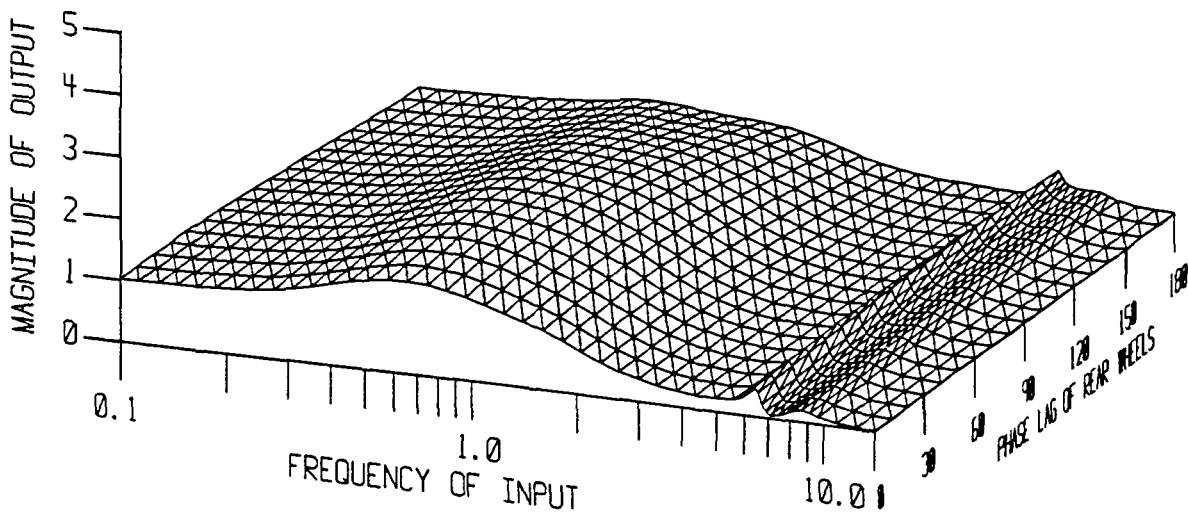


Figure 5.9: Bounce frequency response for varying phase angles between front and rear tires of the active suspension with a second order actuator ($\omega_n = 10$)

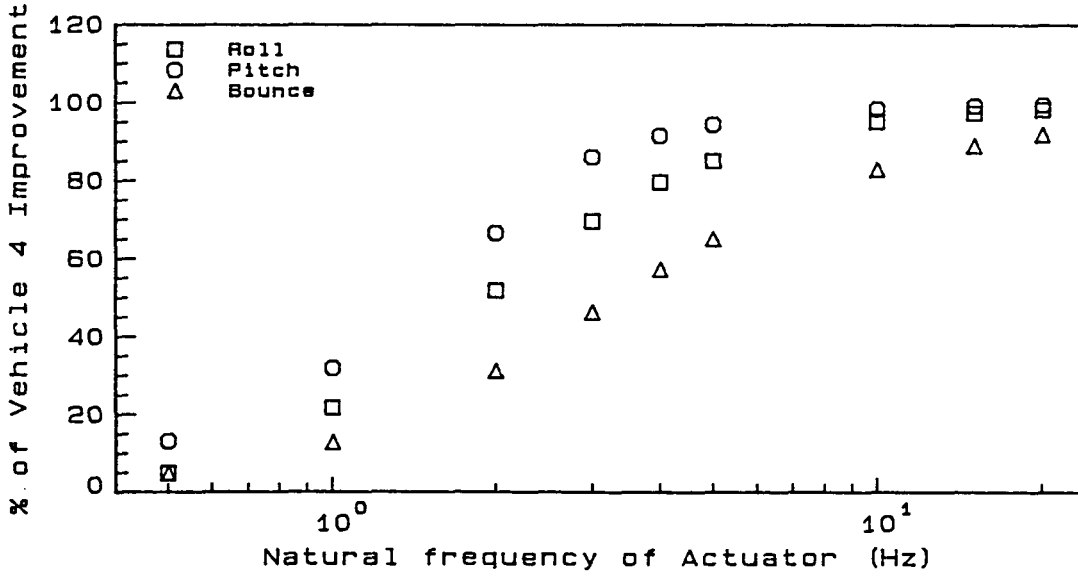


Figure 5.10: Percent improvement in roll, pitch and bounce peak values verses second order actuator frequency for a slanted bump

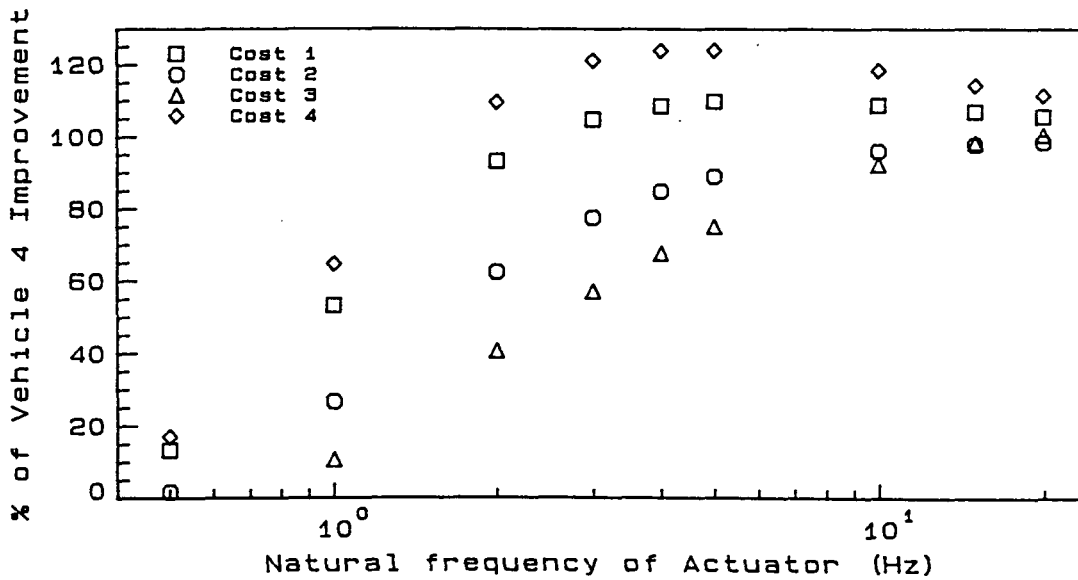


Figure 5.11: Percent improvement in cost integral values verses second order actuator frequency for a slanted bump

are 6.46 Hz and 8.71 Hz respectively, which corresponds to the upper limit of improvement found around 10 Hz. This would indicate as expected that the natural frequency of the actuator need not be significantly larger than the highest natural frequency of the system being controlled to obtain performance close to that of an ideal actuator.

6 VARIABLE DAMPING SEMI-ACTIVE ACTUATORS

The results of Chapter 5 show that an active suspension with a hydraulic actuator is capable of producing significant increases in ride performance as compared to the passive system. This chapter will investigate semi-active actuators which use variable dampers to generate forces. These systems require fewer components than hydraulic actuators and require very little external power to operate and therefore seem a more feasible option for production vehicles.

6.1 On/Off Damper

One type of suspension in the category of semi-active suspensions is a damper that will remove energy from the system but not impart energy to the chassis. The energy imparted per unit time by a force is defined as

$$\text{Energy/time} = \text{Force} \cdot \text{Velocity} \quad (6.1)$$

If the force is from a damper,

$$\text{Force} = -c \times \text{Relative Velocity} \quad (6.2)$$

Therefore, the criterion for turning on the damper is if the energy imparted to the chassis is negative, or

$$(-c \times \text{Relative Velocity}) \cdot \text{Velocity} < 0 \quad (6.3)$$

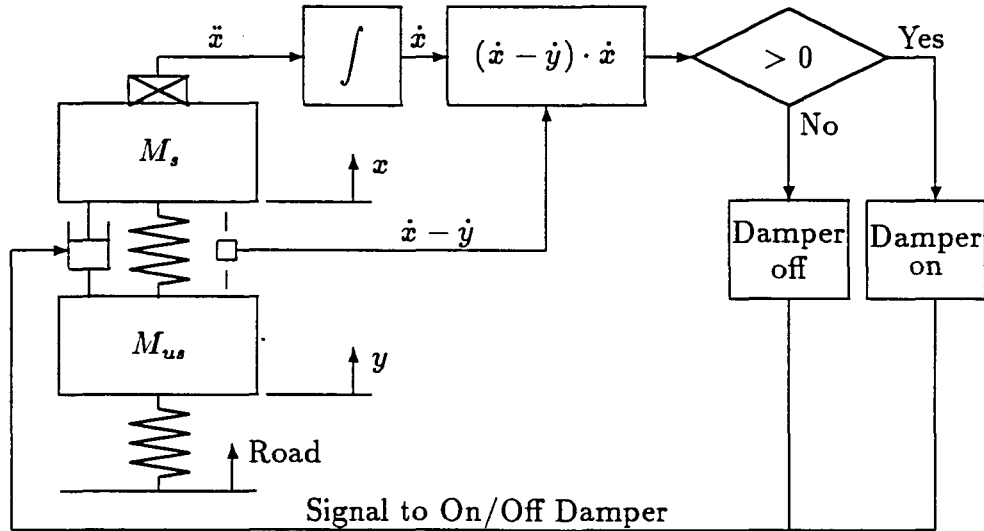


Figure 6.1: Block diagram of on/off suspension system applied to a two degree of freedom model of a vehicle

then the damping is switched on. Otherwise the damper is switched to a very low damping condition.

This scheme requires the measurement of relative velocity of the suspension and the absolute velocity of the chassis attachment point, a difficult variable to measure. However, the control system is less complex than a fully active suspension and the individual suspensions are independent from one another. Figure 6.1 presents a block diagram of the system.

A frequency response analysis as used previously is impossible for this system because of its non-linearity. Therefore, this system will be studied using two different time responses for the worse cases defined earlier, that being the slanted bump in Figure 3.9 and the step in Figure 3.10.

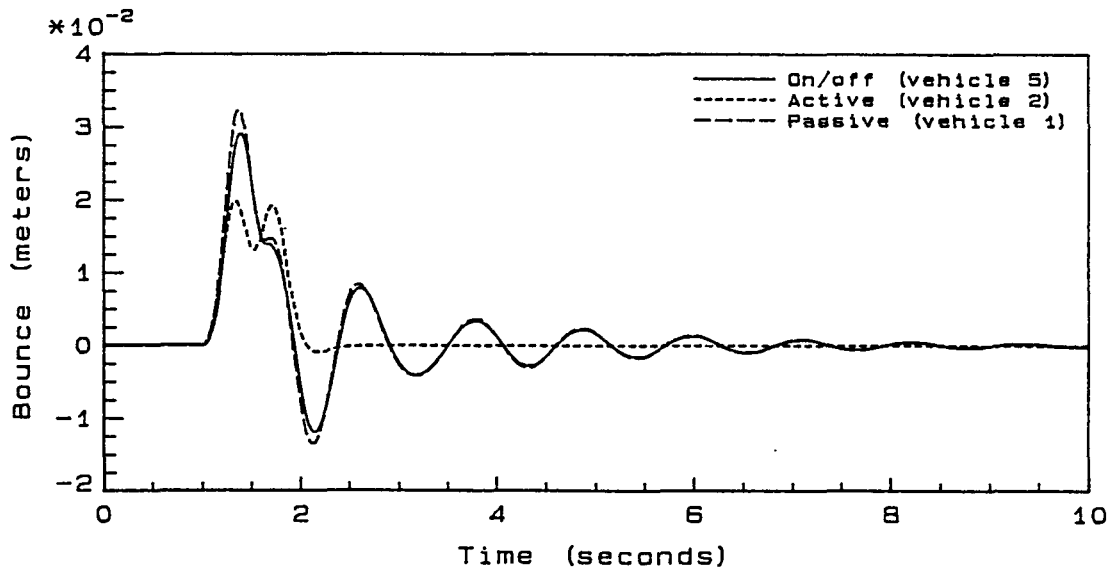


Figure 6.2: Bounce response of the vehicle with an on/off suspension system (vehicle 5) to a slanted bump input compared to that of the passive (vehicle 1) and active (vehicle 2) suspensions

The seven degree of freedom vehicle model with on/off dampers with the same damping rate as the passive suspension is simulated over the slanted bump and step road profiles. Figures 6.2, 6.3 and 6.4 show the bounce, pitch and roll responses of the vehicle with on/off dampers (vehicle 5) to the slanted bump input compared with the passive and active suspensions, and Table 6.1 lists the response parameters. Figures 6.5 and 6.6 show the bounce and pitch responses and Table 6.2 lists the response parameters for the step.

The on/off damper gives a limited improvement in peak bounce, pitch and roll for the case of the slanted bump, but gives a dramatic increase in performance for the step. Note the 40% improvement in peak force transmitted in Table 6.2 for the step. This great improvement is due to the high suspension velocities imparted during the step which give high damping forces for the passive case but which do

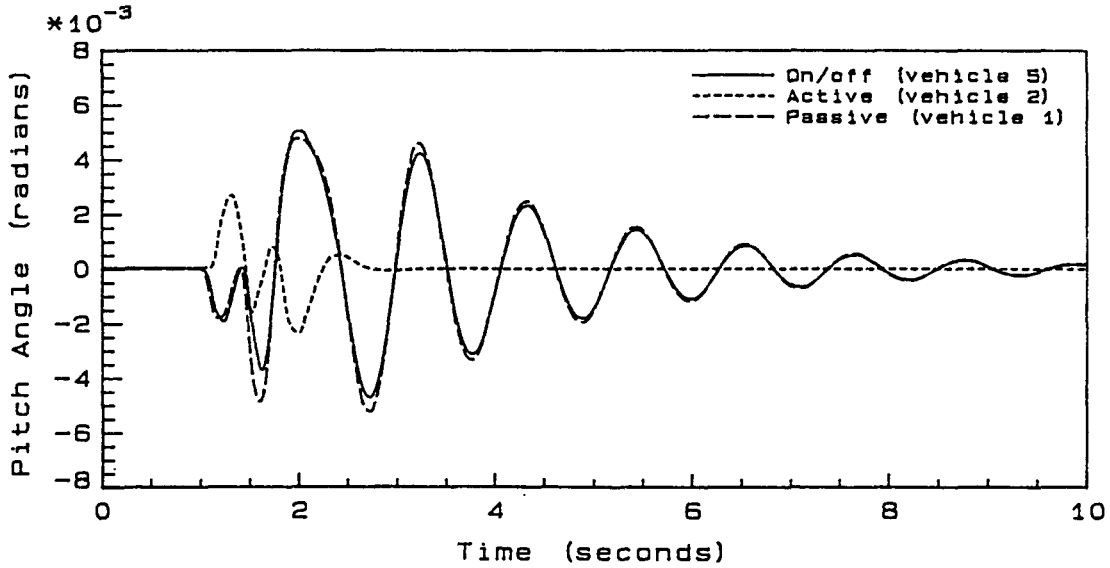


Figure 6.3: Pitch response of the vehicle with an on/off suspension system (vehicle 5) to a slanted bump input compared to that of the passive (vehicle 1) and active (vehicle 2) suspensions

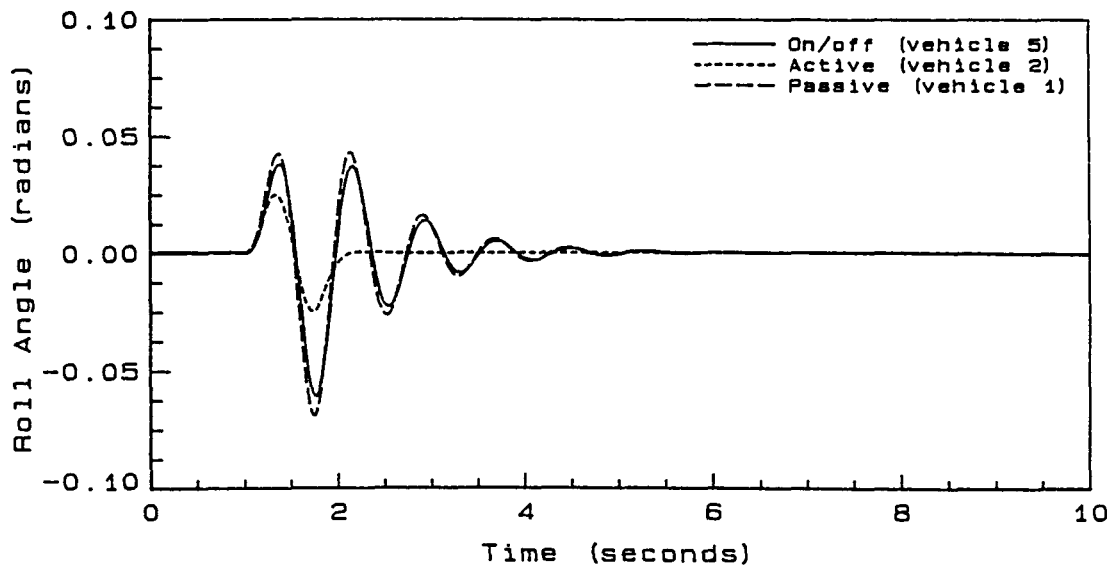


Figure 6.4: Roll response of the vehicle with an on/off suspension system (vehicle 5) to a slanted bump input compared to that of the passive (vehicle 1) and active (vehicle 2) suspensions

Table 6.1: Response characteristics of the vehicle with an on/off suspension system (vehicle 5) to a slanted bump compared to that of the active (vehicle 2) and passive (vehicle 1) suspensions

Vehicle	1	5	% Improvement	
			2	5
Peak Force Transmitted (N)	928.98	822.81	34.55	11.43
$\int_0^t q_1(\dot{\phi}'^2 + \dot{\theta}'^2 + \dot{z}'^2)dt$.0181	.0155	79.56	14.36
$\int_0^t q_2(\dot{\phi}^2 + \dot{\theta}^2 + \dot{z}^2)dt$.9338	.7189	87.30	23.01
$\int_0^t q_3(z_1'^2 + z_2'^2 + z_3'^2 + z_4'^2)dt$.0028	.0029	14.29	-3.57
$\int_0^t (q_4 F_s^2 + q_5 F_{\text{damp}}^2 + q_6 F_{\text{act}}^2)dt$.4752	.4122	52.55	13.26

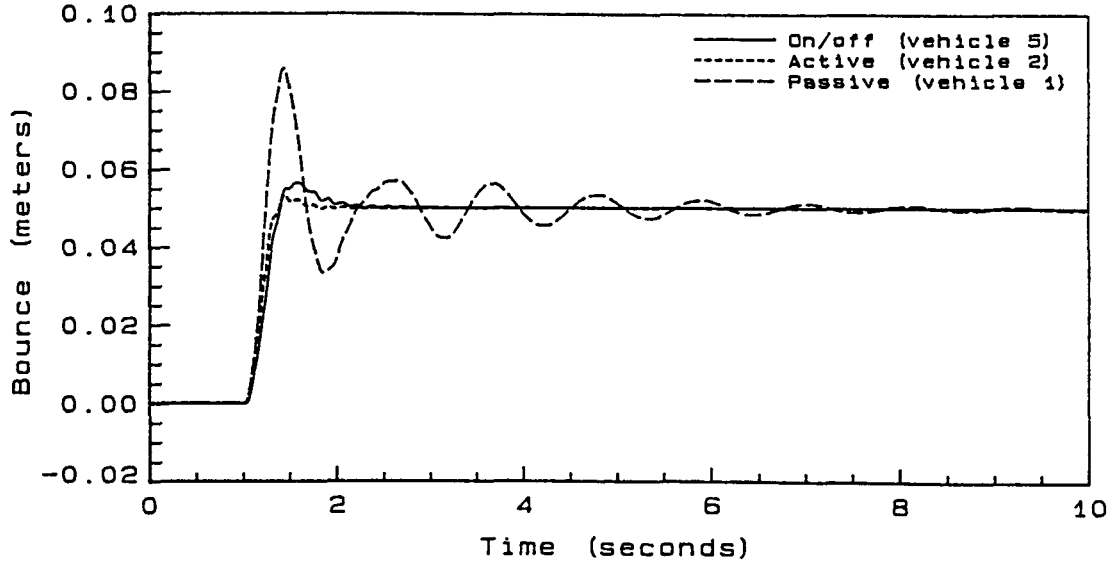


Figure 6.5: Bounce response of the vehicle with an on/off suspension system (vehicle 5) to a step input compared to that of the passive suspension (vehicle 1)

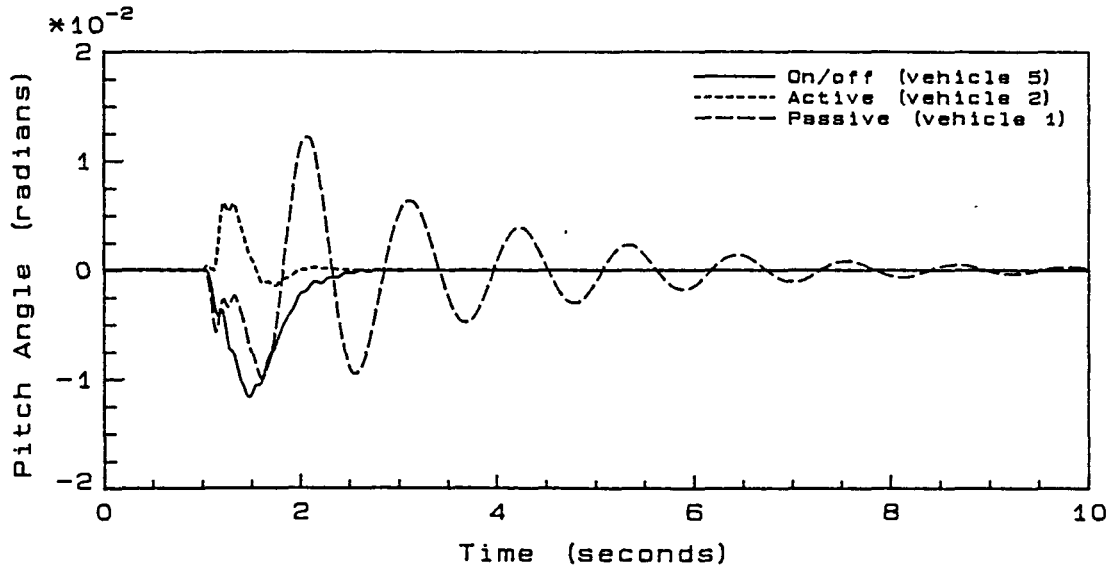


Figure 6.6: Pitch response of the vehicle with an on/off suspension system (vehicle 5) to a step input compared to that of the passive suspension (vehicle 1)

Table 6.2: Response characteristics of the vehicle with an on/off suspension system (vehicle 5) to a step input compared to that of the active (vehicle 2) and passive (vehicle 1) suspensions

Vehicle	1	5	% Improvement	
			2	5
Peak Force Transmitted (N)	2222.9	1347.5	17.68	39.98
$\int_0^t q_1(\dot{\phi}^2 + \dot{\theta}^2 + \dot{z}^2)dt$.0072	.0038	70.83	47.22
$\int_0^t q_2(\dot{\phi}^2 + \dot{\theta}^2 + \dot{z}^2)dt$.2800	.0705	74.11	74.82
$\int_0^t q_3(z_1'^2 + z_2'^2 + z_3'^2 + z_4'^2)dt$.0607	.1085	13.34	-78.75
$\int_0^t (q_4 F_s^2 + q_5 F_{\text{damp}}^2 + q_6 F_{\text{act}}^2)dt$.6724	.6943	16.63	-3.26

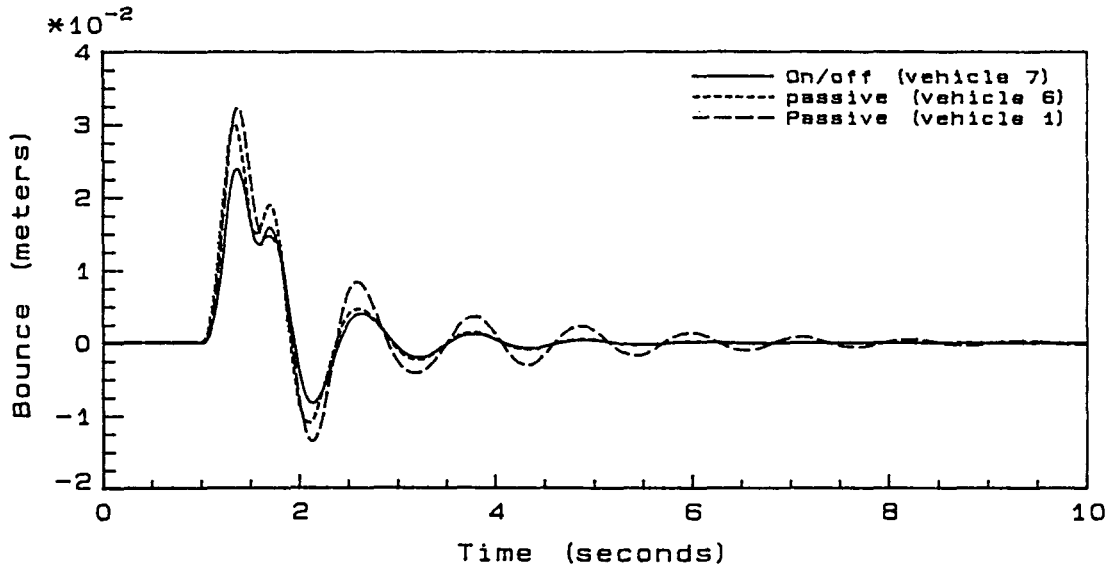


Figure 6.7: Bounce response of the vehicle with an on/off suspension system having twice the damping (vehicle 7) to a slanted bump input compared to that of the passive suspensions (vehicle 1 and vehicle 6, twice damping)

not give damping force when the on/off damper is in the system.

Doubling the damping rate and simulating both the vehicle with the on/off suspension (vehicle 7) and the vehicle with the passive suspension (vehicle 6) result in Figures 6.7 to 6.11 and Tables 6.3 and 6.4. While in both cases, doubling the damping ratio reduces peak sprung mass vibration and settling time significantly, the passive suspension with increased damping gives a peak force 40% higher than the original passive suspension for the step. The on/off damper, however, decreases peak force transmitted by 31% relative to the original passive system. Again, the step responses in Figures 6.10 and 6.11 show remarkable vibration isolation for the on/off damper.

The results of this section show that in traditional passive systems, increasing damping rates improves the low frequency ride performance, but results in a hard

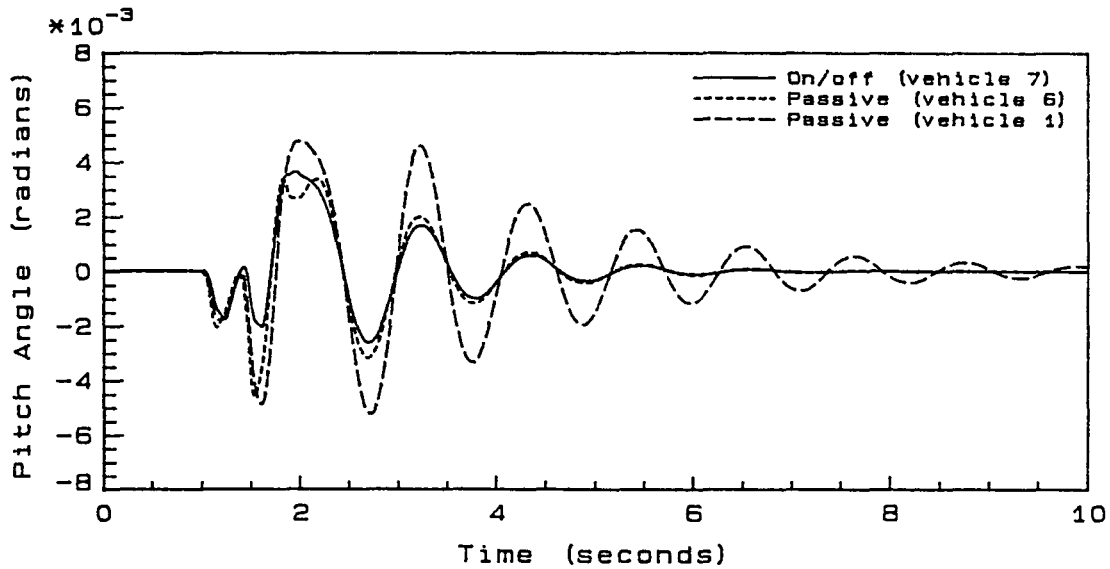


Figure 6.8: Pitch response of the vehicle with an on/off suspension system having twice the damping (vehicle 7) to a slanted bump input compared to that of the passive suspensions (vehicle 1 and vehicle 6, twice damping)

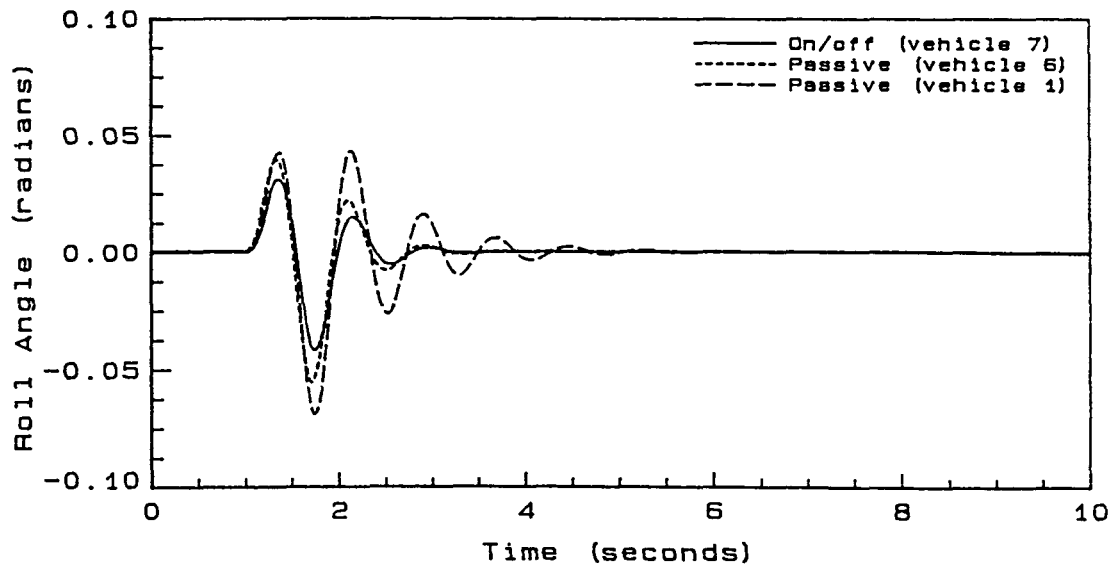


Figure 6.9: Roll response of the vehicle with an on/off suspension system having twice the damping (vehicle 7) to a slanted bump input compared to that of the passive suspensions (vehicle 1 and vehicle 6, twice damping)

Table 6.3: Response characteristics of the vehicle with an on/off suspension system having twice the damping (vehicle 7) to a slanted bump input compared to that of the passive suspensions (vehicle 1 and vehicle 6, twice damping)

Vehicle	1	6	7	% Improvement	
				6	7
Peak Force Transmitted (N)	928.98	897.72	773.52	3.36	16.73
$\int_0^t q_1(\phi'^2 + \theta'^2 + z'^2)dt$.0181	.0083	.0069	54.14	61.88
$\int_0^t q_2(\dot{\phi}^2 + \dot{\theta}^2 + \dot{z}^2)dt$.9338	.5130	.2889	45.06	69.06
$\int_0^t q_3(z_1'^2 + z_2'^2 + z_3'^2 + z_4'^2)dt$.0028	.0022	.0024	21.42	14.29
$\int_0^t (q_4 F_s^2 + q_5 F_{\text{damp}}^2 + q_6 F_{\text{act}}^2)dt$.4752	.3495	.2801	26.45	41.06

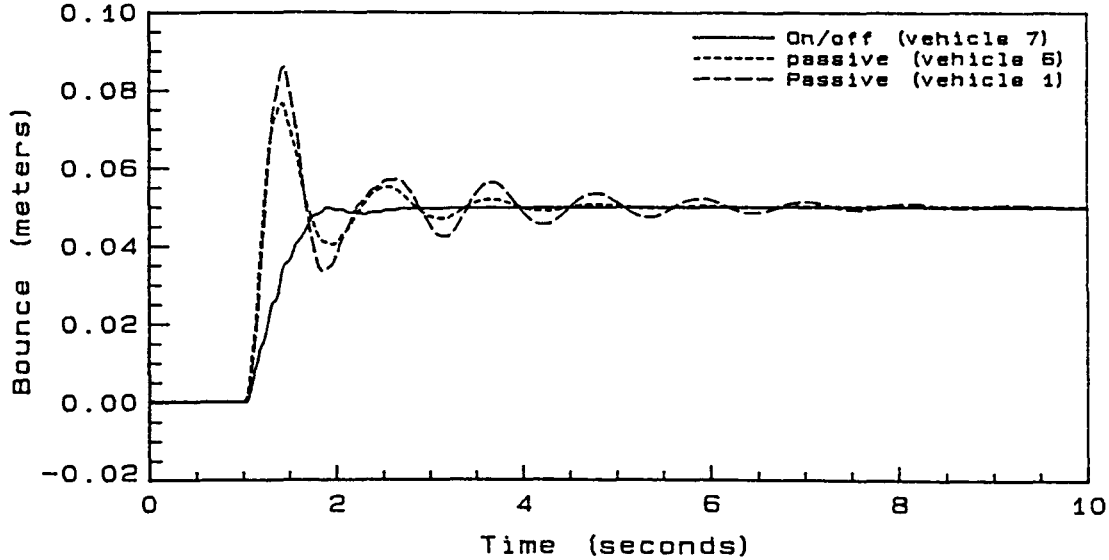


Figure 6.10: Bounce response of the vehicle with an on/off suspension system having twice the damping (vehicle 7) to a step input compared to that of the passive suspensions (vehicle 1 and vehicle 6, twice damping)

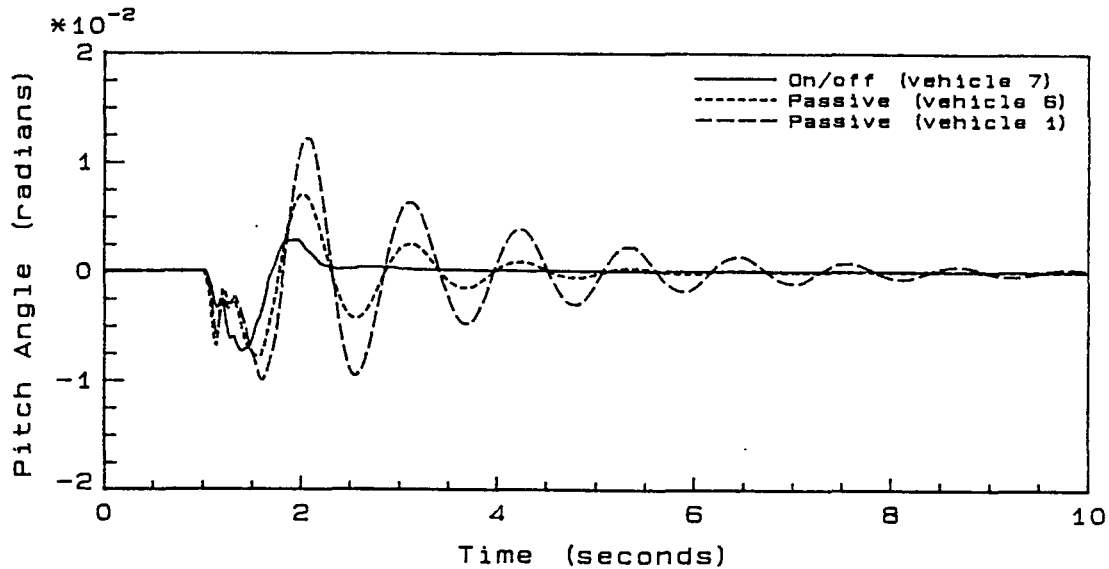


Figure 6.11: Pitch response of the vehicle with an on/off suspension system having twice the damping (vehicle 7) to a step input compared to that of the passive suspensions (vehicle 1 and vehicle 6, twice damping)

Table 6.4: Response characteristics of the vehicle with an on/off suspension system having twice the damping (vehicle 7) to a step input compared to that of the passive suspensions (vehicle 1 and vehicle 6, twice damping)

Vehicle	1	6	7	% Improvement	
				6	7
Peak Force Transmitted (N)	2222.9	3132.0	1548.2	-40.90	30.75
$\int_0^t q_1(\dot{\phi}'^2 + \dot{\theta}'^2 + \dot{z}'^2)dt$.0072	.0042	.0051	41.67	29.17
$\int_0^t q_2(\dot{\phi}^2 + \dot{\theta}^2 + \dot{z}^2)dt$.2800	.1931	.0374	31.04	86.64
$\int_0^t q_3(z_1'^2 + z_2'^2 + z_3'^2 + z_4'^2)dt$.0607	.0321	.0673	47.12	-10.87
$\int_0^t (q_4 F_s^2 + q_5 F_{\text{damp}}^2 + q_6 F_{\text{act}}^2)dt$.6742	.8401	1.0233	-24.94	-52.19

or harsh ride demonstrated by the high force transmitted by vehicle 6. Therefore, increasing the damping is not traditionally used to improve low frequency ride. The on/off damper however, permits the use of increased damping rates without allowing high frequency inputs through the system. This is demonstrated in all simulations where peak transmitted force is reduced for the on/off suspension compared to passive systems especially for high frequency inputs. Therefore, with an on/off suspension, increased damping rates can be used to improve ride, without increasing transmitted force, and resulting in a less harsh ride than a passive suspension with the same increased damping rate.

6.2 Active Damper

An active damper, as described in Section 2.3, is capable of absorbing energy only. However, its output force is varied continuously by changing the damping rate from a value of zero to infinity. The most popular systems use a continuously variable orifice size in a damper.

When using this scheme, the damping force must be zero when the force desired is in a direction opposite to the force available. If, however, the force desired is in the same direction as the force available, then the output force is equal to the force desired if an instantaneous damping change response is assumed.

Again, the frequency response is not possible due to the nonlinearities of this system. Therefore this system will be investigated using time responses. The seven degree of freedom vehicle model with active dampers (vehicle 8) is simulated over the slanted bump and step road profiles. Figures 6.12, 6.13 and 6.14 show the bounce, pitch and roll responses of the on/off damper to the slanted bump input

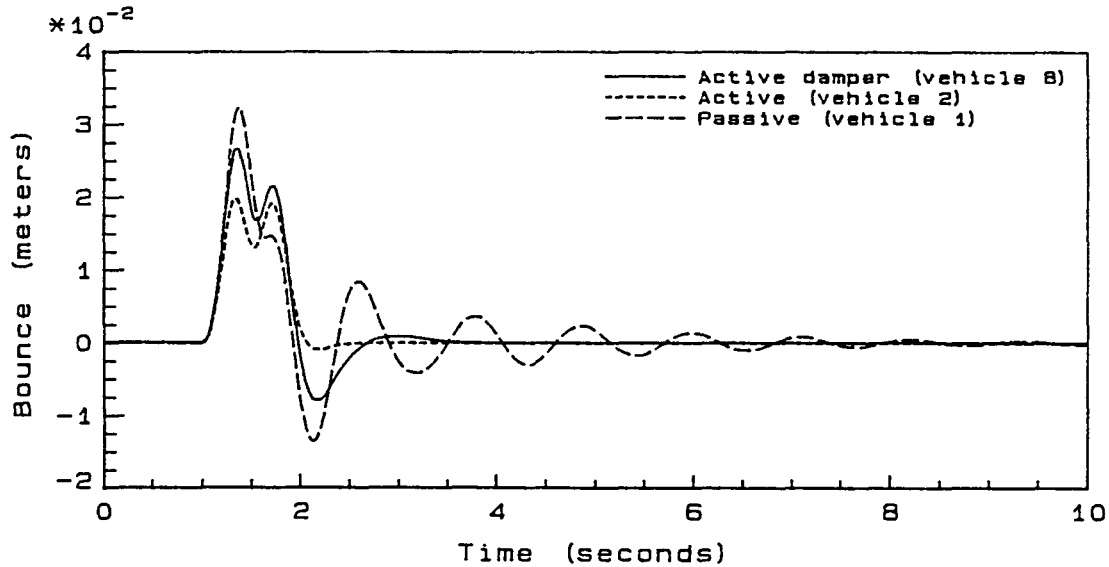


Figure 6.12: Bounce response of the vehicle with an active damper (vehicle 8) suspension system to a slanted bump input compared to that of the passive (vehicle 1) and active (vehicle 2) suspensions

compared with the passive suspension, and Table 6.5 lists the response parameters. Figures 6.15 and 6.16 show the bounce and pitch responses and Table 6.6 lists the response parameters for the step.

The simulation results show that this particular active suspension gives improved low frequency ride response as compared to the passive suspension, but not as improved as the ideal active suspension. In each graph the peak amplitudes and residual vibrations are greatly reduced. Specifically, for the slanted bump, peak bounce is reduced by 17.3%, peak roll by 36.2%, and peak pitch by 32.7%. Roll response settles out 52.4% faster, pitch 71.1% faster, and bounce 66.2% faster. For the step response, peak bounce overshoot is reduced by 12.5% while peak pitch is reduced by 52.5%. The settling time for the step response is 67.2% faster for bounce and 68.9% faster for pitch.

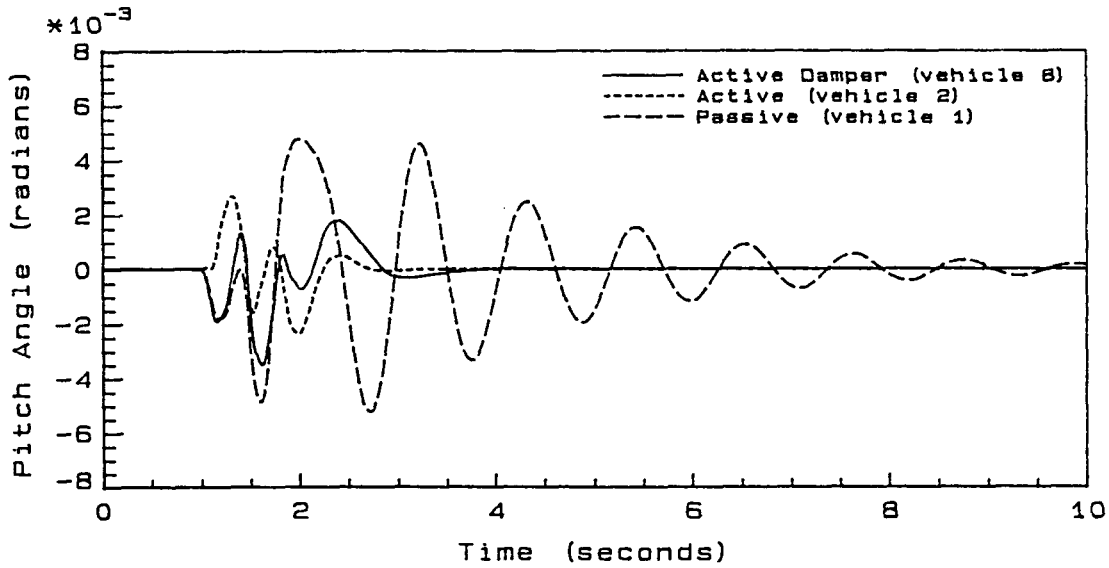


Figure 6.13: Pitch response of the vehicle with an active damper (vehicle 8) suspension system to a slanted bump input compared to that of the passive (vehicle 1) and active (vehicle 2) suspensions

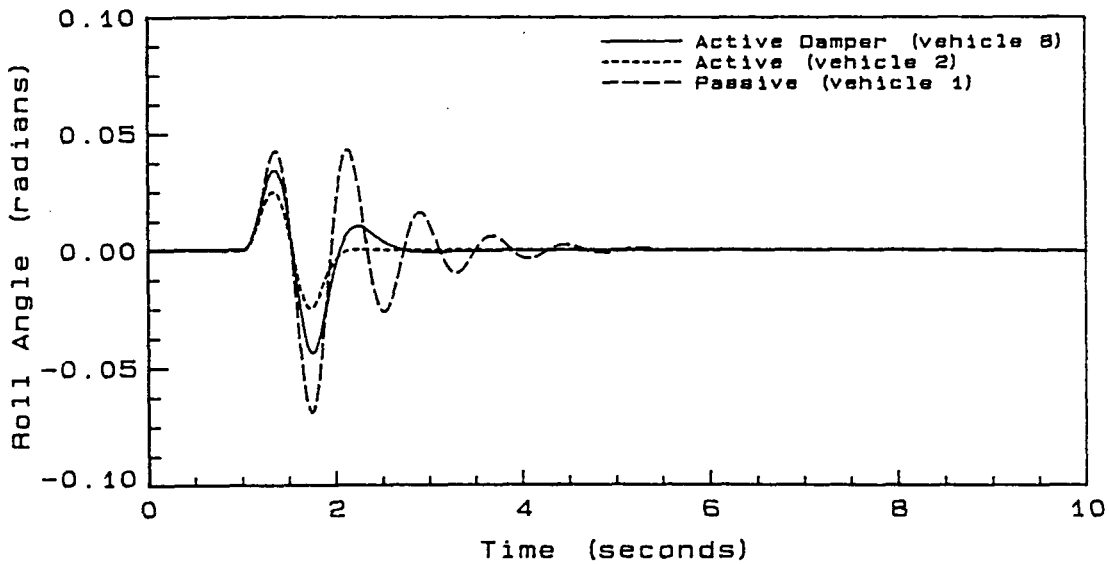


Figure 6.14: Roll response of the vehicle with an active damper (vehicle 8) suspension system to a slanted bump input compared to that of the passive (vehicle 1) and active (vehicle 2) suspensions

Table 6.5: Response characteristics of the vehicle with an active damper (vehicle 8) suspension system to a slanted bump input compared to that of the active (vehicle 2) and passive (vehicle 1) suspensions

Vehicle	1	8	% Improvement	
			2	8
Peak Force Transmitted (N)	928.98	792.91	34.55	14.65
$\int_0^t q_1(\dot{\phi}'^2 + \dot{\theta}'^2 + \dot{z}'^2)dt$.0181	.0073	79.56	59.67
$\int_0^t q_2(\dot{\phi}^2 + \dot{\theta}^2 + \dot{z}^2)dt$.9338	.2880	87.30	69.16
$\int_0^t q_3(z_1'^2 + z_2'^2 + z_3'^2 + z_4'^2)dt$.0028	.0021	14.29	25.00
$\int_0^t (q_4 F_s^2 + q_5 F_{\text{damp}}^2 + q_6 F_{\text{act}}^2)dt$.4752	.2725	52.55	42.66

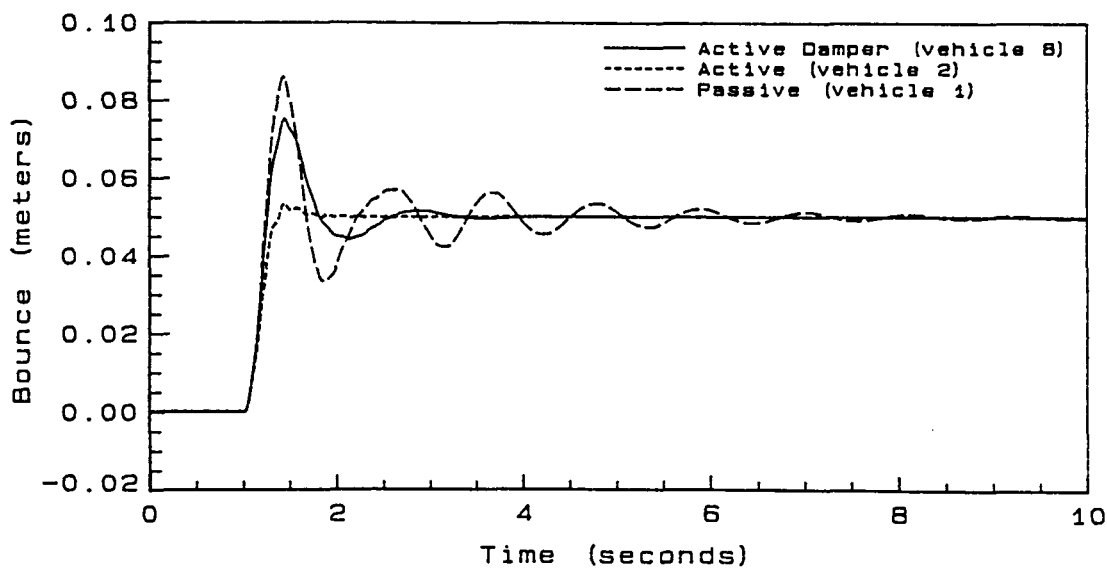


Figure 6.15: Bounce response of the vehicle with an active damper (vehicle 8) suspension system to a step input compared to that of the passive (vehicle 1) and active (vehicle 2) suspensions

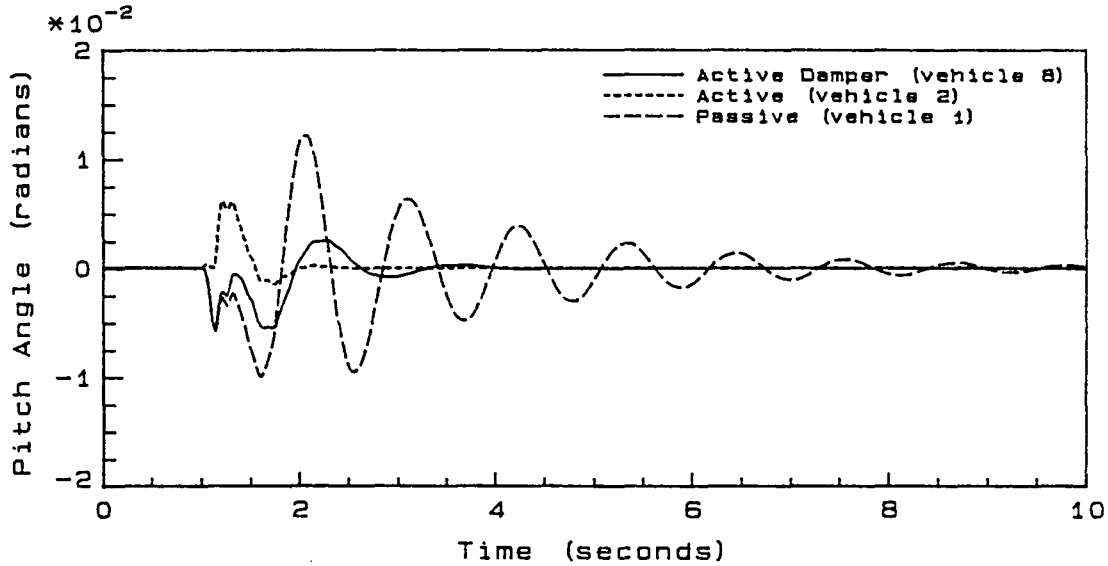


Figure 6.16: Pitch response of the vehicle with an active damper (vehicle 8) suspension system to a step input compared to that of the passive (vehicle 1) and active (vehicle 2) suspensions

Table 6.6: Response characteristics of the vehicle with an active damper (vehicle 8) suspension system to a step compared to that of the active (vehicle 2) and passive (vehicle 1) suspensions

vehicle	1	8	% Improvement	
			2	8
Peak Force Transmitted (N)	2222.9	2237.1	17.68	-0.64
$\int_0^t q_1(\dot{\phi}'^2 + \dot{\theta}'^2 + \dot{z}'^2)dt$.0072	.0040	70.83	44.44
$\int_0^t q_2(\dot{\phi}^2 + \dot{\theta}^2 + \dot{z}^2)dt$.2800	.1475	74.11	47.32
$\int_0^t q_3(z_1'^2 + z_2'^2 + z_3'^2 + z_4'^2)dt$.0607	.0453	13.34	25.37
$\int_0^t (q_4 F_s^2 + q_5 F_{\text{damp}}^2 + q_6 F_{\text{act}}^2)dt$.6724	.5209	16.63	22.53

This section indicates that an active suspension with an active damper as its actuator is capable of giving significant improvement in ride over a passive suspension system and has the advantage of requiring very little external power to operate.

7 CONCLUSIONS

Using a linear seven degree of freedom model, this thesis examined the ride improvements that can be obtained using active suspension systems. Each system was evaluated using frequency response and/or simulation for specific worst case road profiles. The results are summarized below for each system studied in this thesis. In order to quantify the comparisons of the improvement of each suspension type, comparisons are made using the percent improvement in the sum of the four cost integrals for the slanted bump. This does not give a complete evaluation of each system, and therefore other important findings are also summarized.

1. The vehicle with full state variable feedback (vehicle 2) improves the sum of the cost integrals 75.5%. While vehicle 3 gives slightly better improvement, the vehicle with full state feedback has the least force transmitted, peak bounce, peak roll, and settling times of all the vehicles which indicates this vehicle gives the best improvement in ride.
2. The vehicle with road height removed from the state vector (vehicle 3) improves the sum of the cost integrals by 76.0%. Other measures of vehicle ride for this vehicle show slightly less improvement than those for vehicle 2, but are much improved over the other vehicles.
3. The optimal observer used to reconstruct the state vector based on relative suspension deflections (vehicle 4) reduces the cost integral by 62.6% over the passive system. The improvement in peak vibrations and settling times is slightly less than that of vehicles 2 and 3, but still much improved over the passive system.

4. A linearized first order model of an hydraulic actuator included in the optimal observer model gives performance very similar to vehicle 4 when the time constant is below 0.1 seconds. A linearized second order model of an hydraulic actuator gives similar performance when its natural frequency is above 10 Hertz. If the time constant is less than 0.1 seconds or the natural frequency of the actuator is above 10 Hertz, then the dynamics can be neglected since they only slightly effect the results.
5. On/off damping (vehicle 5) gives a 19.6% improvement in cost integrals for baseline damping constants and a 33.8% improvement for two times the baseline damping ratio (vehicle 6). Advantages of on/off damping include the simplicity of the system and that the system requires very little external power to operate. Not shown by the slanted bump input is the ability of the on/off damper to remove high frequency inputs. This was demonstrated by the step response in which the on/off damper dramatically improved the ride performance compared to the passive system.
6. The vehicle with active dampers (vehicle 8) gives a 60.1% improvement in the total cost integral over the passive suspension. An advantage of active damping is that little external power is required to achieve ride performance comparing well to that of an ideal actuator.

This thesis has demonstrated that realistic active and semi-active suspension systems are capable of significantly improving the ride performance of the vehicle. The on/off damper system and the optimal observer system with either hydraulic or active damping actuators are capable of producing improved suspension performance. It remains to be seen, however, whether these are practical for production vehicles when the cost, reliability, and energy consumption of the systems are weighed against the improvements possible.

8 BIBLIOGRAPHY

- [1] Thompson, A. G. "An Active Suspension with Optimal Linear State Feedback". Vehicle System Dynamics 5 (1976): 61-72.
- [2] Thompson, A. G. and Pearce, C. E. M. "An Optimal Suspension for an Automobile on a Random Road". SAE Transactions, paper 790478 (1979).
- [3] Shannan, J. E. "Ride and Handling of a Vehicle with Active Suspensions". Master's Thesis, Iowa State University, Ames, Iowa, 1986.
- [4] Baker, A. "Lotus' Active Suspension". Automotive Engineer, London, 10 (June/July 1985): 26-9.
- [5] Yokoya, Y., Asami, K., Hamajima, T., and Nakashima, N. "Toyota Electronic Modulated Suspension (TEMS) System for the 1983 Soarer". SAE Transactions, paper 840341 (1985).
- [6] Mizuguchi, M., Suda, T., Chikamori, S., and Kobayashi, K. "Chassis Electronic Control Systems for the Mitsubishi 1984 Galant". SAE Transactions, paper 840258 (1984).
- [7] "Programmed Suspension Provides Ride Control". Automotive Engineering, 95, number 2 (February 1987): 122-132.
- [8] Crosby, M. J. and Karnopp, D. C. "The Active Damper - A New Concept for Shock and Vibration Control". 43rd Shock and Vibration Bulletin, Part H, June 1973.
- [9] Sharp, R. and Hassan, S. "Performance and design considerations for dissipative semi-active suspension systems for automobiles". Proc. Institution of Mechanical Engineers, Part D, 201, number D2 (1987): 149-153.
- [10] Sutton, H. "Synthesis and development of an experimental active suspension". Automotive Engineer, London, 4 (October/November 1979): 51-4.

- [11] Merritt, H. Hydraulic Control Systems. John Wiley & Sons, New York, 1967.
- [12] Sherman, S. and Lance, G. "A Design Study of a positioning System with Electrohydraulic Actuation". U.S. Army Tank Automotive Command Contract number DAAE07-83-R032 (1983).
- [13] Lopez, J. and Lance, G. "Integrated Simulation of Agricultural Tractor With Controlled Implement". SAE Transactions, paper 841128 (1985).
- [14] Kwakernaak, H., and Sivan, R. Linear Optimal Control Systems. Wiley-Interscience, New York, 1972.

9 APPENDIX A - PARAMETERS USED IN THIS THESIS

a	$= 0.945 \text{ m}$	q_1	$= 10$
b	$= 1.718 \text{ m}$	q_2	$= 7.5$
c_f	$= 348 \text{ N s/m}$	q_3	$= 50$
c_r	$= 782 \text{ N s/m}$	q_4	$= 5(10)^{-7}$
I_x	$= 438 \text{ kg m}^2$	q_5	$= 5(10)^{-7}$
I_y	$= 2337 \text{ kg m}^2$	q_6	$= 5(10)^{-7}$
k_f	$= 12480 \text{ N/m}$	q_7	$= 1(10)^{-10}$
k_r	$= 15730 \text{ N/m}$	t_f	$= 1.512 \text{ m}$
k_t	$= 240000 \text{ N/m}$	t_r	$= 1.470 \text{ m}$
M_s	$= 876 \text{ kg}$	\bar{w}^2	$= 1(10)^{-6}$
M_1	$= 153 \text{ kg}$	\bar{z}_r^2	$= 6.375(10)^{-7}$
M_2	$= 85 \text{ kg}$		
M_3	$= 153 \text{ kg}$		
M_4	$= 85 \text{ kg}$		

10 APPENDIX B - FEEDBACK GAIN MATRICES

Feedback gain matrix for 18 state variable feedback(type-2):

$$K_r = \begin{bmatrix} 2022.396 & 1912.242 & -2021.458 & -1910.420 \\ -3363.783 & 2742.049 & -3354.376 & 2754.662 \\ 4744.883 & 4374.338 & -4782.329 & -4363.217 \\ -10900.107 & 8062.379 & -10899.791 & 8139.961 \\ 7234.908 & 4965.373 & 7273.676 & 4898.856 \\ 2777.987 & 1576.832 & 2774.325 & 1566.049 \\ -3934.736 & -1860.419 & -722.245 & 1264.983 \\ -128.475 & 45.490 & 9.270 & -27.113 \\ -2553.258 & -5121.686 & 1727.217 & -621.449 \\ 33.799 & 22.884 & -21.366 & 3.034 \\ -541.012 & 935.651 & -2911.566 & -1339.031 \\ 10.244 & -25.957 & -11.093 & 43.059 \\ 1734.301 & -621.806 & -2547.096 & -5115.795 \\ -21.161 & 3.032 & 34.294 & 22.842 \\ 2091.156 & -2408.671 & 2208.658 & -2270.185 \\ -2089.261 & 2410.527 & -2210.080 & 2268.396 \\ 2223.728 & -2278.723 & 2108.987 & -2395.426 \\ -2225.620 & 2276.866 & -2107.561 & 2397.216 \end{bmatrix}$$

Feedback gain matrix for 14 state variable feedback

(types-3, 4 and 9):

$$K_r = \begin{bmatrix} 2022.396 & 1912.242 & -2021.458 & -1910.420 \\ -3363.783 & 2742.049 & -3354.376 & 2754.662 \\ 4744.883 & 4374.338 & -4782.329 & -4363.217 \\ -10900.107 & 8062.379 & -10899.791 & 8139.961 \\ 7234.908 & 4965.373 & 7273.676 & 4898.856 \\ 2777.987 & 1576.832 & 2774.325 & 1566.049 \\ -3934.736 & -1860.419 & -722.245 & 1264.983 \\ -128.475 & 45.490 & 9.270 & -27.113 \\ -2553.258 & -5121.686 & 1727.217 & -621.449 \\ 33.799 & 22.884 & -21.366 & 3.034 \\ -541.012 & 935.651 & -2911.566 & -1339.031 \\ 10.244 & -25.957 & -11.093 & 43.059 \\ 1734.301 & -621.806 & -2547.096 & -5115.795 \\ -21.161 & 3.032 & 34.294 & 22.842 \end{bmatrix}$$

Columns 1 through 4 of optimal observer feedback gain matrix for
14 state variable feedback (types-3, 4 and 9):

$$K_e = \begin{bmatrix} -1.630 & 8.501 & -2.008 & 8.111 \\ 0.675 & -2.305 & -0.921 & 4.028 \\ -0.088 & 1.884 & -0.154 & 1.924 \\ 0.046 & -0.710 & -0.062 & 0.980 \\ -0.086 & 1.470 & -0.083 & 1.197 \\ -1.349 & 5.798 & -1.200 & 5.500 \\ -0.667 & 3.443 & -0.066 & 1.721 \\ -3.342 & -1239.082 & -1.762 & 6.743 \\ 0.001 & 1.718 & -0.692 & 4.206 \\ -1.393 & 7.003 & -4.350 & -2229.262 \\ -0.022 & 0.744 & 0.042 & -1.189 \\ -0.728 & 0.695 & 1.136 & -3.462 \\ 0.007 & -1.188 & -0.026 & 1.498 \\ 1.002 & -3.434 & -1.277 & 5.494 \end{bmatrix}$$

Columns 5 through 8 of optimal observer feedback gain matrix for
14 state variable feedback (types-3, 4 and 9):

1.630	-8.501	2.008	-8.111
0.675	-2.305	-0.921	4.028
0.088	-1.884	0.154	-1.924
0.046	-0.710	-0.062	0.980
-0.086	1.470	-0.083	1.197
-1.349	5.798	-1.200	5.500
-0.022	0.744	0.042	-1.189
-0.728	0.695	1.136	-3.462
0.007	-1.188	-0.026	1.498
1.002	-3.434	-1.277	5.494
-0.667	3.443	-0.066	1.721
-3.342	-1239.082	-1.762	6.743
0.001	1.718	-0.692	4.206
-1.393	7.003	-4.350	-2229.262

11 APPENDIX C - SYSTEM EQUATIONS AND MATRICES

Equations of motion:

$$F_a = F_1 + k_f(z_1 - z_a) + c_f(\dot{z}_1 - \dot{z}_a)$$

$$F_b = F_2 + k_r(z_2 - z_b) + c_r(\dot{z}_2 - \dot{z}_b)$$

$$F_c = F_3 + k_f(z_3 - z_c) + c_f(\dot{z}_3 - \dot{z}_c)$$

$$F_d = F_4 + k_r(z_4 - z_d) + c_r(\dot{z}_4 - \dot{z}_d)$$

$$F_{t1} = k_t(z_{1f} - z_1)$$

$$F_{t2} = k_t(z_{1r} - z_2)$$

$$F_{t3} = k_t(z_{rf} - z_3)$$

$$F_{t4} = k_t(z_{rr} - z_4)$$

$$z_a = z + \frac{t_f}{2}\phi - a\theta$$

$$z_b = z + \frac{t_r}{2}\phi + b\theta$$

$$z_c = z - \frac{t_f}{2}\phi - a\theta$$

$$z_d = z - \frac{t_r}{2}\phi + b\theta$$

$$\dot{z}_a = \dot{z} + \frac{t_f}{2}\dot{\phi} - a\dot{\theta}$$

$$\dot{z}_b = \dot{z} + \frac{t_r}{2}\dot{\phi} + b\dot{\theta}$$

$$\dot{z}_c = \dot{z} - \frac{t_f}{2}\dot{\phi} - a\dot{\theta}$$

$$\dot{z}_d = \dot{z} - \frac{t_r}{2}\dot{\phi} + b\dot{\theta}$$

First four columns of \tilde{A} matrix

$$\tilde{A} = \begin{bmatrix} \frac{-c_f t_f^2 - c_r t_r^2}{2I_x} & 0 & \frac{-k_f t_f^2 - k_r t_r^2}{2I_x} & 0 \\ 0 & \frac{-c_f a^2 - c_r b^2}{I_y} & 0 & \frac{-k_f a^2 - k_r b^2}{I_y} \\ 1 & 0 & 0 & 0 \\ 0 & 1 & 0 & 0 \\ 0 & 0 & 0 & 0 \\ 0 & \frac{2(ac_f - bc_r)}{M_s} & 0 & \frac{2(ak_f - bk_r)}{M_s} \\ 0 & 0 & 0 & 0 \\ \frac{t_f c_f}{2M_1} & \frac{-ac_f}{M_1} & \frac{t_f k_f}{2M_1} & \frac{-ak_f}{M_1} \\ 0 & 0 & 0 & 0 \\ \frac{t_r c_r}{2M_2} & \frac{bc_r}{M_2} & \frac{t_r k_r}{2M_2} & \frac{bk_r}{M_2} \\ 0 & 0 & 0 & 0 \\ \frac{-t_f c_f}{2M_3} & \frac{-ac_f}{M_3} & \frac{-t_f k_f}{2M_3} & \frac{-ak_f}{M_3} \\ 0 & 0 & 0 & 0 \\ \frac{-t_r c_r}{2M_4} & \frac{bc_r}{M_4} & \frac{-t_r k_r}{2M_4} & \frac{bk_r}{M_4} \\ 0 & 0 & 0 & 0 \\ 0 & 0 & 0 & 0 \\ 0 & 0 & 0 & 0 \\ 0 & 0 & 0 & 0 \end{bmatrix}$$

Columns 5 through 11 of the \bar{A} matrix

0	0	$\frac{t_f k_f}{2I_x}$	$\frac{t_f c_f}{2I_x}$	$\frac{t_r k_r}{2I_x}$	$\frac{t_r c_r}{2I_x}$	$\frac{-t_f k_f}{2I_x}$
$2\frac{ak_f - bk_r}{I_y}$	$2\frac{ac_f - bc_r}{I_y}$	$\frac{-ak_f}{I_y}$	$\frac{-ac_f}{I_y}$	$\frac{bk_r}{I_y}$	$\frac{bc_r}{I_y}$	$\frac{-ak_f}{I_y}$
0	0	0	0	0	0	0
0	0	0	0	0	0	0
0	1	0	0	0	0	0
$2\frac{-k_f - k_r}{M_s}$	$2\frac{-c_f - c_r}{M_s}$	$\frac{k_f}{M_s}$	$\frac{c_f}{M_s}$	$\frac{k_r}{M_s}$	$\frac{c_r}{M_s}$	$\frac{k_f}{M_s}$
0	0	0	1	0	0	0
$\frac{k_f}{M_1}$	$\frac{c_f}{M_1}$	$\frac{-k_f - k_t}{M_1}$	$\frac{-c_f}{M_1}$	0	0	0
0	0	0	0	0	1	0
$\frac{k_r}{M_2}$	$\frac{c_r}{M_2}$	0	0	$\frac{-k_r - k_t}{M_2}$	$\frac{-c_r}{M_2}$	0
0	0	0	0	0	0	0
$\frac{k_f}{M_3}$	$\frac{c_f}{M_3}$	0	0	0	0	$\frac{-k_f - k_t}{M_3}$
0	0	0	0	0	0	0
$\frac{k_r}{M_4}$	$\frac{c_r}{M_4}$	0	0	0	0	0
0	0	0	0	0	0	0
0	0	0	0	0	0	0
0	0	0	0	0	0	0
0	0	0	0	0	0	0

Columns 12 through 18 of the \tilde{A} matrix

$\frac{-t_f c_f}{2I_x}$	$\frac{-t_r k_r}{2I_x}$	$\frac{-t_r c_r}{2I_x}$	0	0	0	0
$\frac{-ac_f}{I_y}$	$\frac{bk_r}{I_y}$	$\frac{bc_r}{I_y}$	0	0	0	0
0	0	0	0	0	0	0
0	0	0	0	0	0	0
0	0	0	0	0	0	0
$\frac{c_f}{M_s}$	$\frac{k_r}{M_s}$	$\frac{c_r}{M_s}$	0	0	0	0
0	0	0	0	0	0	0
0	0	0	$\frac{k_t}{M_1}$	0	0	0
0	0	0	0	0	0	0
0	0	0	0	$\frac{k_t}{M_2}$	0	0
1	0	0	0	0	0	0
0	0	0	0	0	$\frac{k_t}{M_3}$	0
0	0	1	0	0	0	0
0	0	0	0	0	0	$\frac{k_t}{M_4}$
0	0	0	0	0	0	0
0	0	0	0	0	0	0
0	0	0	0	0	0	0
0	0	0	0	0	0	0

The \tilde{B}_1 matrix:

$$\tilde{B}_1 = \begin{bmatrix} \frac{t_f}{2I_x} & \frac{t_r}{2I_x} & \frac{-t_f}{2I_x} & \frac{-t_r}{2I_x} \\ \frac{-a}{I_y} & \frac{b}{I_y} & \frac{-a}{I_y} & \frac{b}{I_y} \\ 0 & 0 & 0 & 0 \\ 0 & 0 & 0 & 0 \\ 0 & 0 & 0 & 0 \\ \frac{1}{M_s} & \frac{1}{M_s} & \frac{1}{M_s} & \frac{1}{M_s} \\ 0 & 0 & 0 & 0 \\ \frac{-1}{M_1} & 0 & 0 & 0 \\ 0 & 0 & 0 & 0 \\ 0 & \frac{-1}{M_2} & 0 & 0 \\ 0 & 0 & 0 & 0 \\ 0 & 0 & \frac{-1}{M_1} & 0 \\ 0 & 0 & 0 & 0 \\ 0 & 0 & 0 & \frac{-1}{M_1} \\ 0 & 0 & 0 & 0 \\ 0 & 0 & 0 & 0 \\ 0 & 0 & 0 & 0 \\ 0 & 0 & 0 & 0 \end{bmatrix}$$

The \tilde{B}_2 matrix:

$$\tilde{B}_2 = \begin{bmatrix} 0 & 0 & 0 & 0 \\ 0 & 0 & 0 & 0 \\ 0 & 0 & 0 & 0 \\ 0 & 0 & 0 & 0 \\ 0 & 0 & 0 & 0 \\ 0 & 0 & 0 & 0 \\ 0 & 0 & 0 & 0 \\ 0 & 0 & 0 & 0 \\ 0 & 0 & 0 & 0 \\ 0 & 0 & 0 & 0 \\ 0 & 0 & 0 & 0 \\ 0 & 0 & 0 & 0 \\ 0 & 0 & 0 & 0 \\ 0 & 0 & 0 & 0 \\ 0 & 0 & 0 & 0 \\ 1 & 0 & 0 & 0 \\ 0 & 1 & 0 & 0 \\ 0 & 0 & 1 & 0 \\ 0 & 0 & 0 & 1 \end{bmatrix}$$

Columns 15 through 18 of the D matrix:

0	0	0	0
0	0	0	0
$\frac{-1}{2t_f}$	$\frac{-1}{2t_r}$	$\frac{1}{2t_f}$	$\frac{1}{2t_r}$
$\frac{-1}{2(a+b)}$	$\frac{1}{2(a+b)}$	$\frac{-1}{2(a+b)}$	$\frac{1}{2(a+b)}$
-0.25	-0.25	-0.25	-0.25
0	0	0	0
-1	0	0	0
0	0	0	0
0	-1	0	0
0	0	0	0
0	0	-1	0
0	0	0	0
0	0	0	-1
0	0	0	0
1	0	0	0
0	1	0	0
0	0	1	0
0	0	0	1

Columns 1 through 7 of the C matrix:

$$C = \begin{bmatrix} 0 & 0 & \frac{t_f}{2} & -a & 1 & 0 & -1 \\ \frac{t_f}{2} & -a & 0 & 0 & 0 & 1 & 0 \\ 0 & 0 & \frac{t_r}{2} & b & 1 & 0 & 0 \\ \frac{t_r}{2} & b & 0 & 0 & 0 & 1 & 0 \\ 0 & 0 & \frac{-t_f}{2} & -a & 1 & 0 & 0 \\ \frac{-t_f}{2} & -a & 0 & 0 & 0 & 1 & 0 \\ 0 & 0 & \frac{-t_r}{2} & b & 1 & 0 & 0 \\ \frac{-t_r}{2} & b & 0 & 0 & 0 & 1 & 0 \end{bmatrix}$$

Columns 8 through 14 of the C matrix:

$$\begin{bmatrix} 0 & 0 & 0 & 0 & 0 & 0 & 0 \\ -1 & 0 & 0 & 0 & 0 & 0 & 0 \\ 0 & -1 & 0 & 0 & 0 & 0 & 0 \\ 0 & 0 & -1 & 0 & 0 & 0 & 0 \\ 0 & 0 & 0 & -1 & 0 & 0 & 0 \\ 0 & 0 & 0 & 0 & -1 & 0 & 0 \\ 0 & 0 & 0 & 0 & 0 & -1 & 0 \\ 0 & 0 & 0 & 0 & 0 & 0 & -1 \end{bmatrix}$$